2005

The Structural and Functional Analysis of a Voltage-Dependent Potassium Channel

Vanessa Ruta

THE STRUCTURAL AND FUNCTIONAL ANALYSIS OF A VOLTAGE-DEPENDENT POTASSIUM CHANNEL

A Dissertation

Presented to the Faculty of The Rockefeller University

In Partial Fulfillment of the Requirements for

the Degree of Doctor of Philosophy

by

Vanessa Ruta

June 2005

For my first teachers, my parents

ACKNOWLEDGMENTS

I came to Rockefeller University hoping to work in the MacKinnon lab after hearing Rod give a talk that exemplified his insight, enthusiasm and passion for the discovery process. I feel very fortunate to have spent the past five years as a member of the MacKinnon lab. Rod, I sincerely thank you for all that you have shared with me. It has been a privilege to work with and learn from you. You remain my lasting ideal for a scientist.

For all the time I have been a student, the MacKinnon lab has remained an interesting eclectic group of scientists. I feel every member of the lab has contributed to my education and any progress I have made. I thank you all for your patience, generosity and friendship. I would particularly like to thank Alice, Youxing and Jiayun with whom I worked directly in this long road to understanding of voltage-dependent gating. I also would like to thank Fenny, Raimund, and Seok-Yong for helping me with data collection and for advice on crystallography. Francis, I thank for his critical advice on a variety of different biochemical questions. I also want to thank Wendell for helping me out on numerous occasions. I surely will miss the special environment of the lab.

I would like to thank Martine Cadene and Michelle Trester-Zedlitz from Brian Chait's lab for assistance with mass spectrometry, as well as their advice and friendship.

Thanks to David Gadsby, Brian Chait and Eric Gouaux for their time and attention as members of my thesis committee.

I want to thank the Rockefeller University graduate program for their support and enabling me to work with so few worries about life outside of the lab. Thanks to Sid, Marta, Kristen, and all the members of the Dean's office for their help and support.

Thanks to my family and friends who have tolerated five years of my strange schedule, and remained a source of very happy distractions. My most constant and wonderful distraction is my husband who has kept me laughing through out these years and listened to more discussions on heavy atom phasing than anyone should ever have to. Thanks for being there for me.

TABLE OF CONTENTS

Abstract..... page 1

Chapter 1: Introduction..... page 3

Chapter 2: Functional analysis of KvAP, an archeabacterial voltage-dependent K^+ channel..... page 18

Chapter 3: Localization of the tarantula voltage-sensor toxin receptor on KvAP.....page 29

Chapter 4: Crystal structure of the KvAP-Fab complex..... page 43

Chapter 5: The structure of KvAP in the absence of Fab..... page 60

Chapter 6: Gating charge movement in KvAP..... page 82

Chapter 7: Conclusions and discussion .....page 114

Materials and Methods.....page 145

References.....page 154

LIST OF TABLES

Table 1: Molecular replacement solution statistics for all primitive orthorhombic space-groups.....page 69

Table 2: Data-collection and phasing statistics.....page 73

LIST OF FIGURES

Figure 1: Fundamental structural aspects of a K^+ selective pore..... page 6

Figure 2: Architecture of a voltage-gated K^+ channel..... page 10

Figure 3: A model of voltage-dependent gating..... page 13

Figure 4: Properties of the KvAP ion pathway..... page 20

Figure 5: Voltage-dependent gating properties in KvAP..... page 22

Figure 6: Inhibition of KvAP by *Grammostola spatulata* toxins..... page 25

Figure 7: Sequence analysis of spider toxins that bind to KvAP..... page 27

Figure 8: A conserved target for voltage-sensor toxins in voltage-dependent K^+, Na^+, and Ca^{2+}channels.....page 31

Figure 9: Experimental strategy used to isolate toxins from whole venom that bind to KvAP channel proteins.....page 33

Figure 10: Comparison of tarantula toxin retention profiles for the KvAP isolated voltage-sensor domain and full-length channel.....page 35

Figure 11: Native and recombinant VSTX3 alter KvAP channel gating.....page 37

Figure 12: VSTX2 and GSMTX4 minimally affect KvAP function.....page 40

Figure 13: Structure of the KvAP channel in complex with Fab fragments.....page 44

Figure 14: The KvAP pore.....page 46

Figure 15: The KvAP channel architecture contains a voltage-sensor paddle at the channel perimeter.....page 48

Figure 16: Structure of the KvAP isolated-voltage sensor domain.....page 51

Figure 17: Comparison of the KvAP voltage-sensor domain structures..... page 53

Figure 18: Hypothesis for gating charge movement.....page 55

Figure 19: Inhibition of KvAP by Fabs that bind to the voltage-sensor paddle..... page 57

Figure 20: Phasing of the low-resolution KvAP crystal form..... page 64

Figure 21: Experimental electron density..... page 72

Figure 22: Architecture of the KvAP channel in the absence of Fab fragments..... page 76

Figure 23: KvAP channel supra-structure.....page 78

Figure 24: Using avidin and tethered biotin to measure the positions of amino-acids on KvAP relative to the membrane plane.....page 84

Figure 25: The effective linker length of biotin determines accessibility to avidin..... page 86

Figure 26: Avidin accessibility of biotinylated residues in S5..... page 88

Figure 27: Estimating the extent of biotinylation through gel-shift assays..... page 90

Figure 28: Avidin accessibility mapped onto the KvAP pore..... page 93

Figure 29: Avidin accessibility of biotinylated residues in S1 and S2..... page 97

Figure 30: Avidin accessibility data indicate a transmembrane orientation for S1 and S2.....page 100

Figure 31: Avidin accessibility for biotinylated residues in the voltage-sensor paddle.....page 103

Figure 32: Exposure of the paddle to the extracellular solution requires membrane depolarization.....page 108

Figure 33: Position of the voltage-sensor paddle in the closed and opened channel.....page 110

Figure 34: Conceptual model of the voltage-dependent gating process.....page 119

Figure 35: Gating charge movement in KvAP..... page 122

Figure 36: Comparison of the accessibility of S4 residues in KvAP, *Shaker* and an Nav channel..... page 126

THE STRUCTURAL AND FUNCTIONAL ANALYSIS OF A VOLTAGE-DEPENDENT POTASSIUM CHANNEL.

Vanessa Ruta

The Rockefeller University 2005

Voltage-dependent ion channels are finely tuned to open and allow ion conduction in response to changes in the membrane voltage, a function that lies at the heart of nerve impulse generation and propagation. These channels contain transmembrane voltage-sensing domains that contain highly conserved cationic amino acids known as "gating charges." The gating charge residues move under the influence of the membrane's electric field, a voltage-dependent conformational change that induces pore opening. In this thesis, I explore the structural basis of gating charge movement through crystallographic, biochemical and functional studies of KvAP, a voltage-dependent K^+ (Kv) channel from a thermophilic archeabacterium. I show that KvAP channels possess all the functional properties of eukaryotic Kv channels responsible for nerve impulses. This functional similarity arises from fundamental conservation of the voltage sensor structure as demonstrated by KvAP's sensitivity to tarantula toxins that bind a receptor on its voltage sensor—toxins that evolved to inhibit the voltage-dependent channels of the eukaryotic prey of these spiders. I present a low-resolution crystal structure of the KvAP channel and compare it with a previous structure of the channel crystallized with monoclonal Fab fragments bound to its voltage

sensors. In both structures, we find a canonical K^+ selective pore surrounded by voltage sensors that contain "voltage-sensor paddles"— hydrophobic helix-turn-helix structures located on the channel's outer perimeter. The gating charge residues are embedded in a helical segment of each voltage-sensor paddle. The crystal structures suggest that the voltage-sensor paddles are attached to the channel through flexible hinges and move as rigid units in response to membrane voltage changes, carrying their gating charges through the lipid. I used tethered biotin and avidin as a molecular ruler to measure the depth of residues in KvAP relative to the plane of the membrane and evaluate the gating motions of the voltage-sensor paddles. From this study, I conclude that the voltage-sensor paddles are a uniquely mobile part of the channel and translate the gating charge residues a ~15-20 Å perpendicular to the plane of the membrane to induce pore opening.

CHAPTER 1: INTRODUCTION

All cells are enclosed in a thin lipid membrane whose function is to keep the components of the cell concentrated so that the chemistry of life can occur. However, the ~30 Å hydrophobic core of the lipid membrane presents a formidable barrier to the passage of a number of chemical species into and out of the cell including ions. Nature's strategy to facilitate and regulate the transport of ions through the low dielectric of the membrane includes two classes of membrane-spanning proteins—ion transporters and ion channels that work in concert. The low permeability of the membrane to ions means that ionic gradients can be established and maintained as a vital form of stored energy. The asymmetric distribution of ions across the membrane is created by the activity of ion transporters that harness energy, from ATP hydrolysis for example, to move ions against their concentration gradients. In contrast, ion flow through channel proteins is "downhill" in the direction dictated by the electrochemical driving force. Thus the slow and steady homeostatic work of ion transporters prepares the way for rapid signaling through ion channels that dissipate ionic gradients, making use of this energy currency to accomplish a number of important cellular processes[1]. In neurons and other electrically excitable cells, the highly orchestrated electrical

signaling through ion channels underlies the action potential—a transient fluctuation in the membrane voltage that spreads quickly over the membrane. The rapid, long range transmission of information encoded in action potentials underlies all the complex processes that define our human existence, including sensation, learning, memory and coordinated motion.

The foundations for our modern understanding of ion channel proteins lie in Hodgkin and Huxley's seminal studies of nerve impulse generation published over fifty years ago [2-5]. Hodgkin and Huxley deduced that the membrane currents underlying an action potential could be attributed to separate Na^+ and K^+ conduction pathways and that these conduction pathways were controlled solely by membrane voltage. During the course of an action potential, an initial transient flow of Na^+ ions inward depolarized the membrane and was followed by a slower persistent outward flow of K^+ ions which served to repolarize the membrane. The interplay of the membrane permeability to a given ion, which determines the membrane voltage, and the membrane voltage, which in turn determines the membrane permeability to ions, was central to Hodgkin and Huxley's theory of the action potential. Their model was sufficient to describe all the classical properties of action potential generation and propagation but also showed surprising insight into the essential functional properties of ion channel proteins. In an era preceding any molecular understanding of channel proteins, Hodgkin and Huxley highlighted the two hallmark features of ion channels—selective permeability and gating of the ion conduction pathway.

Ion channels can be exquisitely selective for a particular type of ion. K^+ channels, for example, are able to select K^+ ions over Na^+ ions by a factor of $\sim 10^4$, although both are essentially featureless monovalent spheres differing in radius by less than 0.4Å. The basis for

a K^+ channel's extraordinary selectivity is eloquently illustrated in the crystal structure of the prokaryotic K^+ channel, KcsA (Fig. 1) [6,7]. All K^+ selective pores have evolved a narrow constriction, the selectivity filter, which optimally coordinates dehydrated K^+ ions but not smaller Na^+ ions. The amino-acid sequence that forms the selectivity filter is called the K^+ channel signature sequence and is conserved in all known K^+ channels throughout the tree of life[8]. In the selectivity filter of KcsA, carbonyl oxygens directed towards the pore mimic the coordination of a K^+ ion in aqueous solution, providing the naked ion with a smooth energetic landscape as it traverses the membrane.

The second feature of ion channels which first came to light in Hodgkin and Huxley's observations is that ion conduction pores are "gated"—they open and close in response to an appropriate biological stimulus, such as a change in membrane voltage or the binding of a ligand. Hodgkin and Huxley proposed that the individual voltage-dependent ionic currents were possible only when "activating particles" were to "occupy a certain region of the membrane."[2] Although they state that the "details of the mechanism will probably not be settled for some time,"[2] they had a basic intuition for how voltage-dependent gating might work: charges move in an electric field and the electrostatic work of this charge movement could be coupled to gating of the ion conduction pathway.

Five decades later, we know that Hodgkin and Huxley's selective conduction pathways are ion channel proteins—members of the family of voltage-dependent cation (Na^+, K^+ or Ca^{2+}) channels. These channels open and conduct primarily their namesake ion as a steep function of the membrane voltage. Voltage-dependent K^+ (Kv) channels have been the subject of particularly intense study. Several decades of investigation using molecular biology, biophysical and biochemical techniques have culminated in a basic understanding of

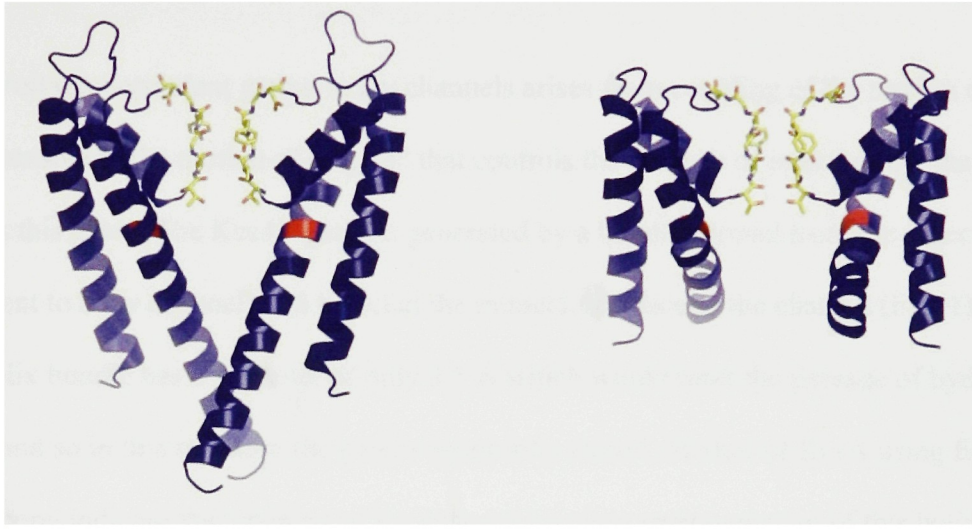

Figure 1

Fundamental structural aspects of a K^+ selective pore. Two subunits of the closed KcsA K^+ channel (left) and the opened MthK K^+ channel (right) are shown. Amino-acids that comprise the K^+ channel signature sequence and form the selectivity filter are shown in yellow. In the KcsA structure the inner helices come together to form a helix bundle that is thought to represent a closed "gate" on the ion-conduction pathway. The inner helices of MthK are bent at a glycine hinge (red) thus allowing the inner helix bundle to open.

channel organization and function. Kv channels are tetramers, with the four identical or similar subunits symmetrically arranged around a central ion conduction pathway[9]. Each subunit has six hydrophobic spanning segments (S1-S6) (Fig. 2). Kv channels are essentially modular proteins. The S5-P-S6 helices contribute to tetrameric architecture of the central ion conduction pore, including the narrow selectivity filter through which K^+ ions pass. The S1-S4 segments each form one of the channel's four voltage sensors which encircle the central pore.

Voltage-dependent gating in Kv channels arises from coupling of the motion of the voltage sensors to the motion of a "gate" that controls the passage of ions through the pore. Where is this gate? The KcsA "gate" is generated by a bundle formed from the inner helices (equivalent to a Kv channel's S6 helix) at the intracellular face of the channel (Fig. 1). The KcsA helix bundle has a diameter of only 3.5 Å which would limit the passage of hydrated K^+ ions and so in this structure the gate is apparently closed. Studies of KcsA using EPR spectroscopy indicate that opening of the channel involves rearrangement of this helix bundle[10]. In eukaryotic Kv channels, several studies have probed the state-dependent accessibility of the pore forming domain using reagents of varying diameter, including quaternary amines, MTS reagents and Ag^+ ions that react with cysteine thiols[11-13]. From these experiments it appears that Kv channels also have an activation gate at their cytoplasmic face that can limit the passage of ions, analogous to the KcsA helix bundle.

A comparison of the KcsA structure (a closed pore) with the crystal structure of a prokaryotic ligand-gated channel, MthK (an opened pore), provides a clear illustration of the conformational changes that can occur in the pore as the channel gates[14] (Fig. 1). In the opened MthK channel, the inner helices are kinked, exposing a wide intracellular mouth that

forms a continuous path for a K^+ ion from the intracellular solution up to the selectivity filter in the upper membrane leaflet. The hinge point of the inner helix in the MthK channel is a conserved glycine, present in most K^+ channels, including those that are voltage-dependent[14]. Mutational studies indicate that the gating hinge glycine is important to the mechanics of pore opening in *Shaker*, the archetypical neuronal Kv channel[15]. The combined structural and functional data suggest that the voltage-induced conformational changes in the voltage-sensors will have to pull on the inner helices (S6) of the pore in order to allow ion conduction.

Opening of the gate in voltage-dependent ion channels follows a very steep function of membrane voltage. Hodgkin and Huxley estimated that at least 6 elementary charges fully cross the membrane electric field during activation of the Na^+ current[2]. Hodgkin and Huxley recognized that the motion of the charged membrane components that governed Na^+ activation should contribute to the total measured current but they were unable to detect "any current associated with the change in Na^+ permeability, apart from the contribution of Na^+ itself."[2] Twenty-two years later Armstrong and Bezanilla, armed with advances in electronics and channel pharmacology, first measured the non-linear capacitive currents associated with Na^+ channel activation—the so-called "gating currents" that arise from movement of protein gating charges[16]. The integrated gating current normalized to the number of recorded channels provides a measure of the gating charge per channel that moves through the field during channel activation. Through gating current measurements, the gating charge in *Shaker* was measured to be 12-14 elementary charges per channel (or approximately 3.0-3.5 elementary charges per subunit)[17-19].

The large gating charge per channel has an interesting implication: there must be a specialized structure—a voltage sensor—to accomplish the charge movement. Voltage sensing could be accomplished by movement of partial charges dispersed throughout the channel or by reorientation of helix dipoles, but that would be unlikely to yield such a high degree of voltage sensitivity. The voltage-sensor domain fulfills this role of a specialized sensory module. When the first voltage-dependent ion channels were cloned it was clear that Hodgkin and Huxley's "activating particles" were located within the S4 segment of the voltage-sensor domain[20-22]. The S4 segment has an unusual conserved motif—repeats of a basic amino acid (mostly arginine but sometimes lysine) followed by two hydrophobic residues (Fig. 2). Gating charge measurements following charge neutralization in the *Shaker* channel indicate that the first four arginine residues in the S4 segment carry most of the gating charge[18,19]. One study has also implicated two conserved acidic residues in the S2 and S3 segments as contributing to the measured gating charge[19].

What types of conformational changes in the voltage sensor account for the transfer of the gating charge across the membrane's electric field? The mechanics of gating charge movement have been extensively investigated using a number of biophysical techniques. One approach has been to measure the state-dependent reactivity of hydrophilic thiol reactive reagents with introduced cysteines on the S4 segment. These accessibility studies have shown that upon membrane depolarization, approximately 10 amino acids on the *Shaker* S4 segment move from an inaccessible location within the membrane to the extracellular solution and at the same time 12 amino acids move from an intracellular to an inaccessible location[23-25]. The accessibility measurements are consistent with an outward motion of the S4 segment with membrane depolarization, in the correct direction to account for the gating

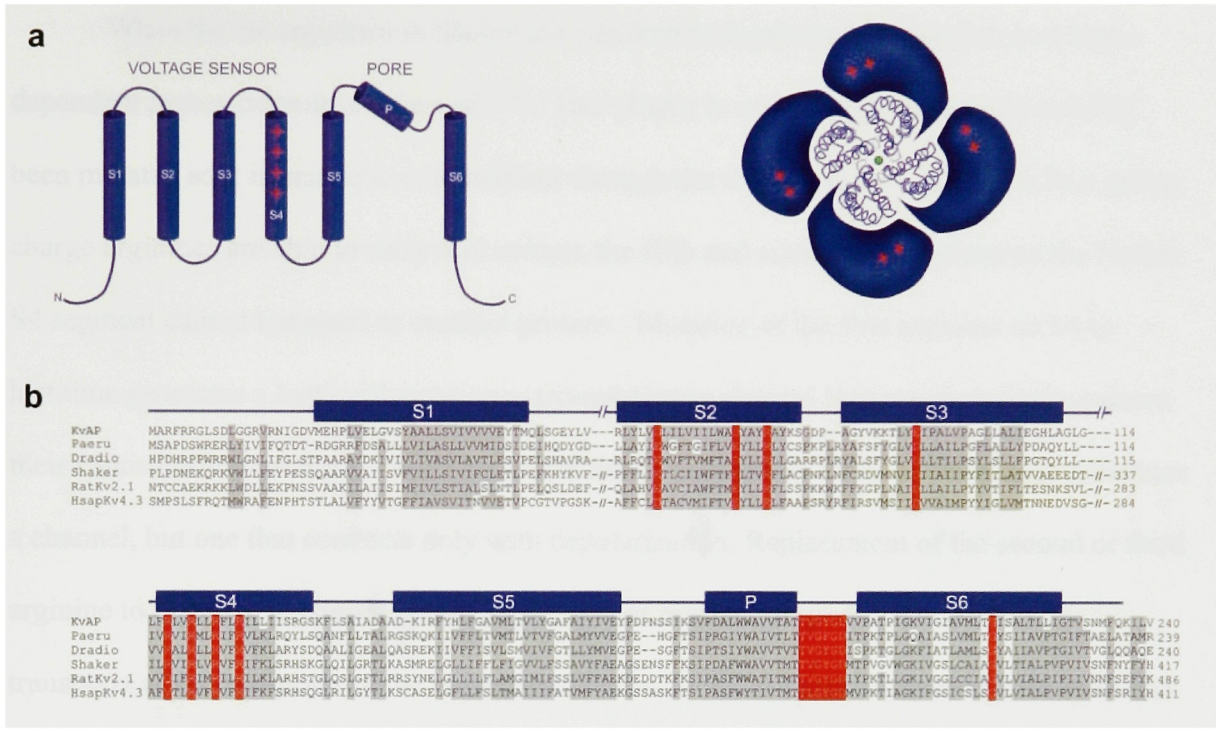

Figure 2

Architecture of a voltage-gated K^+ channel. Transmembrane spanning segments (S1-S6) are labeled (blue segments); four subunits surround the pore. S1-S4 form voltage sensor and S5-S6 the pore, represented by the KcsA K^+ channel structure (backbone model). In sequences of prokaryotic and eukaryotic Kv channels, regions of high homology are colored in grey and functionally important residues in red. Alignment was made with ClustalW followed by manual adjustment and exclusion of loops. K^+ channels: KvAP, *Aeropyrum pernix* (GI: 5104624); Paeru, *Pseudomonas aeruginosa* (GI:15596693); Dradio, *Deinococcus radiodurans* (GI: 15805856); Shaker, *Drosophila melanogaster* (GI:13432103); ratKv2.1, *Rattus norvegicus* (GI:24418849); HsapKv4.3, *Homo sapiens* (GI:5059060)

current. Similarly, in a voltage-dependent Na^+ channel, accessibility measurements show that the second and third basic S4 residues change from the intracellular to the extracellular side of the membrane with depolarization[26,27].

When the S4 arginines in *Shaker* are replaced with protonable histidine a voltage-dependent proton current is observed[28-30]. The current is not through the pore (which has been mutated so it is unable to conduct) but through the voltage sensor. Only the four gating charge arginines are able to carry this current, the fifth and sixth basic residues on the Shaker S4 segment cannot transport or conduct protons. Mutation of the first arginine on S4 to histidine generates a hyperpolarization-activated proton channel that conducts protons down their concentration gradient. Mutation of the fourth arginine on S4 to histidine also generates a channel, but one that conducts only with depolarization. Replacement of the second or third arginine to histidine generates a voltage-dependent proton transporter that maximally transports at the mid-point of the voltage-activation curve, as these residues shuttle back and forth across the membrane interface carrying a proton along with them. These results further substantiate the idea that some S4 residues move across the membrane under the influence of voltage, moving outward with depolarization and inward with hyperpolarization.

Yet another approach has been to study signals from sites on S4 labeled with fluorescent dyes. Many fluorescently labeled residues on different segments of the *Shaker* exhibit voltage-dependent changes in fluorescence intensity and attempts have been made to correlate these changes with the gating motions of the channel[31-34]. Fluorescence resonance energy transfer experiments have been interpreted as indicating that any translation of the S4 segment through the membrane is small and would be accompanied rotation of the S4 helix by ~180 ^{o} [35,36].

These combined observations have led to a model in which the S4 segment lies against the pore in a protein-formed aqueous canal, shielded from the lipid membrane by the S1-S3 segments of the voltage sensor[37-39] (Fig. 3). This model provides a means for the voltage sensor to overcome the energetic cost of having charged residues permanently buried within the hydrophobic core of the membrane, a structural constraint thought to be required in any model of the voltage-sensor architecture. Most residues on the *Shaker* S4 segment are accessible to thiol reactive reagents in either the opened or closed state of the channel and this extensive reactivity was thought to indicate that the S4 segment must lie at the interface of deep invaginations formed within the membrane from both the extracellular and the intracellular solution. The water-filled crevices could be generated by the packing of the remainder of the voltage sensor, for example by two tilted helices. One consequence of these aqueous crevices is that they will sculpt the local membrane potential surrounding the S4 helix, focusing the electric field over a small fraction of the total membrane thickness. It was envisioned that the S4 segment might move only a small distance to slide across the narrow gap between the two crevices or simply rotate and still effectively transfer the full gating charge across the membrane's electric field. In fact, based on fluorescence measurements in the *Shaker* channel, it was hypothesized that S4 translates less than 2 Å perpendicular to the membrane to transfer the gating charge through a highly focused electric field[35].

Despite these advances in our basic understanding of voltage-dependent gating in Kv channels, the molecular "details" of the voltage-dependent gating process have remained unclear. Many questions regarding these details, fundamental to the mechanism, have remained unanswered. What are the voltage-induced conformational changes that occur in voltage-dependent ion channels? How are they coupled to movement of the gate that

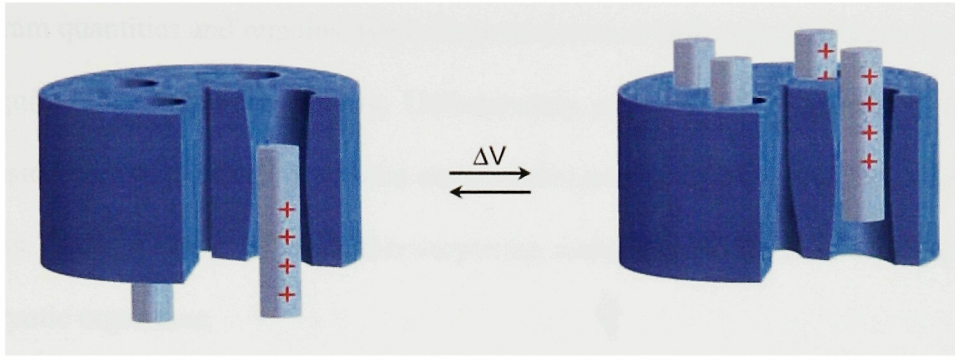

Figure 3
A model of voltage-dependent-gating. The S4 segments of the voltage-sensor (light blue) lie within an aqueous,protein-formed canal and are shielded from the lipid by other segments of the voltage sensor. The gating charges (red) are carried through the protein core by translations and/or rotations of the S4 segments to open the central ion conduction pore.

controls passage of ions through the pore? Ultimately to be able to satisfactorily answer these questions requires an atomic structure of a voltage-dependent channel. A long term goal in the MacKinnon lab has been to understand the structural and mechanistic design of a Kv based on crystallographic images of the channel. This effort began several years prior to my arrival in the MacKinnon lab and was led by Youxing Jiang, with the help of Alice Lee and Jiayun Chen. A prerequisite for any structural study is a protein that can be purified in milligram quantities and remains mono-dispersed even at high concentrations, both of which are required for crystallization trials. Unfortunately, neuronal Kv channels have limited expression both in their native cellular environment and in most heterologous expression systems. Jiang et al. turned to a rather surprising source for abundant Kv channel protein—prokaryotic organisms.

For many years voltage-dependent ion channels were regarded as a unique development of eukaryotes, evolved to accomplish the specialized electrical signaling exemplified in neurons. However, as the database of sequenced prokaryotic genomes grew, a number of prokaryotic genes emerged that appeared to encode voltage-dependent ion channels. One of these genes, a Na^+ selective channel, was shown to exhibit voltage-dependent gating when expressed in a mammalian cell line[40]. Figure 2b aligns three prokaryotic genes (top three sequences) that are very closely related to eukaryotic Kv channels (bottom three sequences). It is clear that there is essential conservation of the basic subunit topology (6 hydrophobic segments, S1-S6) in these prokaryotic genes as well as complete conservation of functionally important residues in the pore and voltage sensor. Highlighted in red are the five 'signature sequence' amino acids between S5 and S6 that form the selectivity filter, conserved inside the pore of all known K^+ channels[8]. Also highlighted

are the arginine residues at every third position in S4 and acidic residues—aspartate or glutamate—in S2 and S3 thought to underlie voltage-dependent gating[18 19]. Conservation of these amino acids implies that these prokaryotic channels may function very much like eukaryotic Kv channels with respect to both K^+ selective conduction and voltage-dependent gating. If this is indeed the case, then these prokaryotic channels could provide an inroad to understanding the structural basis of voltage-dependent gating.

Jiang et al. cloned and expressed a number of different prokaryotic K^+ channels with amino-acid sequences corresponding to the voltage sensor. For six of these channels, they obtained milligram quantities of channel tetramers but in all cases the channels aggregated into higher multimers when the protein was concentrated. They eventually turned to the genomes of extreme thermophiles, hoping to identify an exceptionally stable family member. One of these channels, KvAP, from *Aeropyrum pernix*, a hyperthermophilic archeabacterium isolated from an oceanic thermal vent off the coast of Japan proved to be well suited for structural studies. KvAP provided the first crystallographic image of a Kv channel (solved by Youxing Jiang) and this image was both very enlightening and very provocative, raising many interesting questions on the fundamental mechanism of voltage-dependent gating.

Overview

In my thesis I will present my contribution to this very collaborative effort in the lab. My own effort has involved crystallographic, biochemical and electrophysiological studies of KvAP. In the next chapter I will show that, quite remarkably, KvAP possesses all the functional attributes of Kv channels responsible for nerve impulses; most notably its pore opening is strongly dependent on membrane voltage. Even more remarkable, KvAP is

sensitive to tarantula toxins that evolved specifically to hinder the motions of the voltage sensors in the eukaryotic prey of these spiders. In the third chapter I will make use of a biochemical assay to demonstrate that the tarantula toxin receptor on the KvAP channel is located in the voltage-sensor domain. The results from Chapters 2 and 3 suggest that the conservation of function between KvAP and eukaryotic Kv channels reflects conservation of the essential voltage-sensing structure and mechanism. With this in mind, in Chapter 4 we look at the first crystal structure of KvAP, solved by Youxing Jiang, which shows that the gating charge residues of the S4 segments are located on voltage-sensor paddles, helix-turn-helix structures at the outer perimeter of the channel. The initial structures of KvAP combined with functional studies using Fab fragments, also described in Chapter 4, suggest that the voltage-sensor paddles translate a large distance through the lipid to open the pore. This is quite different from the model of gating shown in Figure 3. To better understand the dynamics of the KvAP channel, we wished to see more structures of the channel. In Chapter 5, I will describe a low-resolution structure of KvAP that I obtained with the help of Alice Lee, crystallized under very different conditions than the first structure of the channel. The low-resolution structure of KvAP described in Chapter 5 strongly supports the idea that the voltage-sensor paddles are very mobile units that lie at the protein-lipid interface. In Chapter 6, I test the hypothesis that the gating charges are carried a large distance through the lipid on voltage-sensor paddle structures, using tethered biotin and avidin as a molecular ruler to measure the membrane depth of residues in the voltage-sensor in the opened and closed channel. In the final chapter, the combined information from the collaborative structure-function studies of KvAP will be synthesized into a conceptual, structure-based model for the

voltage-dependent gating process and considered in the context of the wealth of functional data from studies of eukaryotic Kv channels.

CHAPTER 2: FUNCTIONAL ANALYSIS OF KvAP, AN ARCHEABACTERIAL VOLTAGE-DEPENDENT K^+ CHANNEL

Voltage-dependent ion channels are finely tuned to open and allow ion conduction across the membrane in response to changes in the membrane voltage, a function that lies at the very heart of electrical impulse generation and propagation in excitable cells. Surprisingly, a number of prokaryotic K^+ channels contain amino-acid sequences that appear to encode voltage sensors. In the introductory chapter, I presented an amino-acid sequence comparison of these prokaryotic channels with eukaryotic Kv channels that showed striking conservation of residues in the voltage sensor, including complete conservation of functionally important basic and acidic residues that underlie voltage-dependent gating (Fig. 2b). Are these prokaryotic K^+ channels truly gated by voltage? How similar are the functional properties of these channels to eukaryotic Kv channels responsible for nerve impulses? Until now, essentially nothing has been known about the functional properties of these prokaryotic Kv channels because they cannot easily be studied with the expression systems used for eukaryotic channels. In this chapter, I present the functional characterization

of KvAP, a prokaryotic Kv channel cloned from *Aeropyrum pernix*, a hyperthermophilic archeabacterium isolated from an oceanic thermal vent off the coast of Japan. Although the physiological role of this channel is unknown, I show that it is functionally and structurally very similar to eukaryotic Kv channels.

KvAP channels were expressed in *E. coli*, extracted with decylmaltoside, purified and reconstituted into planar lipid bilayers of 1-palmitoyl-2-oleoyl-phosphatidylglycerol (POPG) and 1-palmitoyl-2-oleoyl-phosphatidylethanolamine (POPE) for functional studies. By controlling the protein to lipid ratio used in the reconstitution we were able to study both single channel and macroscopic current records. KvAP channels have a large conductance—the slope of the single channel current-voltage relationship recorded in solutions containing 150 mM KCl and 10 mM Hepes, pH 7.0 on both sides of the membrane shows a conductance of approximately 170 pS (Fig. 4a,b). The presence of the K^+ channel signature sequence implies that the KvAP pore should be strongly selective for K^+ versus Na^+ ions (Fig. 2b). To examine ion selectivity we measured the reversal potential of macroscopic tail currents in a ten-fold K^+ gradient by substituting 135 mM NaCl for 135 mM KCl in the solution on one side of the membrane (Fig. 4c). The measured reversal potential is -56.5 ± 1.2 mV, which is near the Nernst potential for a perfectly K^+ selective pore at room temperature (21 °C).

How structurally similar is the pore of the KvAP channel to eukaryotic K^+ channel pores? To answer this question we looked for the ability of a small protein toxin from scorpion venom to inhibit the KvAP channel. Venomous animals, like scorpions, exploit the conservation of ion channel structure by producing a toxin that recognizes a structural feature common to an entire family of ion channels[41]. By making many sequence variants of the same basic toxin structure a scorpion can inhibit virtually every member of an ion channel

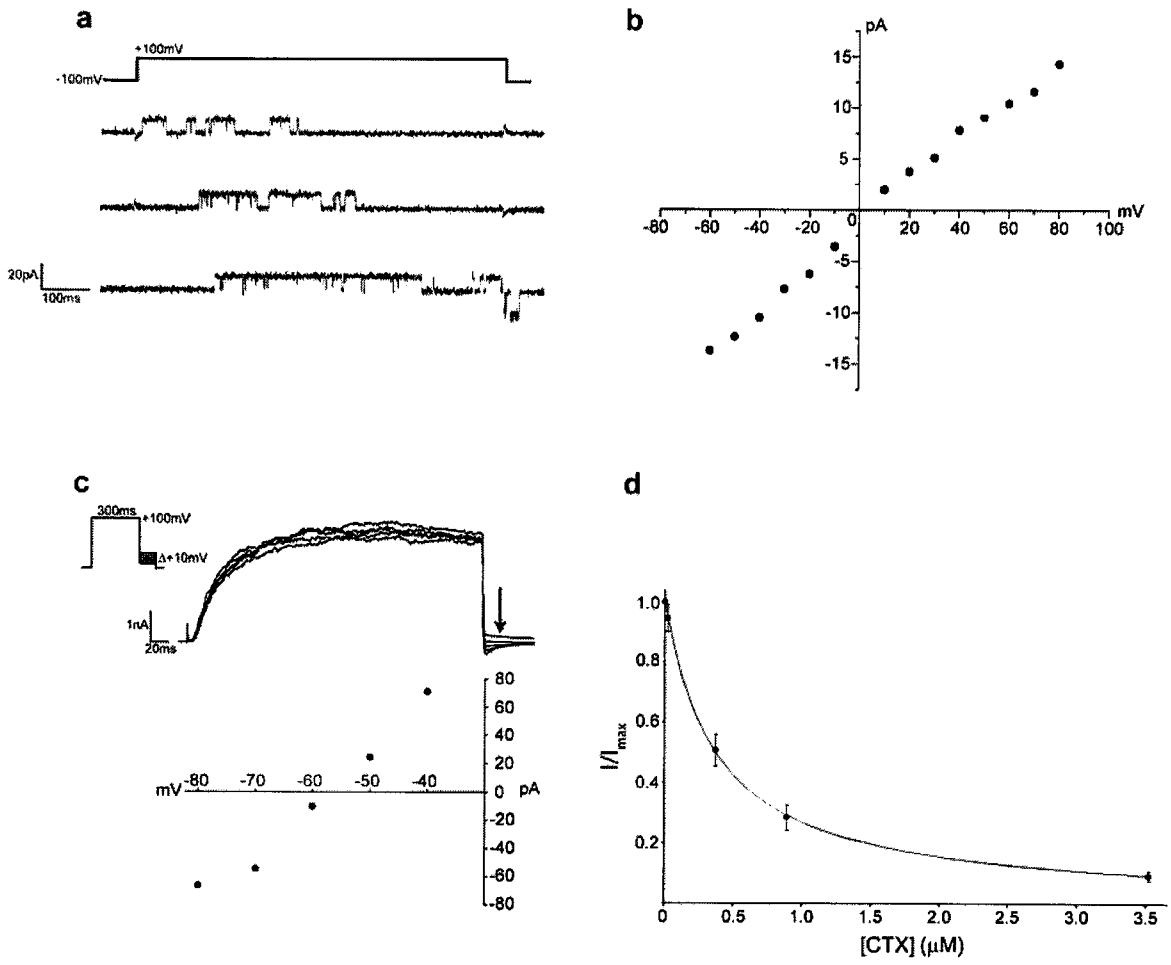

Figure 4

Properties of the KvAP ion pathway. **a,** Single channel traces were recorded at +100 mV in 150 mM KCl, 10 mM Hepes, pH 7.0. **b,** Single-channel current as a function of membrane voltage in above solutions. **c,** Determination of K^+ selectivity. Currents were measured at various test potentials (arrow) after depolarizing to +100 mV in solutions of 150 mM KCl, 10 mM Hepes pH 7.0 inside and 15 mM KCl, 135 mM NaCl, 10 mM Hepes, pH 7.0 outside. Leak and capacitive currents were subtracted by inactivating K^+ channels with a rapid pulse sequence, recording a leak template and subtracting it from traces with active channels. The reversal potential is -56.5± 1.2 mV (n=4). **d,** CTX recognizes a conserved pore structure, fitting like a key in a lock (inset). Fraction of unblocked current (I/Imax) is plotted (mean±SEM) as a function of CTX concentration and fit to $I/Imax = \{1+[CTX]/K_d\}^{-1}$ with a Kd =0.4 μM.

family. The scorpion *Leiurus quinquestriatus hebraeus* specializes in a family of pore-blocking toxins, exemplified by charybdotoxin (CTX), which fit like a key in a lock to the pore entryway of K^+ channels [42,43](Fig, 4d). We find that CTX inhibits the KvAP channel with a Kd of ~0.4 μM. Although the affinity is not very high, we know that single point mutations in the pore of eukaryotic K^+ channels can reduce toxin affinity greater than 1,000-fold[44,45]. The important point is that CTX would not bind to the KvAP channel if its pore were not very similar in structure to that of eukaryotic K^+ channels. Given the high degree of amino acid sequence conservation within the pore, near identity in the three-dimensional structure of the KvAP channel and the *Shaker* channel, for example, is indeed expected (Figure 2b).

Is gating in the KvAP channel voltage-dependent? Data in Figure 5 indicate yes, with qualitative and quantitative properties that are similar to eukaryotic Kv channels. To determine the orientation of channels incorporated into planar lipid bilayers we used CTX, which inhibits by binding only to the extracellular side. We find that KvAP channels open in response to membrane depolarization, that is, when the voltage of the CTX-insensitive (intracellular) side of the membrane is made positive relative to the CTX-sensitive (extracellular) side. Figure 5a shows a representative family of current traces elicited by voltage steps to increasingly positive values from a holding membrane voltage of –100 mV. From such records we evaluated the voltage-dependence of channel opening (Fig. 5b). Data were fit with the Boltzmann equation:

$$\frac{I}{I_{max}} = \frac{1}{1+\exp\left(-\frac{ZF}{RT}\left(V - V_{1/2}\right)\right)} \qquad (1)$$

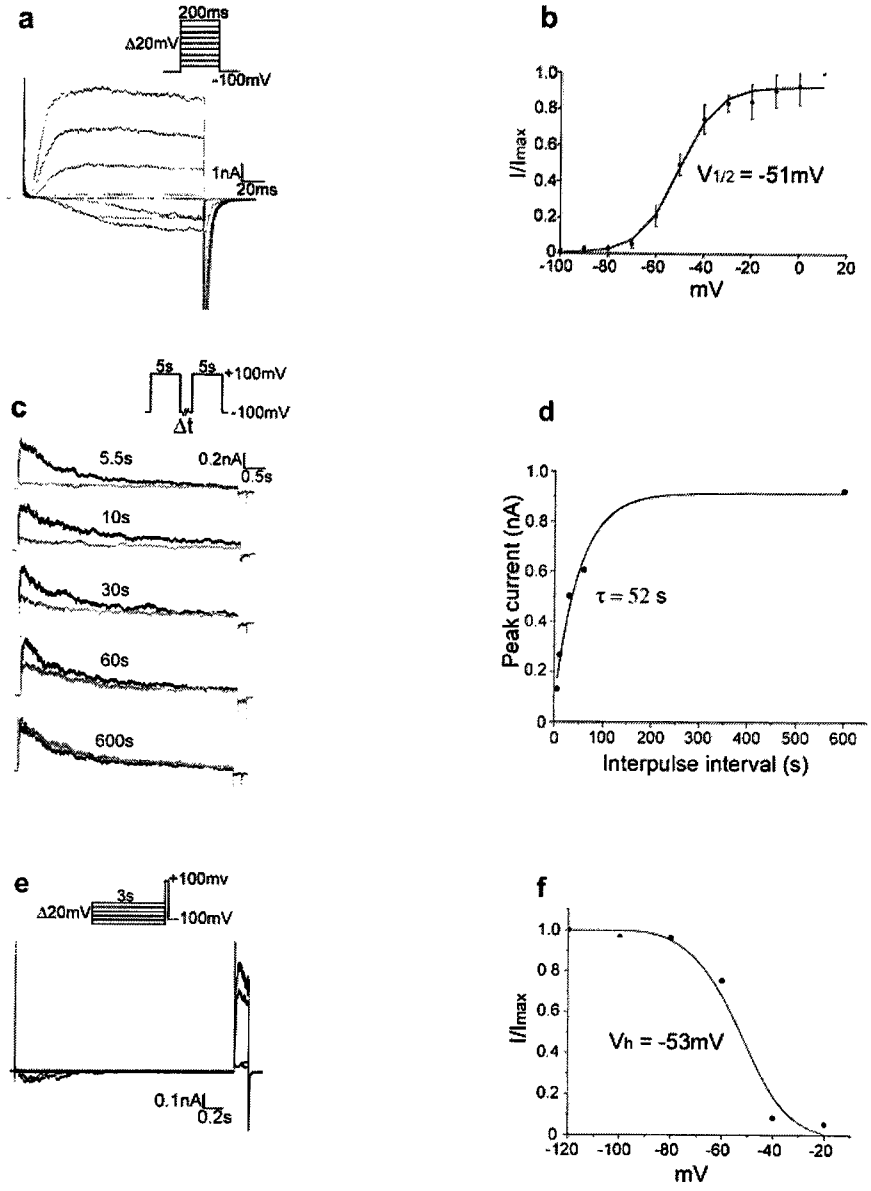

Figure 5

Voltage dependent gating properties. **a,** Channel activation. Currents were recorded during the voltage protocol shown (inset) in the presence of 150 mM KCl. **b,** The voltage activation curve. The fraction of maximal current (I/Imax, mean±SEM, n=6) is graphed as a function of test potential (methods). The smooth curve corresponds to equation 1 with $V_{1/2}$ and Z of –51 mV and 3.2, respectively.**c,** Channel inactivation. Two 5 sec pulses (black first, grey second) to 100 mV are separated by holding at –100 mV for the indicated times. **d,** Fraction of recovery as a function of interpulse duration for currents shown in **c** are fit to a single exponential with time constant 52 sec. **e,** Steady state inactivation. Currents were recorded during the voltage protocol shown (inset) in 150 mM KCl. **f,** Fraction of activatable currents measured in **e** are graphed as a function of holding voltage. The smooth curve is a fit to a two-state Boltzmann equation.

with $V_{1/2}$, the voltage at which the channels have reached 50% of their maximum fraction open, equal to –51 mV and Z, the apparent valence of voltage-dependence, equal to 3.2. We note that the total protein charge moving through the membrane electric field, known as the gating charge, is 12-14 elementary charge equivalents in the *Shaker* K^+ channel[17-19]. But the gating charge should not be confused with Z in the voltage dependence of channel opening, which is around 3.0 for the *Shaker* K^+ channel[46]. KvAP channels are strongly voltage dependent, opening as a function of membrane voltage very much like *Shaker* and other neuronal Kv channels.

Even in many subtle ways the voltage-dependent gating of KvAP is very much like that observed in neuronal Kv channels. For example, the sigmoidal time dependence of opening immediately following depolarization in Figure 5a, thought to reflect multiple transitions along the reaction pathway to opening, looks quite like *Shaker* K^+ channels and Kv channels in squid axons that underlie the Hodgkin-Huxley theory of the action potential[47,48]. The main obvious distinction is the slow over all rates at which KvAP channels open and close. But KvAP is derived from an organism that thrives at temperatures near 95° C and here we are studying the channel's properties at room temperature.

Another aspect of gating in many eukaryotic Kv channels is a phenomenon called inactivation, referring to spontaneous pore closure during sustained membrane depolarization. KvAP channels also exhibit inactivation, as evidenced by the gradual reduction in the current (50% decay in ~800 ms at +100 mV) during long depolarizing steps (Fig. 5c), and slow recovery from inactivation after returning the membrane to its holding voltage (50% in 35 s, 90% in 120 s) (Fig. 5c,d). The fraction of channels that become inactivated as a function of the membrane voltage follows a Boltzmann equation (Fig. 5e, f).

This voltage dependence of 'steady state inactivation' as it is called, is similar to that observed in many eukaryotic Kv channels.

In eukaryotic Kv channels two varieties of inactivation have been described, N-type in which the cytoplasmic N-terminus occludes the pore after the voltage-dependent gate opens[49], and C-type which is less well understood[50]. We do not yet know which mechanism is operating in KvAP, but suspect it is C-type. The important point we wish to make, however, is that voltage-dependent activation and inactivation in the KvAP channel is phenomenologically very similar to what has been observed in eukaryotic Kv channels studied by electrophysiologists for decades.

Do the voltage-dependent gating properties of the KvAP channel arise from a structurally conserved voltage sensor that is shared by prokaryotic and eukaryotic Kv channels? The amino acid sequence conservation argues unequivocally yes (Fig. 2b). But just how conserved is it? If the voltage sensor is conserved to the extent of the K^+ selective pore, then natural toxins intended to inhibit eukaryotic voltage sensors might cross-react with KvAP, just as CTX cross-reacts with the pore. We tested this possibility using venom from the Chilean Rose Tarantula, *Grammostola spatulata*. This venom contains toxins such as hanatoxin and other structurally related proteins that inhibit eukaryotic voltage-dependent ion channels by binding to their voltage sensor[51-53]. Upon addition of a 1:1000 dilution of the whole venom to the extracellular side of the membrane we observed inhibition of KvAP currents elicited by a +120 mV depolarizing step (Fig. 6a). Next, to isolate and identify active components we fractionated the venom by reversed-phase HPLC and tested individual peaks for activity. Several toxins of different masses reproduced the inhibitory effect of the total venom. We focused on one of these, which we call voltage-sensor toxin 1 (VSTX1). VSTX1

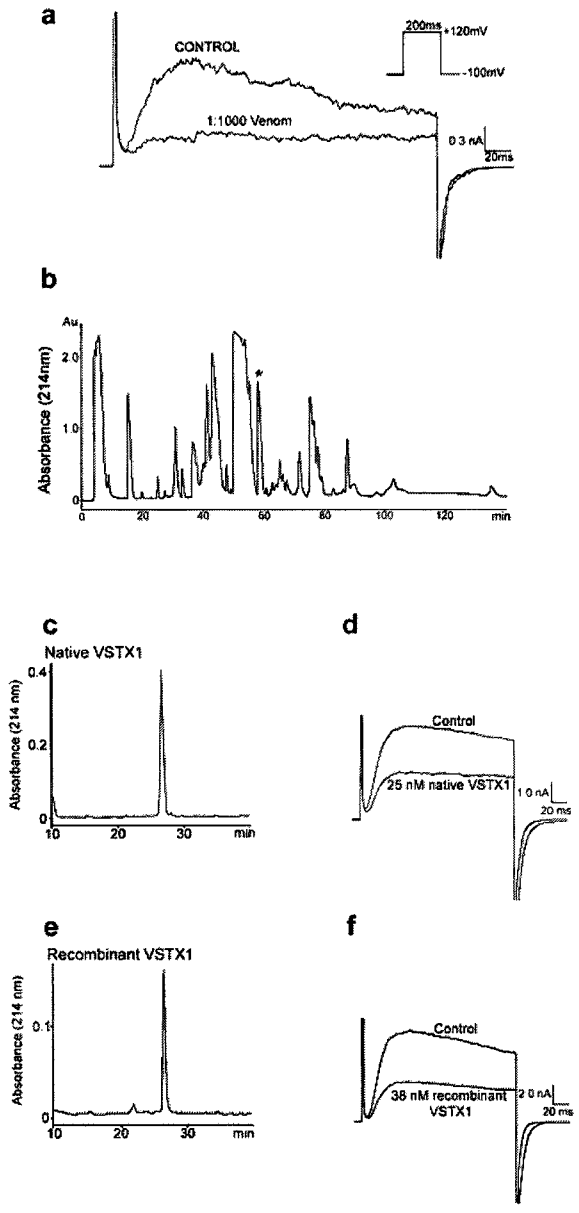

Figure 6

Inhibition by *Grammostola Spatulata* toxins. **a,** A 1:1000 dilution of spider venom inhibits currents elicited by depolarization to +120 mV. **b,** Reverse-phase HPLC chromatogram of venom showing the fraction with VSTX1 (asterix). **c,** VSTX1 is purified to homogeneity by a second HPLC run (methods). **d,** Effect of ~25 nM native purified VSTX1 on the KvAP channel-currents elicited by depolarization to +100 mV, 60 minutes after toxin addition **e,** Reverse-phase HPLC chromatogram of recombinantly expressed VSTX1 following cleavage from purified GST-fusion protein run under the same HPLC conditions as the native toxin shown in **c.** The majority of recombinant VSTX1 elutes with the same retention time as the native toxin. **f,** Recombinant VSTX1 effectively inhibits KvAP channels.

can be purified to homogeneity by two successive HPLC gradients (Fig. 6b,c). This toxin inhibits the KvAP channel with very slow apparent binding kinetics, a characteristic of other voltage-sensor toxins[51,53]. The slow kinetics makes it difficult to reach equilibrium with sub-saturating concentrations before the membrane breaks, but more than half inhibition was achieved after 60 minutes of periodic membrane depolarizing steps in the presence of 25 nanomolar VSTX1 (Fig. 6d). Therefore, VSTX1 likely inhibits KvAP with at least low nanomolar affinity.

For functional assays, VSTX1 was purified from whole venom to a single peak on HPLC of a single mass (Fig. 6c). However this is not a rigorous demonstration that we have correctly isolated the inhibitory component from whole venom that affects KvAP channel function. It is possible that a co-purifying inhibitory contaminant might be present, but below the detection limit. In order to verify that VSTX1 is responsible for inhibition of KvAP channel function, we produced a recombinant version of the toxin. The amino acid sequence of VSTX1 was determined through a combination of N-terminal sequence analysis and MALDI-TOF mass spectrometry. We could then generate a synthetic gene encoding the toxin. Recombinant VSTX1 was expressed as a GST-fusion protein in *E.coli* with an N-terminal thrombin protease recognition site. The recombinant toxin was cleaved from the purified fusion protein and the cleavage reaction then run on HPLC. Figure 6e shows that the majority of recombinant VTSX1 elutes as a single peak with the same retention time as the native toxin despite the addition of two N-terminal residues (glycine and serine) due to the remnant of the thrombin protease site. This peak corresponds to the correctly folded, functionally active toxin—38 nM recombinant VSTX1inhibits KvAP channel function in

```
VSTX1   : -ECGKFMWKCKNSND-CCKDLV-CSSRWKW--CVLASPF- : 34
VSTX2   : -YCQKWMWTCDEERK-CCEGLV-CRLW-----CKKKIEEG : 32
VSTX3   : -DCLGWFKGCDPDNDKCCEGYK-CNRRDKW--CKYKLW-- : 34
GSMTX4  : -GCLEFWWKCNPNDDKCCRPKLKCSKLFKL--CNFSF--- : 34
HATX1   : -ECRYLFGGCKTTSD-CCKHLG-CKFRDKY--CAWDFTFS : 35
HATX2   : -ECRYLFGGCKTTAD-CCKHLG-CKFRDKY--CAWDFTFS : 35
SGTX1   : -TCRYLFGGCKTTAD-CCKHLA-CRSDGKY--CAWDGTF- : 34
GRTX    : -DCVRFWGKCSQTSD-CCPHLA-CKSKWPRNICVWDGSV- : 36
PROTX1  : -ECRYWLGGCSAGQT-CCKHLV-CSRRHGW--CVWDGTFS : 35
PROTX2  : -YCQKWMWTCDSERK-CCEGMV-CRLW-----CKKKLW-- : 30
PATX1   : -YCQKWMWTCDSARK-CCEGLV-CRLW-----CKKII--- : 29
PATX2   : -YCQKWMWTCDEERK-CCEGLV-CRLW-----CKRIINM- : 31
HPTX1   : -DCGTIWHYCGTDQSECCEGWK-CSRQL----CKYVIDW- : 33
HPTX2   : DDCGKLFSGCDTNAD-CCEGYV-CRLW-----CKLDW--- : 30
HPTX3   : -ECGTLFSGCSTHAD-CCEGFI-CKLW-----CRYERTW- : 31
```

Figure 7
Sequence comparison of toxins that bind to KvAP with previously identified tarantula voltage-sensor toxins. Cysteines that determine the tarantula toxin fold are highlighted in gray. Tarantula toxins: VSTX1,VSTX2 and VSTX3, voltage-sensor toxins, *Grammostola Spatulata*; GsMTX4, *Grammostola* mechanotoxin #4[54], *Grammostola Spatulata,* HATX1 and HATX2, Hanatoxins[55], *Grammostola Spatulata*, SGTX1[56], *Scodra griseipes*, GRTX, Grammotoxin[53], *Grammostola Spatulata*; PROTX1 and PROTX2[57], *Thrixopelma pruriens* PATX1 and PATX2, Phrixotoxins[58], *Phrixotrichus auratus*; HPTX1, HPTX2 and HPTX3, Heteropodatoxins[59], *Heteropoda venatoria*.

membranes by slightly more than 50% (Fig. 6f). We can conclude that VSTX1 is a high-affinity inhibitor of the KvAP channel.

Figure 7 shows that VSTX1 is related to hanatoxin and other voltage-sensor toxins from tarantula venoms. The most conserved element of these toxins is the six cysteines that form three disulfide bonds and thus define their rigid three-dimensional structure, a structure that has evolved to recognize and bind to the voltage sensor. It is worth noting that some of these toxins promiscuously react with the voltage sensors of eukaryotic voltage-dependent K^+, Ca^{2+}, and Na^+ channels, underscoring the structural conservation of the voltage sensor in channels whose pores have diverged to allow different cation selectivity[57,60]. It is clear that the KvAP channel, with its sensitivity to tarantula toxins, will be a basic structural model for all members of the voltage-dependent cation channel family (K^+, Na^+ and Ca^{2+} channels.)

In this chapter, we have shown that the KvAP channel is very similar to eukaryotic Kv channels in both its functional and structural properties. The voltage dependence of KvAP channel opening is essentially the same as in eukaryotic Kv channels. The evidence that KvAP is structurally the same as its eukaryotic counterparts is based on amino acid sequence conservation and molecular recognition by inhibitors of both the pore and the voltage sensor. There is no evolutionary pressure for a tarantula native to the dry scrublands of Chile or a scorpion from the deserts of the Middle East to recognize receptor sites on a Kv channel from an archeabacteria that lives near an oceanic thermal vent off the coast of Japan. The specific protein-protein interactions described here, which transcend geographic and traditional evolutionary boundaries, speak to the existence of highly conserved molecular structures underlying both ion selectivity and voltage-dependent gating in Kv channels throughout nature.

CHAPTER 3: LOCALIZATION OF THE TARANTULA VOLTAGE-SENSOR TOXIN RECEPTOR ON KvAP

The activity of voltage-dependent cation channels is essential to the rapid, long range electrical signaling of the nervous system[1]. Given the absolutely critical physiological role of this family of channels, it is no surprise that a variety of venomous animals from scorpions to spiders to snakes cripple their prey with selective, high-affinity protein toxins that inhibit voltage-dependent channel function. All protein toxins known to inhibit voltage-dependent cation channels can be classified into two groups based on the manner in which they impair channel function. Pore-blocker toxins bind to a conserved structural surface at the extracellular entryway of the pore and inhibit the function of the channel by physically occluding the ion conduction pathway[42,43,61-66]. Voltage-sensor toxins bind to a separate conserved receptor on the channel, affecting the gating motions of the voltage-sensor domains and altering the energetics of the voltage-dependent gating process[51-53,55,60,67-72]. Voltage-sensor toxins and pore-blocking toxins have spatially distinct receptors and can co-occupy a single voltage-dependent channel[52].

What structural features of a voltage-dependent channel do voltage-sensor toxins recognize? Only one toxin-channel interface has been thoroughly investigated. Hanatoxin, a well-characterized voltage-sensor toxin isolated from the venom of the Chilean Rose tarantula, *Grammostola spatulata*, inhibits Kv2.1 channel function with 10 to 100 nanomolar affinity[55]. Extensive mutagenesis has been carried out on the Kv2.1 channel in search of the full determinants of the hanatoxin receptor. The results of this mutational scan, that included all residues of the voltage sensor and peripheral regions of the pore, show that only three residues on the C-terminal portion of the S3 segment (I273, F274 and E277 on S3, Figure 8) appear to dominate the energetics of the toxin-channel interaction—all other residues investigated have negligible contributions[52,73]. This result, although surprising considering that the dimensions of a face of hanatoxin (~20 Å x 25 Å) and relatively high-affinity inhibition imply a larger channel interface[55,74], suggests that this family of toxins binds to a very localized receptor on the channel. Less is known about other voltage-sensor toxin-channel interfaces. However, the S3 segment appears to form a common target for a number of structurally diverse voltage-sensor toxin families isolated from other venomous animals including sea anemones, scorpions, and wasps. Mutations at nearly equivalent positions on the S3 segment of different voltage-dependent cation channels (residues highlighted in blue in Figure 8b) markedly reduce the affinity of tarantula toxins for a K_v channel[52,60], a funnel-web spider toxin for a Ca_v channel[74] and sea anenome, alpha-scorpion, beta-scorpion, and wasp toxins for a Na_v channel[75-77].

In this chapter we investigate the location of the tarantula toxin receptor on the KvAP channel using a biochemical assay that exploits the modular nature of Kv channels. Studies by Lu *et al.* indicated that the voltage-sensor domain is effectively a gating module because

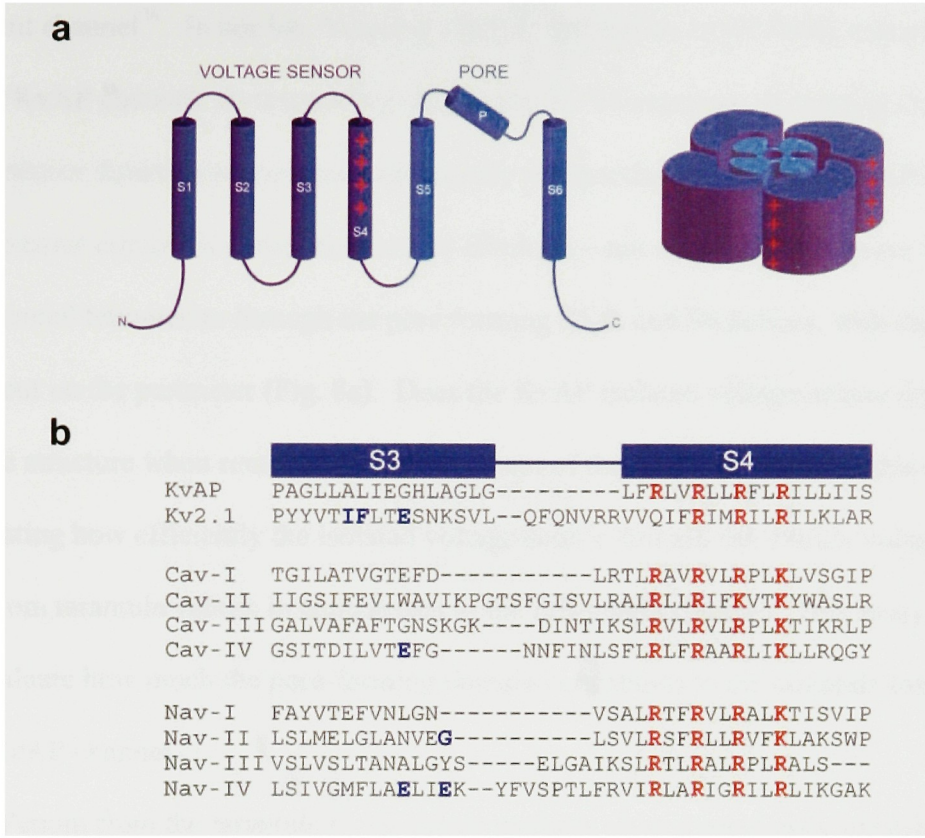

Figure 8

A conserved target for diverse voltage-sensor toxins in voltage-dependent K^+,Na^+ and Ca^{2+} channels. **a,** Topology of a single Kv channel subunit or Cav and Nav channel homologous repeat consists of six hydrophobic segments (S1-S6)—the S1-S4 segments form the voltage-sensor domain and the S5-S6 segments contribute to the pore. Four subunits or repeats assemble to form a central ion conduction pore surrounded by four voltage-sensor domains. **b,** Sequence comparison of a conserved interaction site for voltage-sensor toxins in the voltage-sensor domain. Sequence of the S3-S4 segments from a KvAP channel subunit, a Kv2.1 channel subunit, and the four homologous repeats from αIA-Cav and brain type II-Nav channels are aligned. Gating charge residues are highlighted in red. Residues in S3 highlighted blue alter the channel's affinity for voltage-sensor toxins when mutated. Mutations of I273, F274 and E277 of Kv2.1 decrease the channel's affinity for tarantula toxins, E1658 of the αIA Cav channel decreases the channel's affinity for a funnel-web spider toxin, and G845, E1613, and E1616 of the brain type II Nav channel decrease the channel's affinity for a β-scorpion toxin, sea-anenome and the α-scorpion toxins, and a wasp toxin respectively.

they could graft the *Shaker* voltage sensor onto the KcsA pore to form a functional voltage-dependent channel[78]. In our lab, Youxing Jiang found that he could stably express and purify a partial KvAP channel, corresponding only to the S1-S4 segments, indicating that the voltage-sensor domain can exist as a structurally independent entity. The KvAP isolated voltage-sensor domain is a monomer on gel-filtration—not surprisingly because the subunits of K^+ channel tetramerize through the pore forming S5,P, and S6 helices, with the S1-S4 located out on the perimeter (Fig. 8a). Does the KvAP isolated voltage-sensor domain retain its native structure when removed from the context of the pore? We address this question by investigating how efficiently the isolated voltage-sensor domain can extract voltage-sensor toxins from tarantula venom in comparison to the full-length channel. This assay also allows us to evaluate how much the pore-forming domain contributes to the tarantula toxin receptor on the KvAP channel.

Venom from the tarantula *G. spatulata* contains several previously identified voltage-sensor toxins including hanatoxin. The venom is a rich mixture of dozens of toxins in the ~3.5-5.0 kDa range. Which of these toxins recognize a receptor on KvAP? Figure 9 shows the strategy we used to screen for interacting toxins. Briefly, we generated small affinity columns containing Co^{2+} resin saturated with either purified isolated voltage-sensor domain or full-length channel bound to the resin through a hexahistidine C-terminal tag. We ran diluted whole venom over these two columns or a control column that contained only Co^{2+} resin and no bound protein. After the columns were washed to minimize non-specific interactions, the channel proteins and the bound toxins were eluted with imidazole and reduced with DTT to improve separation by reverse-phase HPLC. Parts a,b and c of Figure 10 compare the retention profiles obtained when equal volumes of the reduced eluate are run

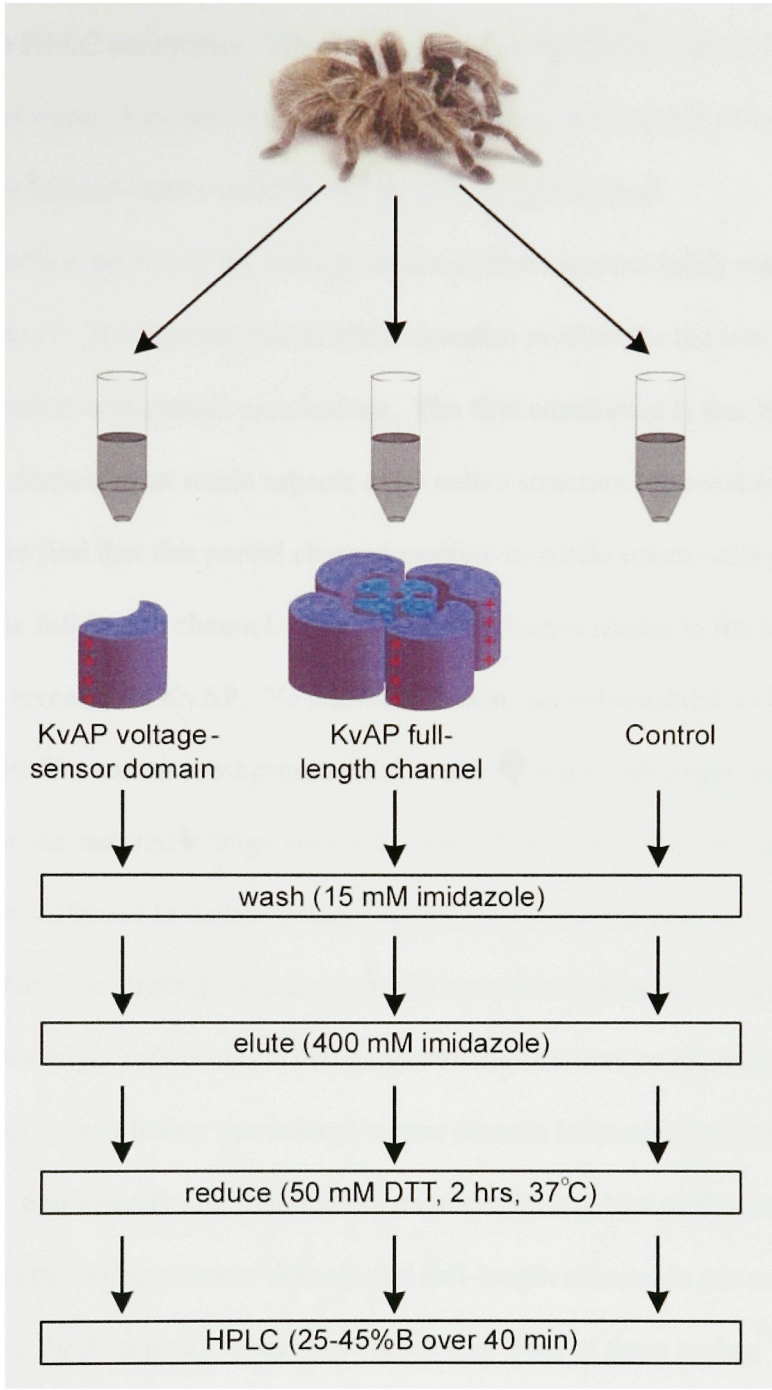

Figure 9

Experimental strategy used to isolate tarantula toxins from whole venom that specifically bind to the KvAP voltage-sensor domain and full-length channel. Venom is applied to Co^{2+} resin columns saturated with either KvAP voltage-sensor domain or full-length channel or a control column that contains Co^{2+} resin alone. After washing to minimize non-specific interactions, the bound protein is eluted, chemically reduced and analyzed by analytical reverse-phase HPLC.

under the same HPLC conditions. The Co^{2+} resin non-specifically retains some toxins but this background signal does not obscure the identification of a number of toxin peaks that bind only to the voltage-sensor domain and the full-length channel.

The retention profile of the voltage-sensor domain is remarkably similar to that of the full-length channel. The equivalence of toxin retention profiles for the two channel proteins allows us to reach two important conclusions. The first conclusion is that the isolated voltage-sensor domain must retain aspects of its native structure removed from its native context since we find that this partial channel purifies tarantula toxins with the same efficiency as the full-length channel. The second conclusion relates to the location of the tarantula toxin receptor on KvAP. No additional toxins are retained due to the presence of the pore domain. The toxins most prominently retained by the full-length channel are equally well retained by the isolated voltage-sensor domain. This argues that the voltage-sensor domain alone is sufficient to isolate voltage-sensor toxins and the pore does not contribute to the toxin receptor. The slight differences in toxin retention that are seen between the two retention profiles might reflect subtle differences in the structure or exposure of the toxin receptor depending on whether the voltage-sensor domain is attached to the pore.

We chose to identify and functionally characterize a subset of the toxins specifically retained by both the voltage-sensor domain and full-length channel in our assay, corresponding to the four peaks labeled in Figure 10a. Two of these toxins, VSTX1 and GSMTX4, have been previously isolated and identified. Two other prominently retained toxins, VSTX2 and VSTX3, were sequenced through a combination of Edman sequencing and tandem mass spectrometry analysis of proteolytic fragments.

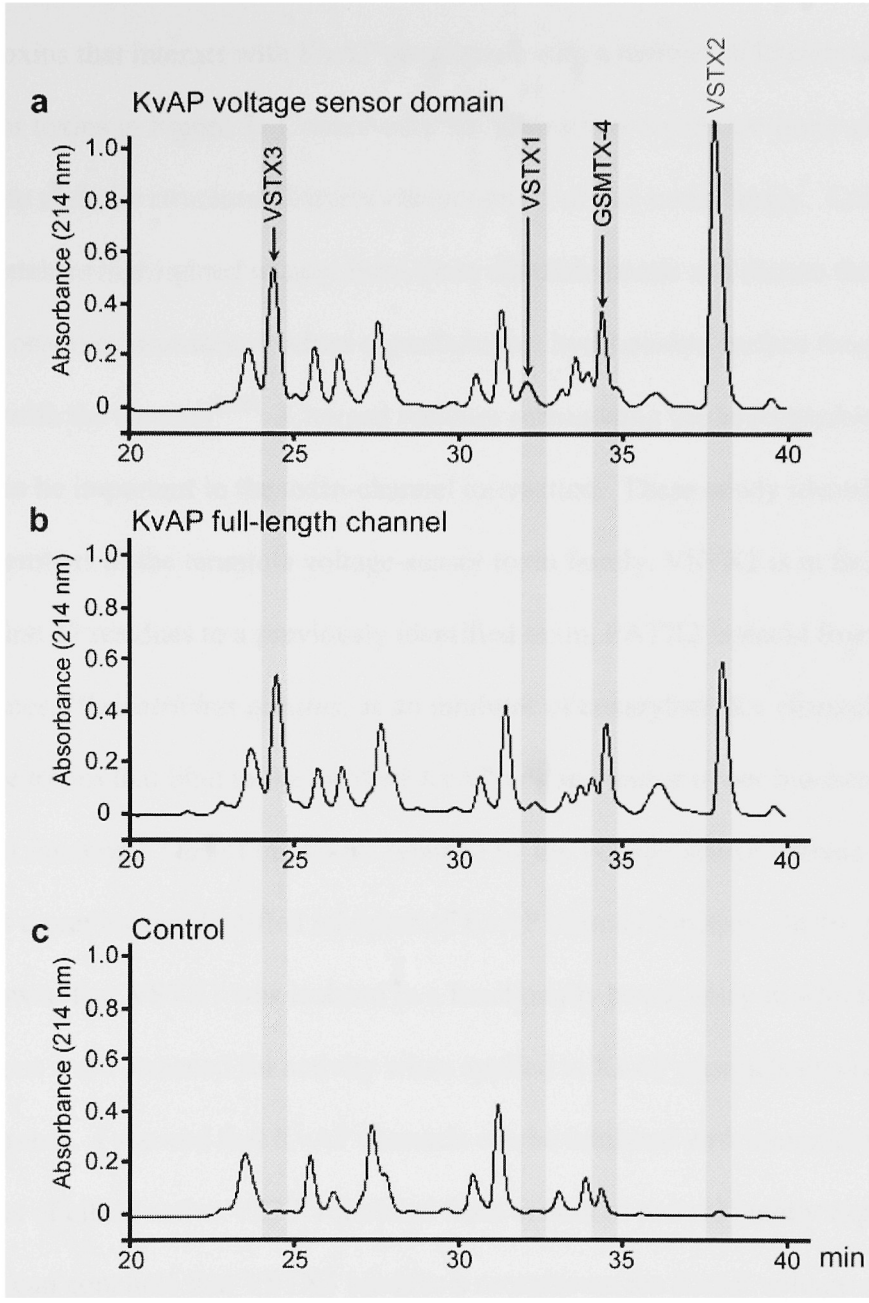

Figure 10

Comparison of the tarantula toxins purified from whole venom by the KvAP voltage-sensor domain and the KvAP full-length channel. Analytical reverse-phase HPLC chromatograms of toxins retained by a KvAP voltage-sensor domain affinity column **(a)** a full-length KvAP channel affinity column **(b)** and a resin only control column **(c)** shows that the channel proteins specifically retain a number of tarantula voltage-sensor toxins. Bound toxins were chemically reduced to enhance separation on a 25-45%B acetonitrile/ H2O linear gradient over 40 minutes. See materials and methods for details on mobile and stationary phase composition. The gray bars highlight toxins that bind only to the channel proteins and were identified and characterized further in this study.

The toxins that interact with KvAP are aligned with a number of known tarantula voltage-sensor toxins in Figure 7. Conserved within these new toxins are many of the amino acids known to underlie structural features characteristic of this toxin family. Completely conserved cysteines highlighted in gray form three disulfide bonds and dictate the toxin fold[74,79-81]. Conserved aromatic residues contribute to a hydrophobic surface thought to form the interface with the channel[82,83]. Charged residues surrounding the hydrophobic surface are also thought to be important in the toxin-channel interaction. These newly identified toxins are clearly members of the tarantula voltage-sensor toxin family. VSTX2 is in fact identical through the first 27 residues to a previously identified toxin, PATX2 isolated from a related tarantula species, *Phrixotrichus auratus*, as an inhibitor of eukarytotic Kv channels[84].

Do the toxins that bind to the purified KvAP voltage sensor in our biochemical assay affect channel function? One of the toxins retained by the voltage-sensor domain we recognized as a previously identified inhibitor of KvAP channel function. In the previous chapter, I showed that VSTX1 was isolated in a functionally based assay in which individual venom fractions were screened for activity when applied to KvAP channels reconstituted into planar membranes. I showed that KvAP channels can be inhibited with nanomolar concentrations of either native VSTX1 purified from venom or recombinantly expressed VTSX1. We can conclude that VSTX1 binds to a receptor on the KvAP voltage-sensor domain and consequently affects channel gating.

VSTX3 is a second functionally active toxin that is selectively retained by the purified voltage-sensor domain and full-length channel in our biochemical assay. In its reduced form (Fig. 10a,b) VSTX3 elutes as a single symmetric peak. However in its native folded form, VSTX3 has an unusually broad elution profile (Fig. 11a) that hindered our

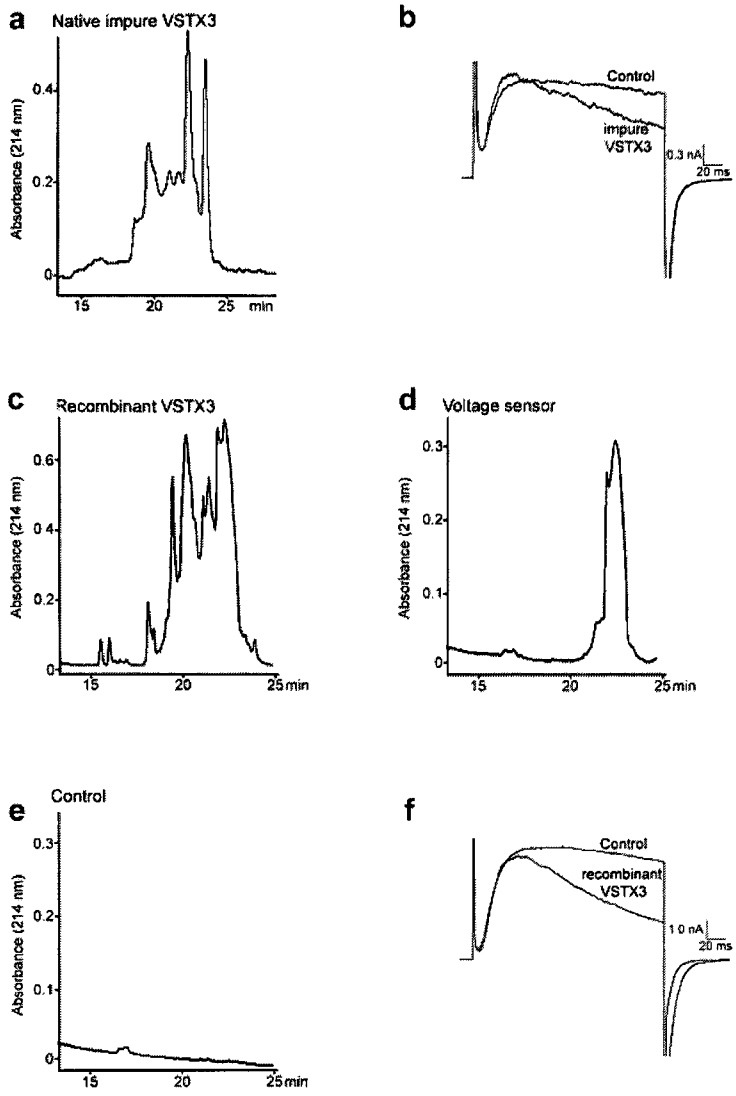

Figure 11

Native and recombinant forms of VSTX3 alter KvAP channel kinetics. **a,** Reverse-phase HPLC chromatogram of an impure fraction of VSTX3 from venom used for functional experiments. **b,** Venom fractions containing VSTX3 alter the kinetics of KvAP channel gating. **c,** Reverse-phase HPLC chromatogram of recombinantly expressed VSTX3 following cleavage from purified GST-fusion protein. Toxin peaks eluting between 18-24 minutes have the correct mass for recombinant VSTX3 and presumably correspond to different toxin folds. **d,** The KvAP voltage-sensor domain purifies the correct fold of recombinant VSTX3. Recombinant VSTX3 fractions were pooled together and passed over a column of Co^{2+} resin saturated with purified KvAP voltage-sensor domain (**d**) or a control column of only Co^{2+} resin (**e**). Toxins retained by the two columns were analyzed by analytical reverse-phase HPLC run under the same conditions as the HPLC chromatogram shown in (**e**). **f,** Recombinant VSTX3 fractions purified by the KvAP voltage-sensor domain alter the function of reconstituted KvAP channels.

ability to isolate it away from co-purifying toxin contaminants. A fraction containing VSTX3 and three other toxins when applied to the extracellular side of the membrane has an interesting effect on KvAP channel function, different from what is seen with VSTX1. Impure VSTX3 alters the gating kinetics of KvAP—speeding the rate of activation and inactivation (Fig.11b).

To further investigate the function of VSTX3, and conclusively determine whether it is responsible for the observed change in gating kinetics, we expressed this toxin recombinantly using the same strategy used to produce functional VSTX1. Recombinant VSTX3 was expressed as a GST fusion protein in *E. coli* with an N-terminal thrombin protease recognition site. The thrombin cleavage of VSTX3 from the purified fusion protein yielded multiple peaks on HPLC, most with the correct mass for the recombinant toxin. These peaks presumably represent different possible toxin folds with different disulfide connectivity (Fig. 11c). We reasoned that only the correctly folded toxins would effectively interact with their receptor on the voltage-sensor domain and that we might be able to purify the correctly folded toxin away from misfolded versions using a voltage-sensor domain affinity column. We pooled together HPLC fractions of recombinant VSTX3 with the correct mass and applied them to a column of Co^{2+} resin saturated with purified voltage-sensor domain or, as a control, Co^{2+} resin without any bound protein. After washing, we eluted the bound protein from the two columns with imidazole and ran equal volumes of the eluate, without chemical reduction, on the same HPLC gradient. Passage of recombinant VSTX3 over the voltage-sensor domain column has partially purified the recombinant toxin (Fig.11d), which does not adhere to the Co^{2+} resin control (Fig. 11e). We cannot explain why affinity-purified, recombinant VSTX3 shows a multiple-peaked broad chromatographic

profile—although it is reminiscent of the elution of the native toxin. Some degree of conformational heterogeneity might be characteristic of certain tarantula voltage-sensor toxins—native hanatoxin for example, displays a less severe form of heterogeneity that gives rise to two chromatographically separated peaks in equilibrium[55]. Nevertheless, the fraction of recombinant VSTX3 selectively retained by the voltage-sensor domain was then applied to KvAP channels in membranes to test for functional activity. Figure 11f shows that this fraction changes the kinetics of channel activation and inactivation in a very similar manner to what is seen with impure native VSTX3.

The two remaining toxins identified through their physical interaction with the purified KvAP voltage-sensor domain show negligible effects on channel function. VSTX2 is the most abundant toxin of this family in the *G. spatulata* venom (data not shown). Purified native VSTX2 inhibits KvAP with at best only weak affinity—20 μM VSTX2 appears to inhibit currents by about 30% (Fig. 12a,b). However, at such high concentrations of a toxin purified from whole venom there is a distinct possibility that the low level inhibition we see is due to a small amount of a higher affinity inhibitory contaminant. GSMTX4 was previously isolated as a low affinity inhibitor of stretch activated channels in astrocytes[54]. Purified GSMTX4 appears to have no effect on the KvAP channel even at micromolar concentrations (Fig. 12 c,d).

If these toxins bind to the voltage-sensor domains, why do we not see a functional consequence of this interaction on KvAP channels in the membrane? One possibility is that the toxins bind to the KvAP voltage sensors in the membrane but do not affect channel function. Another possibility is that they are unable to access their receptor when the channel is immersed in the lipid bilayer. Alternatively, some toxins, like VSTX2, might bind to the

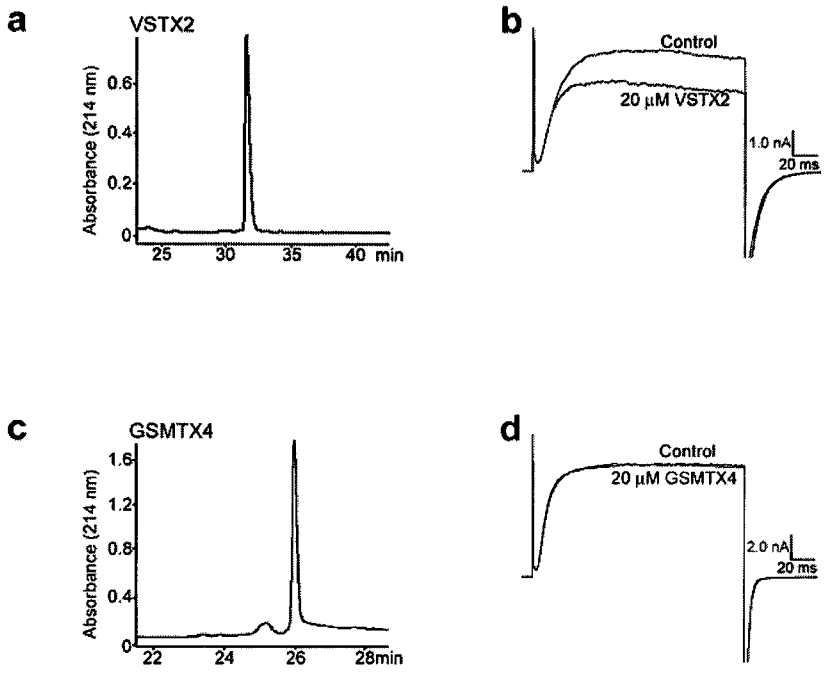

Figure 12

Some voltage-sensor toxins that bind the KvAP voltage-sensor domain do not strongly affect the function of KvAP channels. **a,** VSTX2 can be purified from whole venom with two successive reverse-phase HPLC gradients. The chromatogram of the second HPLC purification step is shown. **b,** Effect of VSTX2 on reconstituted KvAP channels. KvAP channel currents elicited by depolarization to +100 mV in the absence (control) and in the presence of 20 μM VSTX2. **c,** Purification of GSMTX4 from venom. **d,** 20 μM GSMTX4 has no affect on KvAP channel function. Traces of KvAP currents elicited by depolarization to +100 mV in the absence and presence of GSMTX4 are superimposed.

purified voltage-sensor domain with extremely low affinity and are retained in our biochemical assay by virtue of their sheer abundance in the venom. This is a more likely explanation in light of recent evidence that VSTX1 partitions into the membrane and has, in fact, low intrinsic affinity for the purified KvAP channel in the absence of the lipid bilayer[83].

In this chapter I have shown that the determinants for tarantula voltage-sensor toxin binding are contained exclusively within the voltage-sensor domain. The pore and its exterior walls do not appear to contribute to toxin specificity. This conclusion is consistent with functional studies of eukaryotic voltage-dependent Kv channels that suggest a four-to-one stoichiometry (four toxins per channel or one toxin per voltage sensor)[52] and with mutational studies that point to a very localized region of the channel for toxin binding, limited to the S3 segment of the voltage sensor.

Only two of the four toxins that are retained by both the purified voltage-sensor domain and the full-length channel in our assay affect the function of KvAP channels in membranes. Clearly the tarantula toxins interact with the purified voltage-sensor domain with some specificity otherwise we would have seen non-specific selection of toxins by the pore domain which provides an additional potential interaction surface for the toxins. Instead we find that the same toxin retention profile is obtained for both the KvAP voltage-sensor domain alone and for the full-length channel. Moreover, we are able to purify the correctly folded, functionally active form of recombinant VSTX3 through its affinity for the voltage-sensor domain, implying that the voltage-sensor domain specifically selects for toxins with the correct fold and the correct three-dimensional shape.

The fact that the voltage-sensor domain can purify a mixture of functional and non-functional toxins likely reflects that the toxin-channel interaction increasingly appears to be

quite complex and presently not well understood. Recent work has shown that VSTX1 has intrinsically low affinity for purified KvAP channels and much of the binding energy of the toxin-channel interaction comes from the toxin's interaction with lipid membranes[83]. Our selection for interacting toxins using purified channel protein thus necessarily lacks an important component of the system that these toxins have evolved to target—the lipid bilayer. Our assay might therefore capture only relatively weak interactions and may select for toxins with greater abundance in the spider venom. Despite these limitations in our experimental system and our incomplete understanding of how voltage-sensor toxins bind to and inhibit voltage-dependent cation channels, we are able to show that the determinants for tarantula voltage-sensor toxin binding reside exclusively in the voltage-sensor domain.

CHAPTER 4: CRYSTAL STRUCTURE OF THE KvAP-FAB COMPLEX

The preceding chapters have shown that the prokaryotic KvAP channel possesses all the functional attributes of classic neuronal Kv channels. This conservation of function reflects structural conservation in the voltage sensor as revealed by specific interactions with tarantula venom toxins that have evolved to bind to the voltage sensors of eukaryotic Kv channels. Thus the conservation of amino-acid sequence, functional characteristics and pharmacological properties all suggest that KvAP can serve as a basic structural model for eukaryotic Kv channels like the *Shaker* channel (Fig. 13a).

After an intense five-year effort, Youxing Jiang with the help of Alice Lee and Jiayun Chen, solved a crystal structure of KvAP and provided the first image of a Kv channel's fundamental architecture. This structure was an especially technically challenging crystallographic feat due to the fact that the voltage sensor is intrinsically flexible—a property required for a domain that undergoes voltage-dependent rearrangements within the membrane but one that hinders crystal formation. In order to coax the KvAP channel to crystallize, Jiang et al., raised monoclonal antibodies against the channel and selected for those that bound to the voltage-sensor domain. They reasoned that if they could "hold" the

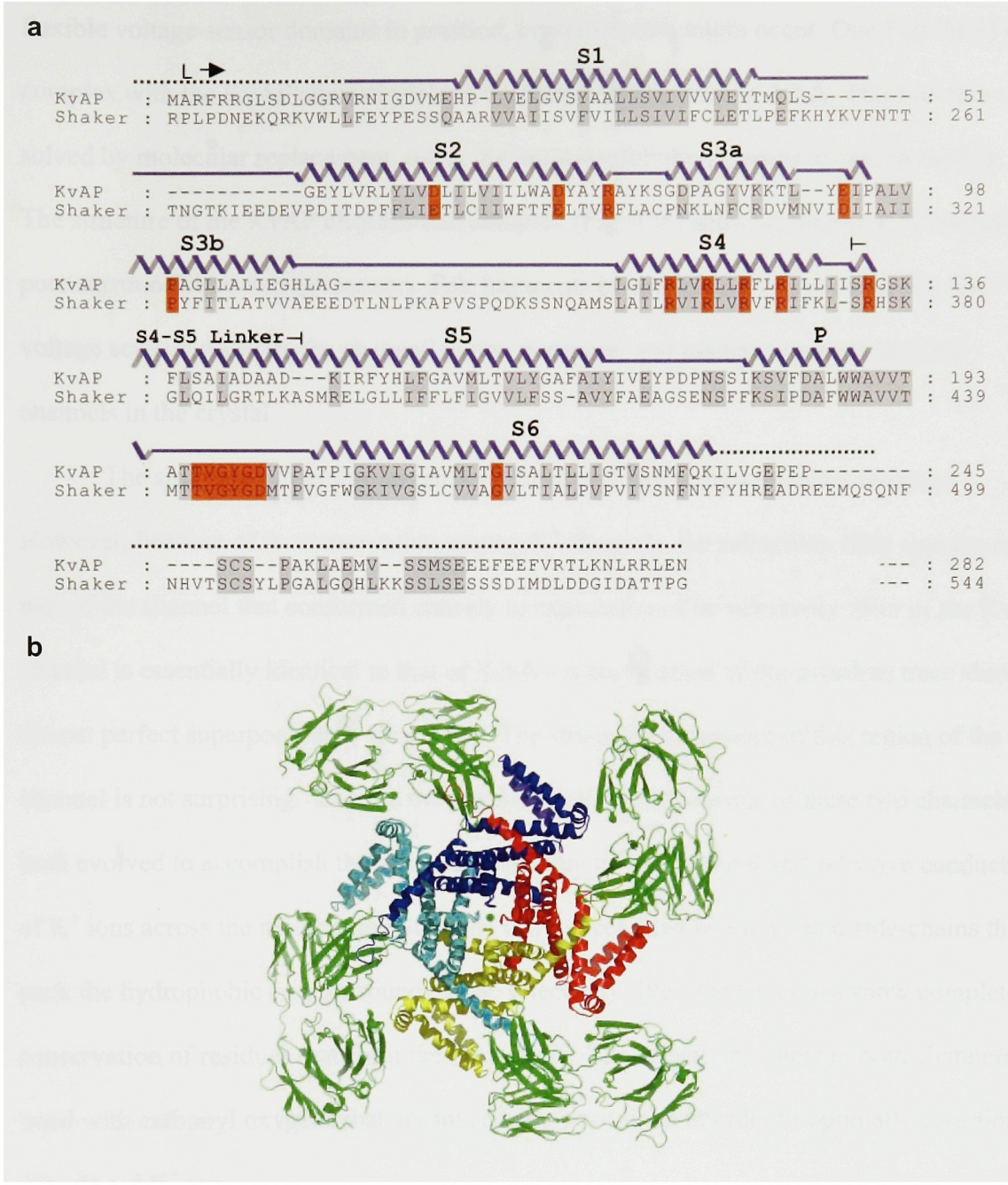

Figure 13
Structure of the KvAP channel in compex with Fab. **a**, Sequence alignment of KvAP and the *Shaker* K^+ channel. Regions of high homology are colored grey, and residues known to be important for K^+ selectivity and voltage-dependent gating are colored red. Secondary structure elements show S1–S6 and P (pore) α-helices on the basis of the crystal structure. Disordered regions are shown as black dotted lines. **b**, Structure of the KvAP channel (blue, yellow, cyan and red helical structures) bound to four Fab fragments (green), viewed down the four-fold axis from the intracellular side.

flexible voltage-sensor domains in position, crystallization might occur. One Fab (6E1) in complex with the KvAP channel yielded crystals that diffracted to 3.2 Å. The structure was solved by molecular replacement, using the immunoglobulin domains as search models. The structure of the KvAP channel-Fab complex (Fig. 13b) shows a canonical K^+ selective pore surrounded by voltage sensors. Fab fragments bound to each of the channel's four voltage sensors decorate the channel's outer perimeter and mediate contacts between channels in the crystal.

The structure of the full-length KvAP channel has many surprising features. However, because of its conservation among K^+ channels, the selectivity filter was the one part of the channel that conformed entirely to expectation. The selectivity filter of the KvAP channel is essentially identical to that of KcsA—a comparison of the α-carbon trace shows almost perfect superposition[6,7] (Fig. 14a). The structural invariance of this region of the channel is not surprising. Despite the different gating mechanisms of these two channels, both evolved to accomplish the same essential function—the rapid and selective conduction of K^+ ions across the membrane. So while differences exist in amino-acid side-chains that pack the hydrophobic core surrounding the selectivity filter, the structures show complete conservation of residues that form the filter itself. The selectivity filters in both channels are lined with carbonyl oxygens that are invariantly positioned in order to optimally coordinate dehydrated K^+ ions.

Deviations between the KvAP and KcsA structures are visible beneath the selectivity filter, at the level of the inner leaflet of the membrane (Fig. 14b). In the structure of KcsA, the inner helices which line the ion conduction pathway form a bundle at the intracellular face of the channel with an impenetrably small diameter that would prevent the passage of K^+ ions in the

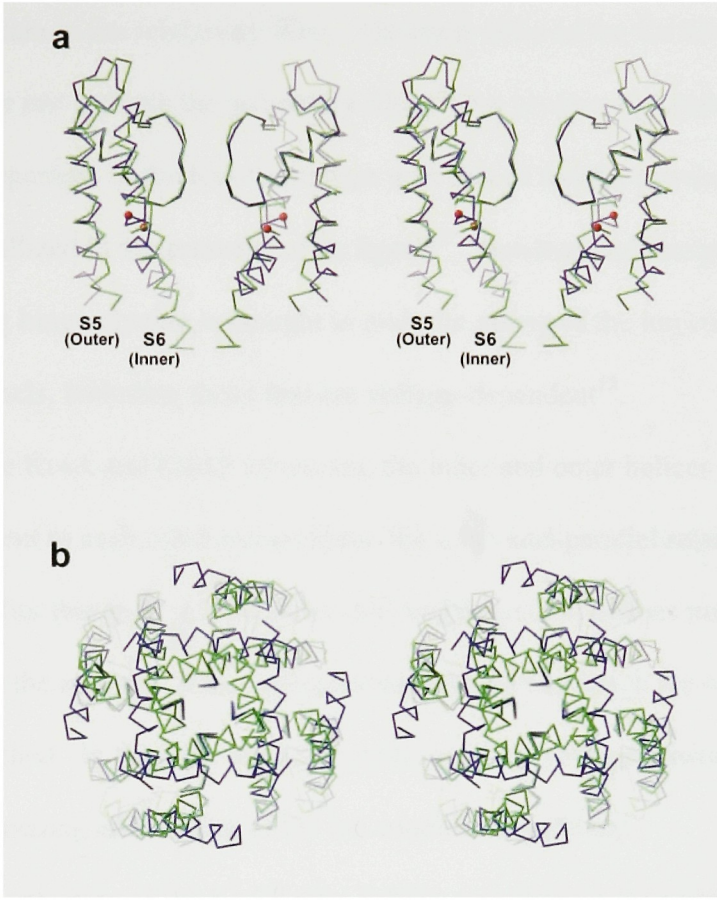

Figure 14

The KvAP pore. **a,** Stereo diagram of two subunits of the KvAP pore (blue) superimposed on the KcsA K^+ channel (green) from within the membrane or **b,** from the intracellular side of the membrane (with all four subunits shown). The glycine gating hinge residue is shown as a red sphere.

hydrated state[6]. In contrast the KvAP pore is in an "opened" presumably conductive conformation. In the KvAP channel, the inner helices (S6) are bent and splayed open, exposing a wide intracellular mouth that forms a continuous path for a K^+ ion from the intracellular solution to the selectivity filter. The inner helix of the KvAP pore is bent at a conserved glycine just beneath the selectivity filter. This glycine was identified as a gating hinge from a comparison of the KcsA structure with that of MthK, a prokaryotic Ca^{2+}-gated K^+ channel crystallized in the presence of its ligand[85]. Bending and straightening of the inner helix at the gating hinge glycine is thought to underlie gating of the ion conduction pathway in many K^+ channels, including those that are voltage-dependent[15].

In both the KcsA and KvAP structures, the inner and outer helices of each subunit of the pore lie adjacent to each other and maintain the same anti-parallel relationship. This raises the possibility that in KvAP the inner (S6) and outer (S5) helices may move laterally as a unit directed by the motions of the voltage-sensor domain to which the outer helix (S5) is immediately attached. In this way the conformations of the voltage-sensor domain could directly control opening and closing of the ion conduction pathway.

While the structure of the KvAP pore fulfills expectations for a prototypical K^+ selective channel, the voltage-sensor domains that encircle the pore contain many unexpected features. Figure 15a shows the channel from the intracellular perspective, viewed down the ion conduction pathway. Immediately surrounding the pore are the S1-S2 helices, which form an extended helical belt about the middle of the channel. The S3 and S4 helices are at the very outer perimeter of the channel. Viewed from within the plane of the membrane in Figure 15b, the KvAP voltage sensor is formed from a number of helical segments: S1, S2, S3a, S3b and S4. None of the helical segments of the voltage sensor is transmembrane based

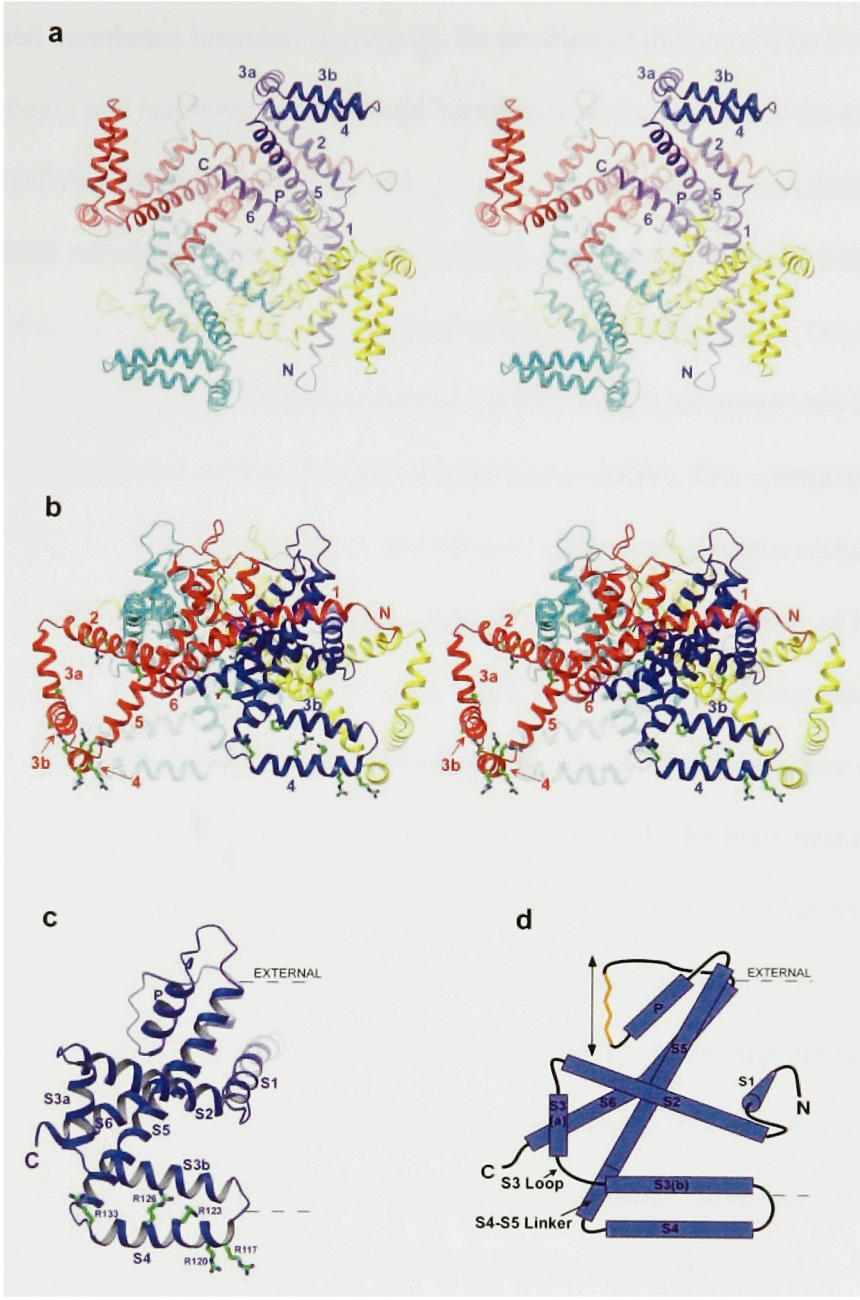

Figure 15

The KvAP channel architecture contains a voltage sensor paddle at the perimeter of the channel. **a,** Stereo image of the KvAP channel tetramer, viewed from the intracellular side of the membrane. Each subunit is a different color and the helices of one subunit (S1-S6) are labeled. **b,** Stereo image of the KvAP channel tetramer, viewed from within the membrane. Highly conserved residues known to be involved in voltage sensing are shown for two subunits. **c,** A single KvAP subunit viewed from the same perspective as in **(b)** with its transmembrane helices labeled (S1-S6) and the conserved arginine residues that account for most of the gating charge highlighted. **d,** A schematic diagram of the KvAP subunit topology. All ribbon figures in this chapter are made with the program Ribbons[86].

on the assumed membrane boundaries given by the position of the pore. The S1 and S2 helices both begin and end within what would correspond to the interior of the membrane, closer to the external membrane surface, with the short S1-S2 loop between them lying near the middle of the membrane. Most unexpected of all is the position of the S4 helix which lies near the intracellular membrane boundary, parallel to the membrane plane. The N-terminal portion of the S4 segment forms a tightly packed helix-turn-helix structure with the S3b segment and we call this structural unit, the voltage-sensor paddle. The voltage-sensor paddle is mostly hydrophobic with the important exception of conserved arginine residues staggered along one face of the S4 helix. In the *Shaker* channel, the first four arginines of the S4 helix account for most of the 12-14 charges that move fully through the membrane electric field during voltage-dependent activation of the channel[18,19]. The corresponding four arginines in KvAP reside within the voltage-sensor paddle. The position of the S4 helix in the KvAP structure is surprising because numerous electrophysiological studies of eukaryotic Kv channels have shown that the N-terminal portion of S4 can react with thiol reactive compounds and spider toxins from the extra-cellular side of the membrane but never the intracellular side[23-25,52]. How can we understand the discrepancy between the position of the S4 segment in the crystal structure and the electrophysiology data? In the KvAP crystal structure, the tip of each voltage-sensor paddle is bound by a Fab fragment (Fig. 13b). Could the crystal packing forces imposed by the Fab fragments have pulled the voltage sensor into a non-physiological conformation?

A second structure—that of the isolated voltage-sensor domain (S1-S4) expressed, purified, and crystallized in the absence of the pore forming domain—helped to address this question by highlighting regions of the voltage sensor that are flexible and can adopt more

than one conformation. In the previous chapter I showed that the isolated voltage-sensor domain purifies the same complement of voltage-sensor toxins from tarantula venom as the full-length KvAP channel. Some of the tarantula toxins that bind to the purified isolated voltage-sensor domain are high-affinity inhibitors of reconstituted KvAP channels in membranes. This result indicates that the isolated voltage-sensor domain, removed from its context within the full channel, still retains aspects of its native structure or else it would not exhibit molecular specificity for these spider toxins that evolved to bind to the voltage-sensor[52,73].

The structure of the isolated voltage-sensor domain was obtained as a complex with a monoclonal Fab fragment and again solved by molecular replacement using the Fab fragment as the search model (Fig. 16a). Both the 6E1 Fab used in crystallization of the full-length channel and 33H1 Fab used in crystallization of the isolated voltage-sensor domain, bind to precisely the same epitope with the same relative orientation at the tip of the voltage-sensor paddle. In the isolated voltage-sensor domain structure we find an identical helix-turn-helix structure corresponding to the voltage-sensor paddle but it has adopted a different relative orientation to other segments of the voltage-sensor. This conformational difference emphasizes the flexible attachments of the voltage-sensor paddle which enable it to move as a unit to accommodate crystal packing.

An important feature of the isolated voltage-sensor domain structure is that it shows a number of ionic interactions between highly conserved basic and acidic amino acids in the voltage sensor (Fig. 16b). The four gating charge arginines on S4 (R117, R120, R123, and R126) face the solvent in the crystal. A fifth arginine on the S4 helix, R133, makes a salt bridge with D62 in S2, pinning the S4 and S2 helices together. A salt-bridge network is also

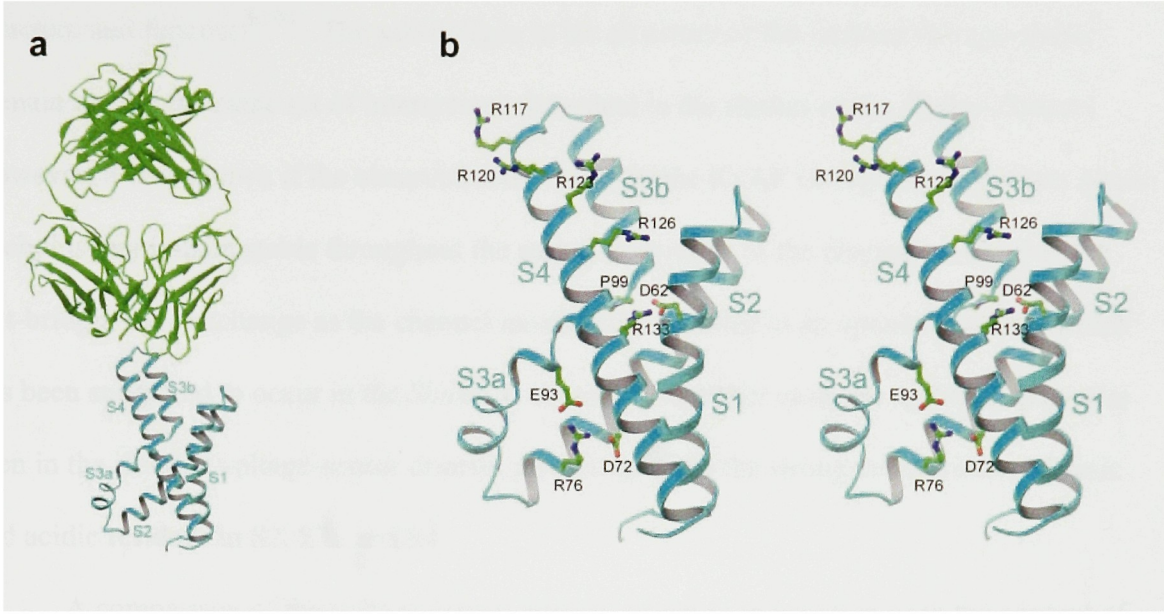

Figure 16

The KvAP isolated voltage-sensor domain. **a,** The structure of the isolated voltage-sensor domain (blue) complexed with the 33H1 Fab fragment (green). **b,** Stereo view of the isolated voltage-sensor domain shows a voltage-sensor paddle. Highly conserved, functionally important residues are shown, including the arginines in S4 that carry the majority of the gating charge as well as charged residues in S2 and S3 that form salt bridges in the structure.

visible involving R76 in S2, D72 one helical turn away in S2, and E93 in S3a, and appears to fasten S3a to the C-terminal half of S2. Studies by Papazian et al. have suggested that specific salt-bridge pairs are formed between acidic residues in S2 and S3a with basic residues on S4 in the *Shaker* channel and these ionic interactions are critical to the channel's structure and function[87-90]. The salt-bridges in the structure of the isolated voltage-sensor domain are not the same set of interactions described in the studies of the *Shaker* channel. However, it is unknown if the observed salt-bridges in the KvAP voltage-senor domain act as linchpins that remain stable throughout the gating transitions of the channel or whether the salt-bridges may exchange as the channel moves from a closed to an opened position, which has been suggested to occur in the *Shaker* channel[89,90]. In either case, the specific ionic pairs seen in the isolated voltage-sensor domain give insight into the strong conservation of basic and acidic residues in S2, S3a and S4.

A comparison of the voltage-sensor domain structure in isolation or in the context of the channel is shown in Figure 17. Two striking differences in the voltage-sensor structures are immediately evident. Figure 17a shows that in the full-length channel, S1 extends away from S2 to make contact with a neighboring subunit but is folded back in the isolated voltage-sensor domain. A second difference is that in the full-length channel, the S4 helix makes a sharp bend at a glycine residue immediately after the voltage-sensor paddle, redirecting the helix into S5 (Fig. 17b). In contrast, the S4 helix in the isolated voltage-sensor domain, without the constraint of its connection to the pore runs straight from the voltage-sensor paddle (Fig. 17c). This conformational difference defines the S4-S5 linker (colored yellow), a mostly hydrophilic helix that directly connects the voltage-sensor paddle to the pore.

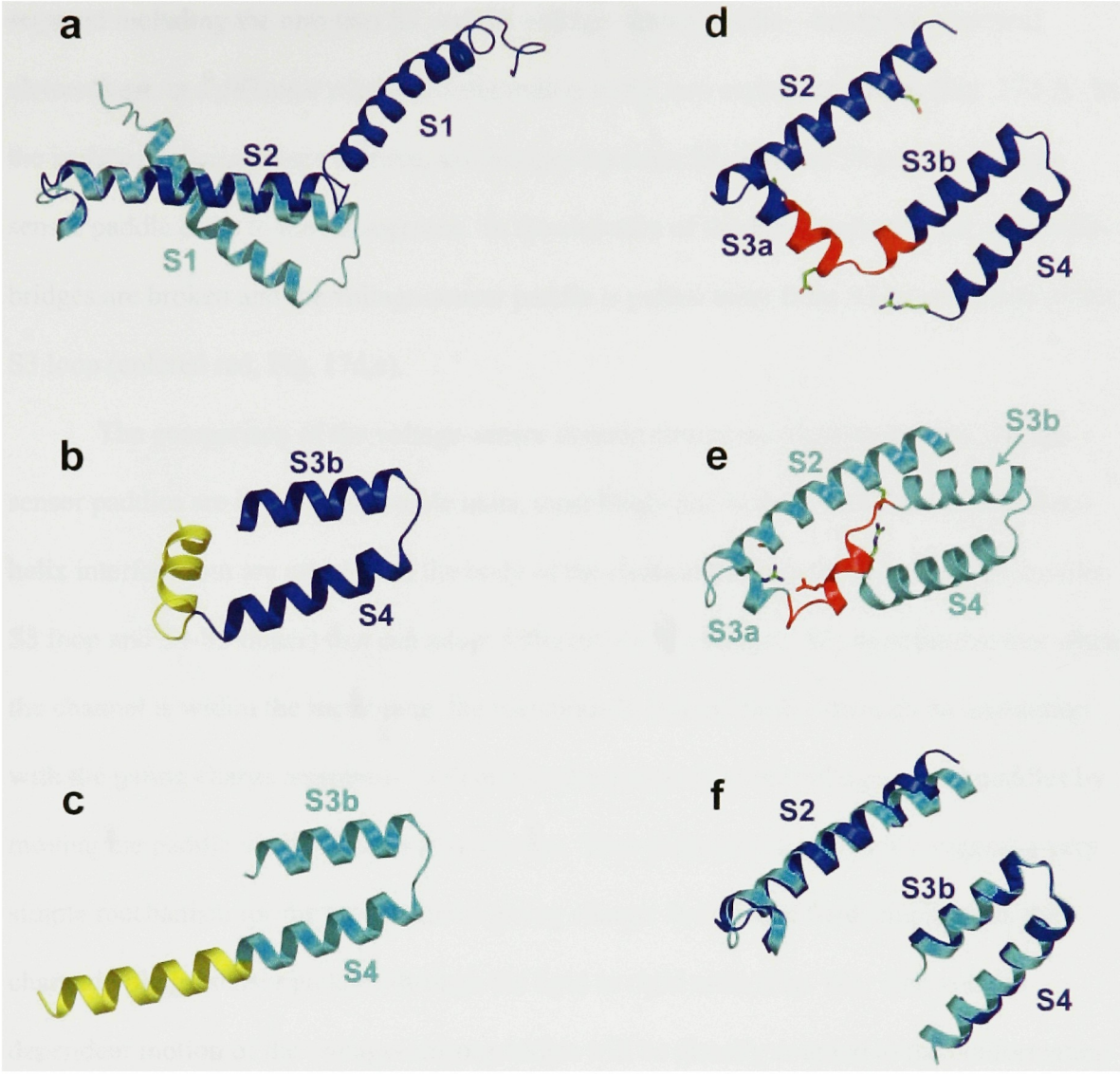

Figure 17

Comparison of the KvAP voltage-sensor domain structures. **a,** The S1 and S2 helices of the voltage sensor are shown for the full-length channel (blue) and the isolated voltage sensor (cyan) with the S2 from both structures superimposed. **b-c,**The voltage-sensor paddle is attached to the pore through the flexible S4-S5 linker (yellow) which is bent in the full-length channel (**b**) and is straightened in the isolated voltage sensor (**c**). **d-f,** The voltage sensor from the beginning of S2 to the end of the voltage-sensor paddle is shown for the full-length KvAP channel (**d**), for the isolated voltage sensor (**e**), and with S2 and the voltage-sensor paddle from both structures superimposed (**f**). Amino acids forming salt bridges in the isolated voltage sensor are shown, and the S3 loop is colored red.

Two regions of both voltage-sensor structures are essentially identical—the S2 segment including the turn into S3 and the voltage-sensor paddle—but these structural elements are in a different relative configuration in the two crystal structures (Fig. 17d-f). In the isolated voltage-sensor domain, salt bridges between S2, S3a and S4 pin the voltage-sensor paddle close to the S2 segment. In the structure of the full-length channel, these salt-bridges are broken and the voltage-sensor paddle is pulled away from S2 by extension of the S3 loop (colored red, Fig. 17d,e).

The comparison of the voltage-sensor domain structures suggests that the voltage-sensor paddles are intrinsically stable units, most likely due to their well packed helix-turn-helix interface, but are attached to the body of the channel through flexible connections (the S3 loop and S4-S5 linker) that can adopt different conformations. We hypothesize that when the channel is within the membrane, the membrane's electric field—through its interaction with the gating charge arginines—will dictate the positions of the voltage-sensor paddles by moving the paddle via its flexible attachments. Thus these structures readily suggest a very simple mechanism for the movement of gating charge: the electric field simply pulls the charged voltage-sensor paddles through the lipid as rigid units (Fig. 18). The voltage-dependent motion of the voltage-sensor paddles will be directly coupled to the conformation of the S4-S5 linker and hence the gating state of the pore. This conceptual model of voltage-dependent gating is quite different from previously conceived models in which S4 lies next to the pore within a protein-lined canal, shielded from the hydrophobic core of the lipid membrane by the S1-S3 segments of the voltage-sensor [37-39](Fig. 3). Instead we find the KvAP voltage sensor is inverted, with the charged S4 helix lying at the very perimeter of the

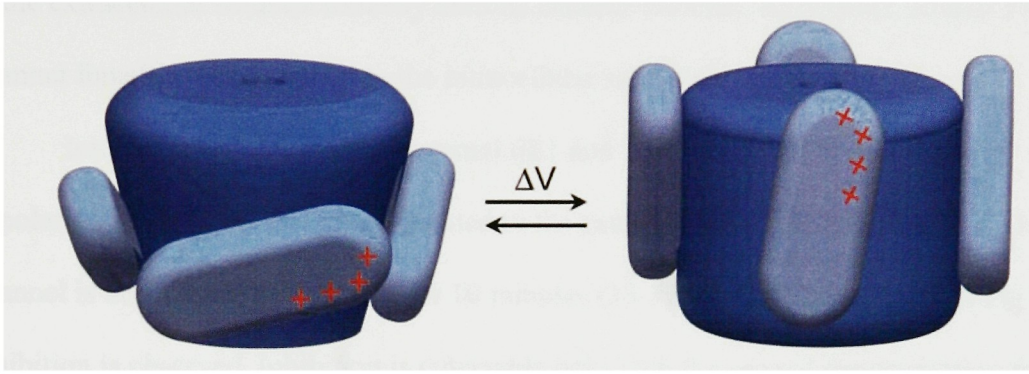

Figure 18

Hypothesis for gating charge movements. Gating charges (red plus signs) could be carried through the membrane from inside (bottom) to outside (top) by movements of the voltage-sensor paddles against the lipid membrane, which in turn could open the pore.

channel, at the protein-lipid interface, poised to move through the lipid with its cargo of gating charges.

To learn more about the mobility of the voltage-sensor paddles within the membrane, we studied the effects of the Fab used for crystallization on KvAP channels reconstituted into planar membranes. Figure 19 shows that both 6E1 and 33H1 Fabs bind their epitope on the voltage-sensor paddle from only the external side of the membrane. Addition of 500 nM Fab to the extracellular solution robustly inhibits channel currents. In contrast, neither Fab affects channel function when applied to the intracellular side of the membrane.

Interestingly inhibition by external 6E1 and 33H1 Fabs requires membrane depolarization. When 33H1 Fab is added to the external side of the membrane while the channel is held closed at -100 mV for 10 minutes (15-25 minute time interval in Fig.19c), no inhibition is observed. Inhibition is detectable only with the second depolarization following Fab addition. Thus by holding the membrane voltage negative, the channel is protected from inhibition by Fab and only with membrane depolarization is the epitope on the paddle (encompassing the tip of the paddle, two helical turns of S3b and one helical turn of S4) accessible to the Fab fragment.

Why do the Fabs inhibit the channel? If the Fab is recognizing the depolarized conformation of the voltage-sensor paddle, why do we not see constitutively activated channels, held open with the Fab fragment? Inhibition can be explained by the fact that the KvAP channel, like most voltage-dependent K^+ channels, inactivates. That is the pore of the channel spontaneously stops conducting during prolonged depolarizations of the membrane, even though the voltages ensors remain in their opened conformation. When Fabs bind and

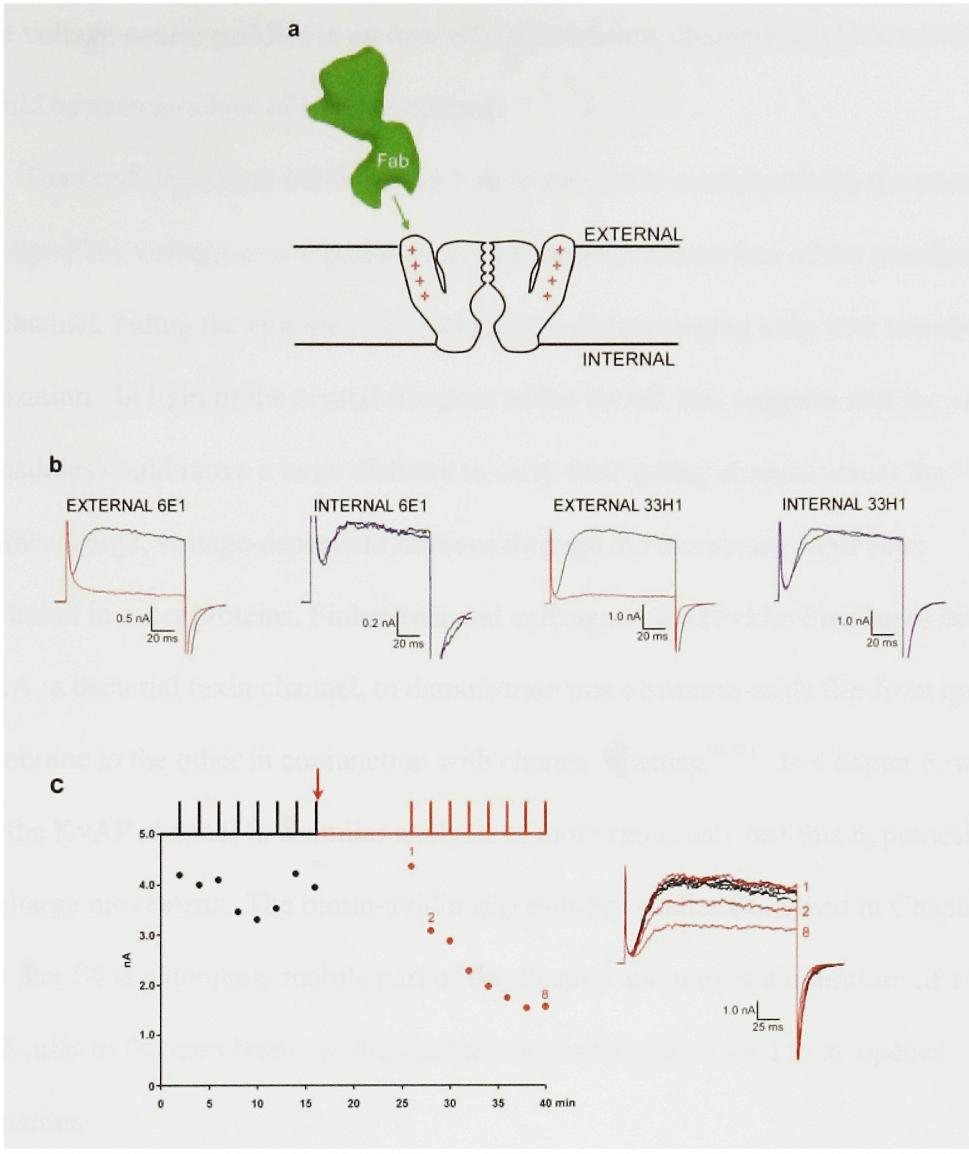

Figure 19

Inhibition of KvAP channels by Fabs that bind to the voltage-sensor paddles. **a,** Experimental strategy: Fab (green) is added to the external or internal side of a planar lipid membrane to determine whether the epitope is exposed. **b,** Fabs used in crystallization (6E1 and 33H1) inhibit from the external (red traces) but not the internal (blue traces) side of the membrane. Currents before (black traces) and after the addition of about 500 nM Fab (red and blue traces) were elicited by membrane depolarization to 100 mV from a holding voltage of -100 mV. **c,** Fab 33H1 binds to the voltage-sensor paddle only when the membrane is depolarized. Current elicited by depolarization from -100 mV to 100 mV at times indicated by the stimulus trace (above) in the absence (black symbols) or presence of 500 nM Fab (red symbols) is presented as a function of time. Selected current traces corresponding to the numbered symbols are shown (right).

hold the voltage-sensor paddles in an opened conformation, channels could inactivate and this would be seen as a loss of channel current.

The state-dependent inhibition by Fab fragments is consistent with the possibility that the tip of the voltage-sensor paddle descends beneath the surface of the membrane in the closed channel, hiding the epitope from recognition and remerging only with membrane depolarization. In light of the crystal structure of the KvAP, this suggests that the voltage-sensor paddles could move a large distance to carry their gating charges across the membrane. Large, voltage-dependent motions through the membrane have been demonstrated in other proteins. Finkelstein and colleagues used avidin binding to biotinylated colicin1A, a bacterial toxin channel, to demonstrate that 68 amino acids flip from one side of the membrane to the other in conjunction with channel opening[91-93]. In Chapter 6, we will subject the KvAP channel to a similar analysis to more rigorously test this hypothesis for gating charge movement. The biotin-avidin accessibility studies described in Chapter 6 indicate that S4 is a uniquely mobile part of the channel and moves a minimum of 15 Å, perpendicular to the membrane, as the channel moves from its closed to its opened conformation.

This first structure of KvAP led to a working model of voltage-dependent gating that is very different from previously postulated models derived from more indirect techniques, and challenges previous conceptions about the dynamics of voltage-dependent channels in the membrane. However a number of very important questions remain after this first structural study. Some of these questions relate to regions of the channel that are likely distorted due to the crystal packing forces imposed by the Fabs on this very flexible protein. Some are mechanistic questions not answered when analyzing a dynamic protein with a

single structural snapshot. What is the relationship of the voltage-sensor paddle to the remainder of the channel in the native structure? Is the interface across the voltage-sensor paddle maintained throughout the channel's gating motions? How is the configuration of the S1 and S2 helices in the crystal structure related to their configuration within the membrane? Do the S1-S2 helices undergo voltage-dependent conformational changes? It was clear that in order to address these questions and understand the mechanistic details of the voltage-dependent gating process more structures of the KvAP channel under different conditions and in different conformations would be needed.

CHAPTER 5: THE STRUCTURE OF KvAP IN THE ABSENCE OF FAB

Voltage-dependent gating in Kv channels arises from the coupling of voltage-sensor movements to pore opening. The voltage sensors must therefore possess some flexibility to allow them to carry out their gating motions within the membrane. Unfortunately the inherent flexibility of the voltage-sensor domains has made crystallization of Kv channels a challenge. One strategy to overcome this obstacle, employed in the first crystal structure of the KvAP channel, was to bind monoclonal Fab fragments to each of the channel's four voltage sensors to "hold" them in place. The Fab fragments in the first KvAP channel structure are bound to the channel's voltage-sensor paddles—helical hairpins that lie at the perimeter of the channel. Highly conserved gating charge residues are located within the voltage-sensor paddle and the displacement of these charged amino acids, driven by changes in the membrane electric field, has been hypothesized to underlie the gating motions of the voltage sensors[34,94].

A structure of the isolated KvAP voltage-sensor domain—expressed, purified and crystallized in the absence of the pore-forming domain—was also obtained as a complex

with a Fab fragment attached to its voltage-sensor paddle. A comparison of these two crystal structures suggested that the voltage-sensor paddles are attached to the channel through flexible hinges and move as rigid units in response to membrane voltage changes, carrying their gating charges part way through the membrane. One consequence of the flexible attachment of the voltage-sensor paddles is that in the full-length KvAP channel structure, the paddles have been pulled into a non-physiological conformation by crystal packing forces imposed by the Fabs. So while the Fab fragments have permitted crystallization they do not prevent distortion in the structure. What would the structure of the KvAP channel look like without the Fabs bound to it? Would we find the voltage-sensor paddles in a more physiological conformation? The Fab fragments used for crystallization inhibit functioning KvAP channels in membranes indicating that the epitope corresponds to a physiological conformation. But could this be a rare conformation of the voltage sensor that is trapped by Fab binding, leading to the observed inhibition? Could the voltage-sensor paddle structure that we see in the crystal structures be an artifact of Fab binding?

In initial trials (conducted by Youxing Jiang and Alice Lee) KvAP channels failed to crystallize on their own. During attempts to identify new crystal forms of KvAP in complex with different Fab fragments, Alice Lee and I serendipitously identified a low-resolution crystal form containing only channel and no Fab. Apparently under the crystallization conditions the Fab-channel complex was unstable and dissociated, leaving the channel to crystallize on its own. I solved this structure of the KvAP channel at 6.4 Å by multiple isomorphous replacement with anomalous signal (MIRAS) using thallium and tantalum derivatives. The structure reveals a fascinating crystallographic solution to hold the voltage-sensors in a uniform configuration. The structure of KvAP without Fab fragments has

remarkably similar architecture to the first structure of the KvAP channel crystallized in complex with Fab fragments. This similarity emphasizes that it is the intrinsic flexibility of the channel and the lack of lipid membrane, and not the binding of the Fab fragment *per se*, that gave rise to the non-physiological conformation of the first structure. Importantly, the similarity of the two channel structures extends to the voltage-sensor paddle, which appears identical with and without Fab fragments bound to it.

Protein purification and crystallization

In initial trials, purified KvAP channels were mixed with 7D12 Fab fragments in 1: 2.5 molar ratio and the complex was purified on a Superdex-200 (10/30 column) in 20 mM Tris pH 8.0, 100 mM KCl, and 30 mM βOG. Following purification, the complexes were concentrated to ~10 mg/ml using a 50 kDa molecular-mass cutoff Centricon (Amicon) for crystallization. Initially small 50 μm crystals grew out of several similar conditions in a grid screen. Protein gel and western blot assays indicated that these crystals contain only the KvAP channel and no Fab fragments. For subsequent crystallization trials, channels were purified directly in 20 mM Tris pH 8.0, 100 mM KCl, and 30 mM βOG and concentrated to ~10 mg/ml.

For structure determination, crystals were grown by sitting drop vapor-diffusion at 20 °C with a 1:1:0.2 mix of the protein, reservoir solution and detergent additive. The reservoir solution was 10–15% (w/v) PEG 400, 50 mM sodium cacodylate, pH 5.5-6.0 and the detergent additive was 109 mM DDAO (N,N-dimethyldecylamine-β-oxide). Cryoprotection of the crystal was achieved through vapor-diffusion by increasing the concentration of PEG 400 in the reservoir slowly to 40%. Cryoprotected crystals were flash frozen in liquid propane.

To obtain thallium derivatives, purified, concentrated KvAP channels were dialyzed against 50 volumes of 20 mM Hepes, pH 8.0, 100 mM $TlNO_3$, and 40 mM βOG overnight and then used for crystallization trials. While crystals grew in $TlNO_3$, the thallium derivatives used for phasing were obtained by the transfer of cryoprotected crystals grown in KCl to wells of cryoprotected mother liquor containing $TlNO_3$ for 24 hours before freezing. Tantalum derivatives were obtained by transfer of cryoprotected crystals to wells containing cryoprotected mother liquor with 2 mM $Ta_6Br_{12}^{2+}$ and soaked 24 hours before freezing.

Structure determination

Crystals initially diffracted to 8.9 Å Bragg spacing. Diffraction patterns could be indexed as a primitive orthorhombic lattice with unit cell dimensions a = 149 Å, b = 250 Å and c = 289 Å. Systematic absences indicated screw axes along all three unit cell axes suggesting that the space group was $P2_12_12_1$. With this large unit cell, 4-8 channels could likely be within a single asymmetric unit giving a solvent content of 55.4-77.7%. The multiple copies of the channel in the asymmetric unit are related through both rotational and translational non-crystallographic symmetry. Calculation of a self-rotation function using the native data-set showed non-crystallographic rotational symmetry—including 6 strong four-folds and a 3-fold—reflecting the complex packing of the channels within the crystal (Fig. 20a). Calculation of a self-Patterson function using the native data set showed a large peak approximately 25% of the origin at the position u = 0.2, v = 0.5, w=0.25 (Fig. 20b). This pseudo-translation is a special form of non-crystallographic symmetry. It can arise from the direct translation of non-crystallographic symmetry related molecules within the asymmetric unit or alternatively it can arise from the positioning of a non-crystallographic symmetry axis parallel to a crystallographic symmetry axis. In either case pseudo-translational symmetry

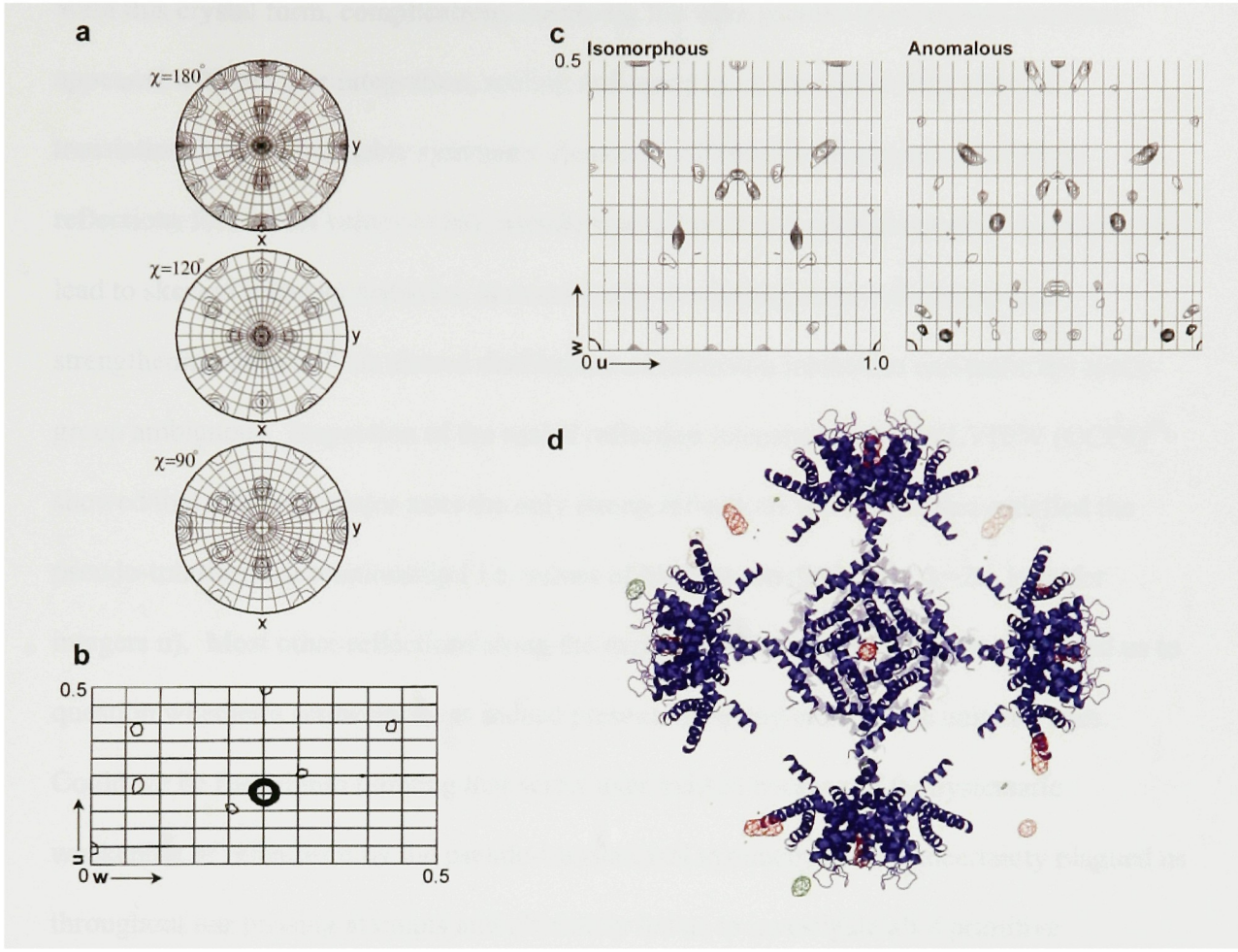

Figure 20

Phasing of a low-resolution crystal form of KvAP without Fab. **a,** Self-rotation function calculated in MOLREP shows the presence of 2-fold (top), 3-fold (middle) and 4-fold (bottom) non-crystallographic rotational symmetry. **b,** Self-Patterson map calculated in $P2_12_12_1$ shown for 1 asymmetric unit for v=0.5. Peak at u=0.2,v=0.5,w=0.25 is due to pseudo-translational symmetry. **c,** Thallium isomorphous difference Patterson map (left) and anomalous difference Patterson map (right) calculated from two different thallium derivatives, contoured at 2σ in 0.5σ increments. v=0 plane is shown. d, Molecular replacement solution in $P2_12_12_1$ shows an assembly of 6 channels within an asymmetric unit. F_{Tl} - F_{native} isomorphous difference density (red) and F_{Ta} - F_{native} isomorphous difference density (green) are superimposed, both contoured at 4σ.

presents an additional challenge to phasing since most phasing methods are Patterson based. With this crystal form, complications stemming from the pseudo-translational symmetry appeared with the first integration, scaling and merging of the native data. Just as translational crystallographic symmetry elements will result in systematically absent reflections for certain values of hkl, pseudo-translational non-crystallographic symmetry will lead to skewed intensity statistics, systematically weakening some reflections and strengthening others. This altered distribution of reflection intensities can make the space-group ambiguous. Inspection of the scaled reflection intensities with HKLVIEW (CCP4)[95] showed that along the major axes the only strong reflections were those that satisfied the pseudo-translational relationship (i.e. values of hkl that satisfied h=5n, k=2n, l=4n for integers n). Most other reflections along the major axes were weak or absent. This led us to question whether a screw axis was indeed present along any or all of the unit cell axes. Could we be fooled into thinking that screw axes existed because of the systematic weakening of reflections by the pseudo-translational symmetry? This uncertainty plagued us throughout our phasing attempts and ultimately led us to investigate all 8 primitive orthorhombic space-groups containing all combinations of 0-3 screw axes.

Initially we reasoned that heavy atom clusters would be the best first attempt for phasing due to their large mass, density of electrons and strong anomalous signal—something that would likely be necessary due to the large scattering mass of the asymmetric unit and the low resolution of the data. Heavy atom clusters diffract as superatoms at resolutions below the dimensions of the cluster giving a clear signal in isomorphous or anomalous difference Patterson maps[96]. However, despite obtaining fairly isomorphous $Ta_6Br_{12}^{2+}$ and $K_{10}[\alpha_2\text{-}P_2W_{17}O_{61}]\cdot nH_2O$ derivatives, we were unable to locate heavy atom sites

using SHELXS[97], SOLVE[98], or RSPS (CCP4)[95] in any of the primitive orthorhombic space groups. The pseudo-translational symmetry worked against us in these attempts. All anomalous and isomorphous Patterson maps were dominated by the pseudo-translation vector peak. Moreover, the correlation of reflections through the pseudo-translational symmetry led to "ghosting" of heavy atom sites in difference Fourier maps rendering this form of validation worthless. A difference Fourier map calculated using phases from a single heavy atom input site would always show a second site related to the first by the pseudo-translation vector.

Frustrated by the complications of the pseudo-translational symmetry in this crystal form, we attempted to grow crystals in the presence of a variety of additives with the hope that the crystals might grow with slightly altered packing and transform some of the non-crystallographic symmetry to crystallographic symmetry. While the presence of heavy metals, detergents and organic and inorganic additives did not induce a change in the crystal packing as we had hoped, we were able to identify a number of detergent additives which produced crystals with higher resolution diffraction. Detergent additives including DDAO (N,N-dimethyldecylamine-β-oxide), MEGA-8 (Octanoyl N-methylglucamide), and HEGA-8 (Octanoyl N-hydroxyethylglucamide) added directly to the crystal well at their respective critical micelle concentrations during crystal trial setups yielded crystals that diffracted to 5.8-6.5 Å.

The higher resolution diffraction certainly contributed to the ultimate success in phasing this crystal form. But more critical was obtaining a good thallium derivative. Thallium is a permeant ion of K^+ channels. Previous studies have shown that on average ~2.5 thallium ions bind within the 12 Å selectivity filter making the queue of ions effectively a heavy atom

cluster specific for K^+ channels[99]. Thallium's 80 electrons provide a strong diffraction signal and at its X-ray absorption edge thallium also provides a fairly strong anomalous signal—10.1 f'' electrons at the L-III edge (12.65 keV). We obtained thallium derivatives by soaking crystals grown in KCl in mother liquor where the KCl was replaced with $TlNO_3$. Although TlCl precipitation occurred at the surface of the crystal, the crystals rarely cracked and remained quite isomorphous with native crystals.

An isomorphous difference Patterson map of the thallium derivative calculated in $P2_12_12_1$ showed strong peaks (up to 9 sigma) many of which had an elongated appearance as we would expect for interatomic vectors coming from a queue of ions (Fig. 20c). We observed similar peaks in anomalous difference Patterson maps from a different thallium derivative dataset collected at 0.9735 Å, close to the wavelength of the L-III transition for thallium (Fig. 20c). Despite the promising Patterson maps we were still unable to locate any thallium sites using the programs SHELXS, SOLVE and RSPS to search in all primitive orthorhombic space groups. Although we could not directly use the thallium derivative as a source of initial phases, we hoped we could make use of the thallium derivative in an alternate manner—as validation for molecular replacement solutions using as search models components of KvAP from the previous structure determined in the presence of Fab fragments. We expected that molecular replacement would be non-trivial for this crystal form due to the large number of copies of the channel in the asymmetric unit and the limited resolution of the diffraction. In addition, because of the dynamic nature of the KvAP voltage sensors, we were limited to using the KvAP pore (residues 139-240) as a search model. Assuming there are 6 channels in the asymmetric unit, our search model of the pore would account for less than 8 % of the total scattering mass.

Nevertheless, molecular replacement was carried out with MOLREP[100] for the 8 primitive orthorhombic space-groups, using data between 30-5.8 Å. We carried out a multiple copy search with the assumption that the asymmetric unit likely contained 6 channels. None of the 8 solutions was statistically outstanding (Table 1). However we could assess the validity of a solution by calculating thallium difference Fouriers using the molecular replacement model as the source of phases. A difference Fourier, $(|F_{tl}| - |F_{nat}|)\phi_{model}$, with the $P222_1$ molecular replacement solution used for calculating phases revealed elongated thallium density (4.5 -7σ) in the selectivity filters of 4 of the 6 pores in the solution and confirmed that this solution was at least partially correct. Thallium difference Fouriers indicated that partially correct solutions were also obtained for the space-groups P222 and $P2_12_12_1$ but these space-groups exhibited weaker thallium density in difference Fourier maps.

MOLREP identified solutions in all space-groups as pairs of channels related through the pseudo-translation vector. We saw a similar "ghosting" phenomenon from correlated noise that had frustrated our search for heavy atom sites: if pore A and B from the molecular replacement solution were related through the pseudo-translation vector, calculation of phases with only pore A would give rise to strong density for pore B. Therefore the validity of pores A and B in the molecular replacement solution could not be evaluated independently.

We proceeded by using the queue of thallium ions in the selectivity filters of 4 pores from the molecular replacement solution to calculate phases by SIRAS in SHARP[101]. The calculated thallium phases were then used in a difference Fourier to identify 2 $Ta_6Br_{12}^{2+}$ sites (7-8 σ). The $Ta_6Br_{12}^{2+}$ sites were included in subsequent phase calculation in SHARP

Table 1

Space-group	Rfactor	Correlation Coefficient
$P2_12_12_1$	0.617	0.499
$P2_12_12$	0.625	0.460
$P2_122_1$	0.648	0.414
$P22_12_1$	0.631	0.446
$P222_1$	0.602	0.496
$P22_12$	0.634	0.446
$P2_122$	0.636	0.437
P222	0.613	0.547

Space-group	Rfactor	Correlation Coefficient
$P2_12_12_1$	0.532	0.708
$P2_12_12$	0.596	0.555
$P2_122_1$	0.638	0.481
$P22_12_1$	0.657	0.446
$P222_1$	0.584	0.638
$P22_12$	0.650	0.467
$P2_122$	0.649	0.471
P222	0.584	0.637

MOLREP molecular replacement solution statistics for all primitive orthorhombic spacegroups using either 1 KvAP pore as a search model (top) or 3 KvAP pores with their corresponding S1 and S2 helices (bottom).

although their contribution to phasing was weak. After 4-fold averaging along each channel's central 4-fold axis, electron density corresponding to the pore became clearly visible. Remarkably, we observed tubes of density encircling the pore that corresponded very well to the configuration of the S1and S2 segments from the first KvAP channel structure crystallized with Fab fragments. As we expanded our model to contain the pore and the S1 and S2 segments from the first KvAP channel structure, we recognized that several of the channels in the molecular replacement solution generated very interesting packing. Three KvAP channels and their crystallographic symmetry mates formed an octahedral bipyramid of channels—a supra-structure that clearly could not arise by coincidence. While this was promising, it still seemed unlikely that $P222_1$ was the correct space-group. The three channels that gave rise to this supra-structure of channels did not generate the observed pseudo-translational symmetry of the crystal. Three additional channels, related to the three that form the bipyramid through the pseudo-translation vector, could be included with minimal clashes. However structure factors calculated from this model of six channels did not give rise to the systematic absences we observe in the data.

Molecular replacement was again tried in all 8 primitive orthorhombic space groups. We redefined our search model based on the $P222_1$ solution to consist of the three KvAP pores with their S1 and S2 segments that formed half of the bipyramid of channels. With this search model, a single molecular replacement solution of 6 channels had clearly outstanding statistics in $P2_12_12_1$ (Table 1). In $P2_12_12_1$, six channels related through only non-crystallographic symmetry come together to form the assembly of channels found in $P222_1$ generated through a combination of non-crystallographic symmetry and crystallographic symmetry (Fig. 20d). In this crystal packing, the pseudo-translational symmetry is generated

through the positioning of a non-crystallographic symmetry axis parallel to a crystallographic symmetry axis.

Difference Fourier maps using phases from the $P2_12_12_1$ molecular replacement solution now showed 12-13 σ thallium sites in the selectivity filters of all 6 channels and a single 12 σ $Ta_6Br_{12}^{2+}$ site (Fig. 20d). A queue of thallium sites in the selectivity filter of 6 channels (24 thallium sites total) and 1 $Ta_6Br_{12}^{2+}$ site were used to calculate phases to 6.4 Å by MIRAS in SHARP followed by solvent flattening in DM[102]. Phasing statistics (Table 2) and the density of the pore (shown without averaging in Fig. 21a,c and with 4-fold averaging in Fig. 21 b,d) in the experimental map shows the high quality of the heavy atom phases. Tracing of the α-carbon chain through the density was vastly simplified by the similarity of this structure to the first KvAP channel structure crystallized with Fab fragments. Model building (main chain only) consisted of simple rigid body transformations of the first KvAP channel structural model to fit helical segments into the un-averaged experimental electron density in the program O[103]. Iterative cycles of model building in O were followed by rigid body refinement carried out in CNS[104] and phases from the model then combined with the heavy atom phases using SIGMAA (CCP4). Electron density was fairly continuous for most of the 24 channel subunits in the model with the exception of the region corresponding to S3a which was broken or missing in the un-averaged map for the majority of subunits.

Structure of KvAP channels without Fab

We have solved a structure of the KvAP channel crystallized without Fab fragments using MIRAS phases calculated to 6.4 Å resolution. We traced the main chain for the six channels in the asymmetric unit into the un-averaged electron density map in order to prevent

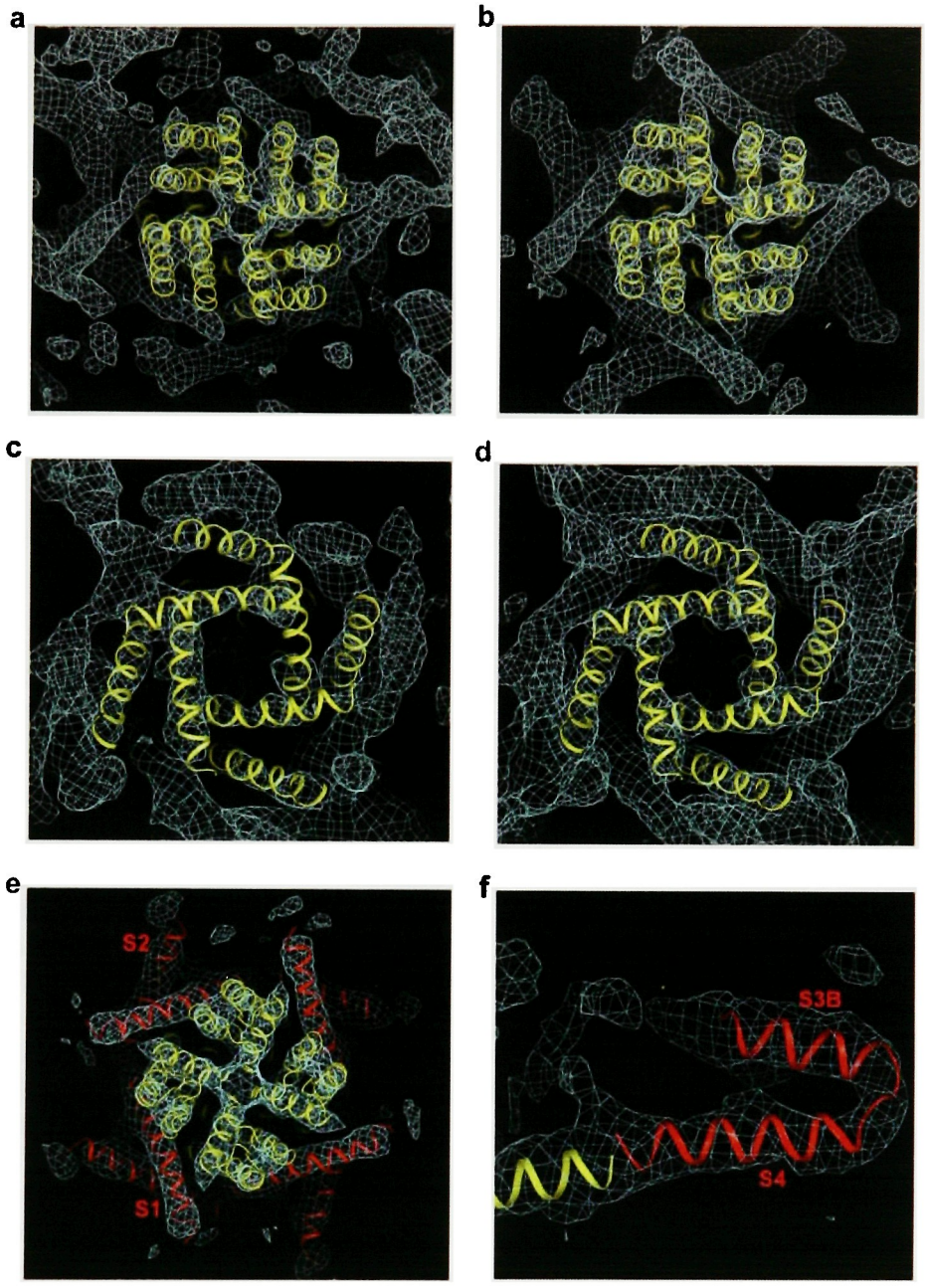

Figure 21

Experimental electron density. Electron density map calculated from native amplitudes and solvent-flattened unaveraged phases, contoured at 1 σ (**a,c**) or averaged phases contoured at 2 σ(**b,d-f**) . **a-d,** Model of the pore from the KvAP-6E1 Fab structure was placed into the experimental density without adjustment and is viewed looking down the ion conduction pathway from the extracellular **(a,b)** or intracellular **(c,d)** perspective. **e,** The S1-S2 helices (red) encircle the pore (yellow). **f,** Experimental density for the voltage-sensor paddle (red). Model of the paddle from the KvAP-6E1 Fab structure has been placed in the experimental density without adjustment. Figures 21-23 were prepared with Pymol[105].

Table 2

Data Collection					
Dataset	Native	TI 1	TI 2	TI 3	$Ta_6Br_{12}^{2+}$
Source	CHESS F1	CHESS F1	BNL X25	ALS 8.2.1	BNL X25
Wavelength (Å)	0.919	0.919	0.976	0.9735	1.25
Resolution (Å)	50-5.8	50-6.4	40-7.1	40-6.8	40-7.4
R_{sym} (%)[a]	6.0 (64.0)	6.4 (62.8)	8.3 (54.6)	7.5 (59.8)	8.7 (42.0)
I/σI	17.6 (3.3)	15.2 (2.8)	16.7 (3.2)	19.9 (4.5)	12.0 (3.5)
Redundancy[b]	5.5	4.4	5.6	6.0	3.2
Completeness (%)	99.7 (99.9)	98.3 (97.8)	96.2 (96.8)	93.4 (95.9)	96.8 (97.5)
Phasing					
Number of sites		24	24	24	1
R_{cullis}(isomorphous)[c] acentric/centric		0.54/0.65	0.60/0.69	0.85/0.87	0.98/0.95
R_{cullis}(anomalous)[d]		0.90	0.90	0.89	1.0
Overall FOM[e] acentric/centric	0.44/0.41				

[a] $R_{sym} = \Sigma|I - \langle I \rangle|/I$, where I is observed intensity and $\langle I \rangle$ is average intensity obtained from multiple observations of symmetry-related reflections.

[b] Redundancy represents the ratio of the total number of measurements to the number of unique reflections.

[c] $R_{cullis}(iso) = = \Sigma| F_{PH} \pm F_P| - F_H(calc)/ \Sigma| F_{PH} \pm F_P|$ where $F_H(calc)$ is the calculated contribution of the heavy atom.

[d] $R_{cullis}(ano) = = \Sigma| \Delta_{ano}(obs) - \Delta_{ano}(cal)| / \Sigma|\Delta_{ano}(obs)$ for acentric reflections, where Δ_{ano} is the anomalous difference.

[e] $FOM = \langle | \Sigma P(\alpha) e^{i\alpha} / \Sigma P(\alpha) | \rangle$, where α is the phase and $P(\alpha)$ its probability distribution.

any potentially interesting deviations in channel conformation from being lost due to inappropriate assumptions about non-crystallographic symmetry. However at the resolution of this structure, the basic architecture of all the KvAP channels that form the asymmetric unit appears to be invariant. The equivalent structure of these non-crystallographic symmetry related channels is not surprising in the context of the unusual packing of this crystal form. Most structural features of each KvAP channel are immediately recognizable in the electron density map calculated with experimental phases including the ion conduction pore, the S1-S2 helices and the voltage-sensor paddle structure formed from the S3b and S4 segments (Fig. 21). Recognition of these features of the channel is facilitated by the remarkable similarity of the channels in this structure to the first KvAP channel structure crystallized in complex with Fab fragments (called the KvAP-6E1 Fab structure from here on). In both structures we find a canonical K^+ pore, encircled by S1-S2 helices, with the voltage-sensor paddles at the channel's perimeter.

Figure 21a-d shows that the pore from the KvAP-6E1 Fab structure fits well into the experimental density from this new crystal form. We expect that the structure of the selectivity filter and the region of the pore surrounding it should be invariant since this part of the channel is responsible for selective ion conduction[6,7]. However, the positions of the S5 and S6 helices at the level corresponding to the intracellular membrane leaflet have been observed in different conformations in different K^+ channel structures and this variation is thought to represent different gating states of the ion conduction pathway[6,14]. Within the limits of the resolution, we find no detectable differences in the conformations of any part of the pore in the two structures of the full-length KvAP channel. In both structures, the pore is in an "opened" configuration, with the S6 helices bent at the gating-hinge glycine to open the

diameter of the inner mouth of the pore and allow access to the ion conduction pathway. The S5 helices are also found in the same relationship to the S6 helices in both KvAP channel structures although the crystal packing forces applied to them are clearly different. In the KvAP-6E1 Fab structure, the S5 helices turn into a bend at the S4-S5 linker (Fig. 22c). In this new structure of the channel without Fab fragments, the S4-S5 linker is held straight, similar to what is seen in the isolated voltage-sensor domain structure, allowing the S5 helix to run directly into the voltage-sensor paddle (Fig. 22a,b).

Also seen in the KvAP-6E1 Fab structure, the S1 and S2 helices form a helical cuff that encircles the pore (Fig. 21e). A comparison of a channel subunit from the KvAP channel structures with and without Fab fragments shows that the configuration of the S1 and S2 helices is in fact essentially superimposable (Fig. 22b,c). In both we see the S1 and S2 helices running nearly parallel to the plane of the membrane with the short S1-S2 loop dipping downward towards the internal side of the channel. Glycosylation studies[106] and experiments with tethered pore blockers[107] both indicate that the S1-S2 loop in eukaryotic channels resides near the external membrane boundary. In addition, a recent study of KvAP channels in lipid vesicles using EPR spectroscopy indicates that residues N-terminal to the S1 helix, the S1-S2 loop and residues at the C-terminus of S2 are all water-accessible[108]. This would suggest that the position of the S1-S2 helices within the membrane is not the same as what we observe in the crystal structures. However, given that we see the very same configuration of the S1-S2 helices in two different structures of the full-length channel, we must take seriously the proposition that S1and S2 in the crystals are not too far from their membrane positions. In Chapter 6, we will investigate this possibility using functional

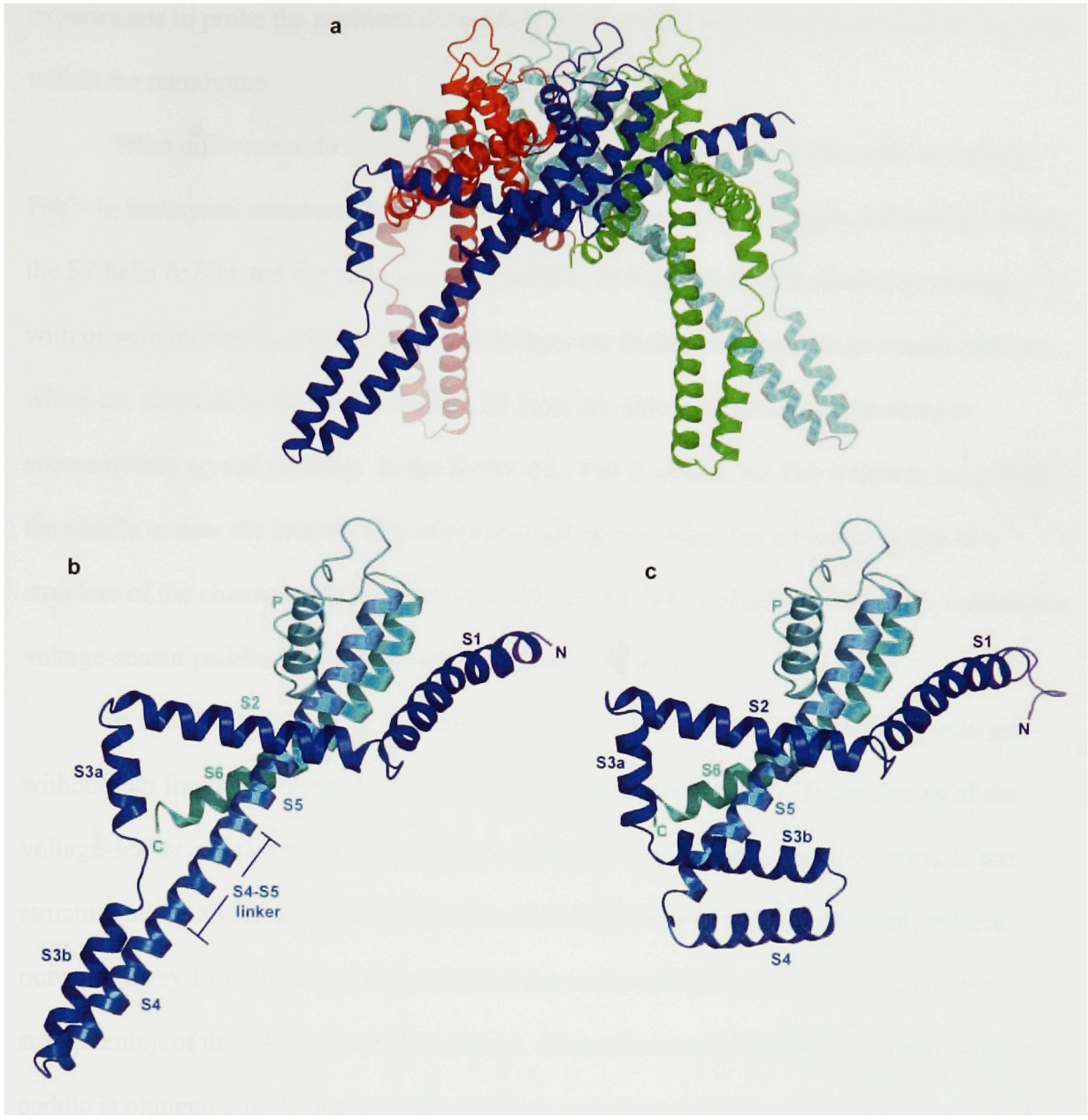

Figure 22

Architecture of the KvAP channel in the absence of Fab fragments. **a,** A representative channel from the asymmetric unit viewed from within the plane of the membrane with the intracellular solution below. Each subunit is colored differently. **b-c,** Comparison of the KvAP channel structure crystallized in the absence **(b)** or presence of Fab **(c)**. One subunit from each channel structure is shown from the same perspective. Helical segments are different shades of blue and labeled. N and C mark the termini.

experiments to probe the positions of residues within the S1and S2 helices in KvAP channels within the membrane.

What differences do we see between the KvAP channel structures, with or without Fab? In the crystal structure of the isolated KvAP voltage-sensor domain, salt bridges fasten the S2 helix to S3a and the voltage-sensor paddle. In both full-length channel structures, with or without Fab fragments, these salt bridges are broken and the voltage-sensor paddles, which are attached to S2 via the flexible S3 loop, are able to reposition themselves to accommodate crystal packing. In the KvAP-6E1 Fab structure, the Fab fragment has pulled the paddle to near the internal side of the channel by extending the S3 loop. In this new structure of the channel without Fab fragments, the S3 loop is also extended to re-position the voltage-sensor paddles in an even more extreme orientation.

In fact, the only striking difference between the KvAP channel structures, with and without Fab fragments, is the location of the voltage-sensor paddles. The positions of the voltage-sensor paddles in the two structures are related by a simple transformation. In the structure of the KvAP channel without Fab, the voltage-sensor paddle has simply rotated outward, away from the body of the channel due to the extension of the S3 loop and the straightening of the S4-S5 linker (Fig. 22b,c). From this transformation the voltage-sensor paddle is plunged into the intracellular solution, with the tip of the paddle lying nearly 50 Å beneath the internal membrane boundary. Why has such a non-physiological conformation been adopted? The mobility of the voltage-sensor paddle unit, unconstrained by the membrane, allows it to adapt to crystal packing.

Figure 23a shows that the six channels of the asymmetric unit come together to form an assembly with 4-3-2 symmetry—a bipyramid with a channel at each vertex. Every

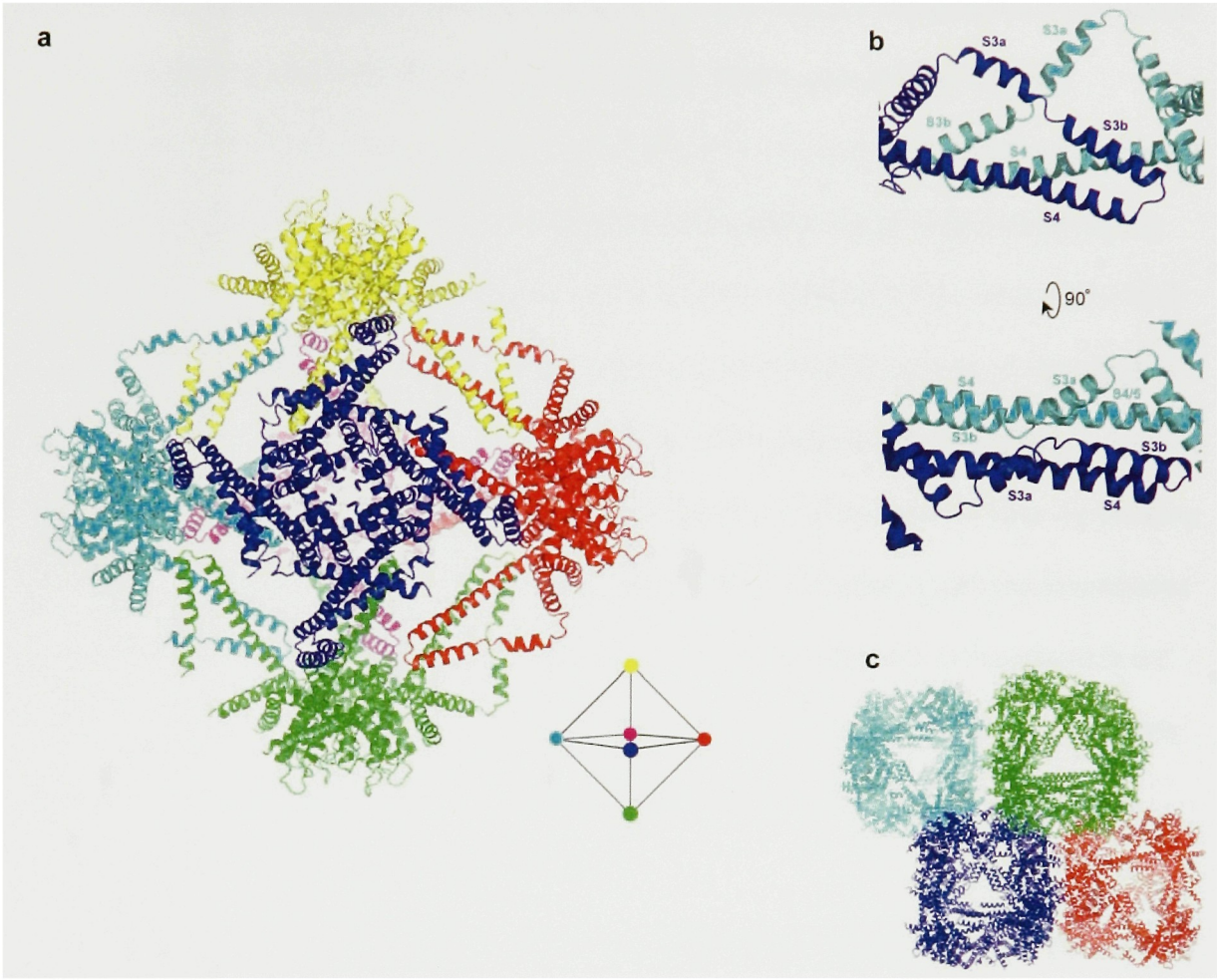

Figure 23

KvAP channel supra-structure. **a,** Each assymetric unit contains 6 KvAP channels (colored differently) that form a bipyramid with approximate 4-3-2 symmetry (inset). **b,** Each KvAP channel within the bipyramid makes symmetric contacts with 4 four other channels. Reciprocal channel contacts are formed between S3b and the S4-S5 linker of a neighboring channel. **c,** Packing of channel bipyramids with the unit cell.

channel in this supra-structure interacts identically with four other channels. Fairly extensive contacts are formed between channels in a set of symmetric interactions. In Figure 23b it can be seen that the S3b segment of the blue channel interacts with the straightened S4-S5 linker of the neighboring cyan channel and the S3b segment of the cyan channel interacts reciprocally with the straightened S4-S5 linker of the blue channel. The paddles are oriented so that the N-terminal portion of the S4 segment and its gating charge arginines are facing into the large cavity in the center of the channel assembly. This cavity is a little over 100 Å in diameter. This devilishly clever crystallographic solution binds all the mobile voltage-sensor paddles in a uniform way, holding them in a rigid configuration that allows crystallization to occur. Although more heterogeneous contacts are formed from the packing of channel assemblies against each other in the crystal (Fig. 23c), the symmetric interactions of the channels within a single bipyramid explains why all the channels in the structure are maintained in the same conformation. Ironically, without Fab fragments present to mediate crystal contacts, the channel found an alternate way of packing that was ultimately more "unnatural" than the KvAP-6E1 Fab structure.

This impressive packing has an important implication. In response to crystal packing forces, the voltage-sensor paddles do not come apart. In fact, the helix-turn-helix structure of the paddle is (within the limits of the resolution of this structure) identical to what we see in both the structures of KvAP-6E1 Fab and the isolated voltage-sensor domain-Fab complex (Fig. 21f.) This suggests that the structure of the paddle unit itself is uninfluenced by the Fab fragment bound to it. The repositioning of the paddle to accommodate very different crystallographic contacts reemphasizes that the paddle is a rigid unit but is attached to the channel through flexible connections that allow it to move. In the context of the channel

within the membrane, it is the planar 2-phase (aqueous-organic) constraint of the membrane that orients the voltage-sensor paddle with respect to the pore and the changing electric field that allows it to move within the membrane imposed constraints. When the channel is extracted from its native lipid environment, the dynamic voltage-sensor paddles are freed from these constraints and can move to extremes to form crystal contacts. Thus the non-physiological position of the voltage-sensor paddles in both structures of the KvAP channel can be explained by the fact that the detergent micelle is simply an inadequate substitute for the special physical and chemical properties of the planar membrane. The detergent micelle cannot mimic the planar arrangement of electrostatic and hydrophobic forces that confine the paddle to a physiological range of motion within the membrane. In contrast to the varied position of the paddles in the two KvAP channel structures, we find near superimposition of the pore and the S1-S2 helices. This difference highlights the unique mobility of the voltage-sensor paddle and makes sense in light of the paddle's functional requirement to move within the lipid in response to changes in membrane voltage.

We believe that the crystal structure of the KvAP channel without Fab fragments lends strong support to the idea that the voltage-sensor paddles are rigid units that exist at the protein-lipid interface, are attached to the body of the channel through flexible connections and are intrinsically very dynamic. While these properties enable the voltage-sensor paddle to transport gating charges through the lipid to open the pore, they also allow the paddles to move into unnatural conformations in the absence of the membrane.

The structure of the KvAP channel without Fab inspired us to return to functional assays to learn more about the native conformations of the channel. In the next chapter, we

use a biotin-avidin accessibility assay to probe the channel's structure within the membrane and learn more about the channel's voltage-dependent conformational changes.

CHAPTER 6: GATING CHARGE MOVEMENT IN KvAP

The first crystal structures of KvAP revealed that the gating charges reside in voltage-sensor paddles—helix-turn-helix structures that lie at the periphery of the channel and are attached to the pore through flexible hinges. In these structures the voltage sensors have adopted a non-native conformation, probably as a result of crystal packing constraints and the absence of a membrane. Despite uncertainties in the relationship between the KvAP crystal structures and the physiological conformations of the channel in the membrane, the first structural image of the channel suggested a simple mechanism of how gating charge could be translocated across the membrane: the voltage-sensor paddles act as hydrophobic cations attached to levers and are pulled through the lipid by the membrane's electric field. How much do the voltage-sensor paddles move as the channel gates? How can we relate the architecture of the channel in the crystal structures to the conformations of the channel functioning within a membrane? To address these questions we have developed a method to probe the structure of KvAP while the channels are embedded in the membrane undergoing voltage-dependent gating. By evaluating the accessibility of biotin tethered at different sites

on the channel to avidin, we generate constraints on the position of these amino acids relative to the plane of the membrane. We are thus able to map the topology of the voltage sensor and compare it to what we observe in the crystal structures. Importantly, we can use the membrane voltage to drive the channel into different voltage-dependent conformations and investigate the resulting differences in avidin accessibility. In this study we first calibrate our assay on the pore of KvAP whose structure and orientation within the membrane we know. With increased confidence that this assay is truly reporting a position's depth within the membrane we apply this molecular measurement to the voltage sensor.

The idea behind the experiment is outlined in Figure 24a. Single cysteine residues are introduced at different sites on the channel, the cysteines are reacted with tethered biotin reagents and then the channels are reconstituted into planar membranes. In functioning channels we then determine whether avidin binds from the internal or external side of the membrane and whether binding depends on membrane depolarization. In addition, we investigate whether the accessibility to avidin for a given site on the channel changes if a longer or shorter biotin tether is used. Using biotin tethers of different lengths allows us to access nearly every site studied on the channel and gives us multiple independent constraints on the depth of a single site within the membrane.

Avidin is a large (~ 56 by 50 by 40 Å) rigid protein[109] (Fig. 24b). It is far too large to fit into any clefts on the channel, and it should not be able to penetrate into the membrane or be sensitive to local distortions of the lipid membrane that may occur immediately surrounding the channel. Biotin accessibility to avidin should therefore depend on the depth of the biotinylated residue beneath the surface of the membrane and the length of the biotin tether. In this way this assay reports distinctly different information than what is conveyed by

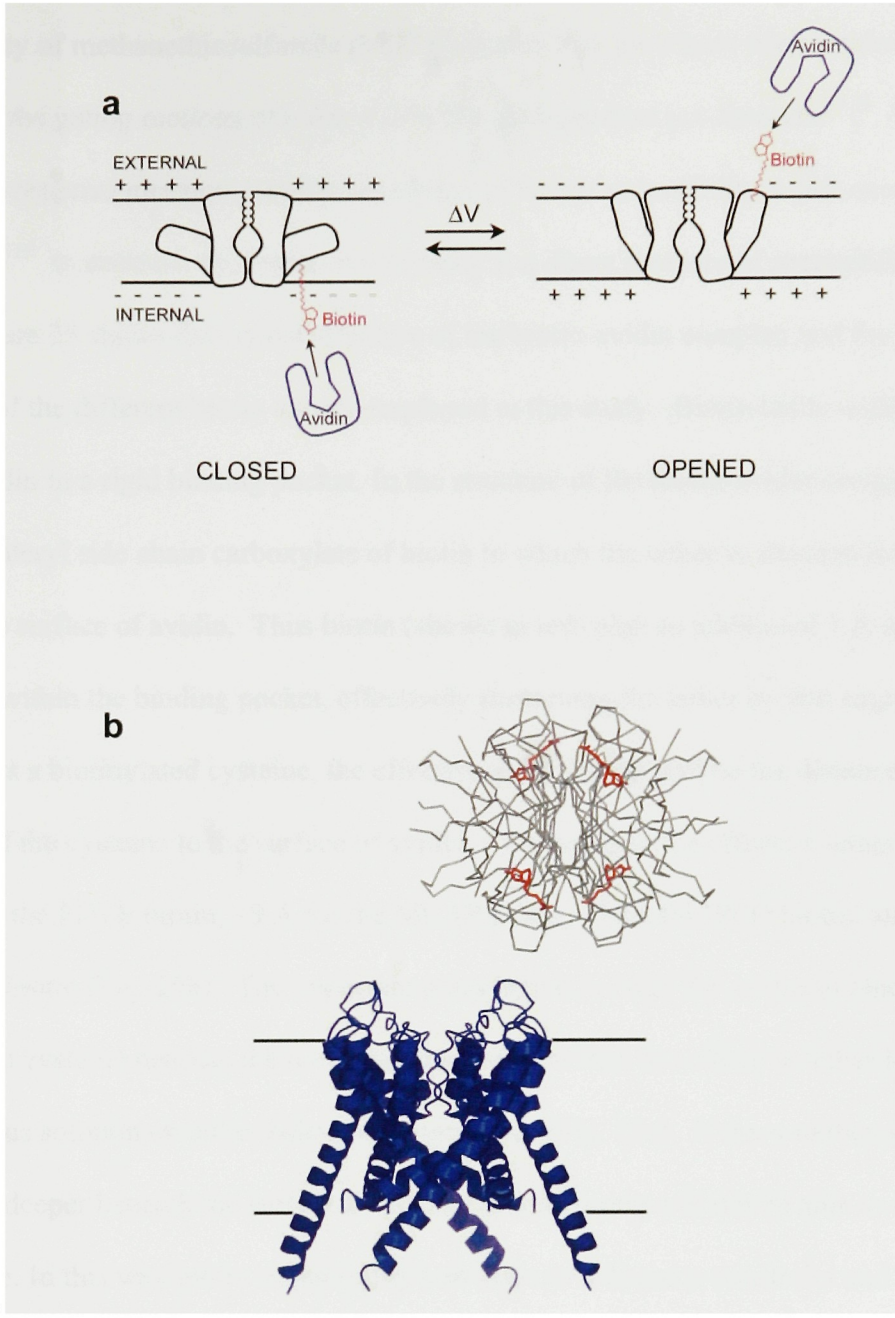

Figure 24
Using avidin and tethered biotin as a molecular ruler to measure the positions of amino-acids on the channel relative to the membrane plane. **a,** Experimental strategy: KvAP channels with biotin tethered to a cysteine can be "grabbed" by avidin in solution to affect channel function and indicate accessibility. b, Comparison of the size of the KvAP pore with the avidin tetramer. KvAP pore shown in blue ribbon as viewed from the side with the approximate membrane boundaries marked. Avidin tetramer (Cα trace, Protein Data Bank code 1AVD) with biotin (red) in its binding pockets.

the reactivity of methanethiosulfonate (MTS) reagents that have been used extensively to investigate the gating motions of eukaryotic voltage-dependent ion channels[23-25]. Studies using MTS reagents measure cysteine reactivity, of which accessibility is just one component[110]. In contrast, the biotin-avidin assay is a direct measure of accessibility.

Figure 25 shows the crystal structure of the biotin-avidin complex and the chemical structures of the different biotin tethers employed in this study. Biotin binds within a deep cleft in avidin in a rigid binding pocket. In the structure of the biotin-avidin complex (Fig. 25a), the valeryl side chain carboxylate of biotin to which the tether is attached lies 7 Å beneath the surface of avidin. Thus biotin (shown in red) plus an additional 7 Å of the tether are buried within the binding pocket, effectively shortening the tether by that amount. When avidin binds a biotinylated cysteine, the effective tether length will be the distance from the α-carbon of the cysteine to the surface of avidin. We estimate the effective tether length to be ~1Å for the PDTE biotin, ~9 Å for the MCAP biotin, ~10Å for IPEO biotin, and ~17Å for the BCAC biotin (Fig. 25b). The important point is that in order for avidin to bind to a biotinylated cysteine residue, the α-carbon must come within the effective tether length of the bulk aqueous solution on either side of the membrane (Fig. 25a). If the α-carbon is positioned deeper beneath the surface of the membrane, biotin will not be able to reach its binding site. In this way biotin accessibility translates to a distance constraint and by using tethers of multiple lengths we obtain multiple constraints for a given position.

How effectively can our assay measure positional depth within the membrane? To test the limits of our assay we investigated the accessibility of sites on the pore and then mapped the results onto the KvAP pore structure. Wild-type KvAP channels contain a single cysteine (C247) on the C-terminus, which was mutated to serine (without affecting function)

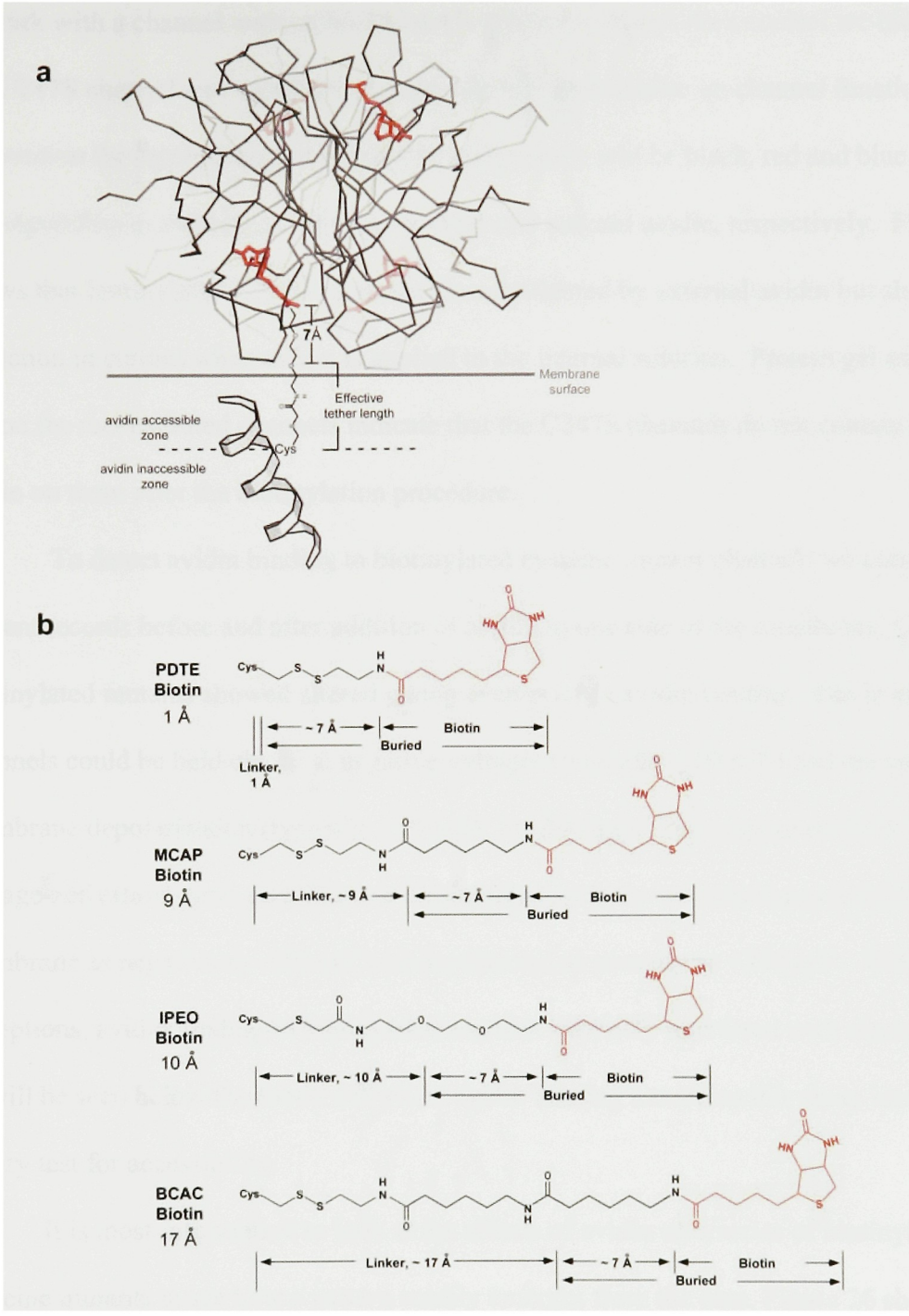

Figure 25

The effective linker length of biotin determines accessibility to avidin. **a,** Crystal structure of biotin (red) bound in a deep pocket in avidin (Cα trace, black wire). A scaled chemical structure of the IPEO tether is shown attached to biotin. Biotinylated cysteine residues will only be able to bind to avidin if their Cα lies within the effective tether length from the membrane surface (in the avidin accessible zone.) **b,** Chemical structures of the biotin reagents used in this study and their estimated effective linker lengths.

to work with a channel without background cysteine residues. As a control we biotinylated the C247S channel and tested for non-specific effects of avidin on channel function. Our convention for representing data throughout this study will be black, red and blue traces corresponding to control (no avidin), external and internal avidin, respectively. Figure 26a shows that biotinylated C247S channels are not affected by external avidin but show a small reduction in current when avidin is applied to the internal solution. Protein gel assays carried out on the reconstituted channels indicate that the C247S channels do not contain detectable biotin on them after the biotinylation procedure.

To detect avidin binding to biotinylated cysteine mutant channels we compared current records before and after addition of avidin to one side of the membrane. Certain biotinylated mutants showed altered gating even prior to avidin binding. But in all cases channels could be held closed at negative voltages (typically -100 mV) and opened with membrane depolarization (typically +100 mV for 200 ms). To compensate for the shifted voltage-activation curve seen in some biotinylated mutants, we sometimes held the membrane as negative as -140 mV and depolarized as strongly as +200 mV. With few exceptions, avidin binding to biotinylated mutants markedly interfered with channel function; as will be seen below the robust effects of avidin binding transform this assay into a virtually binary test for accessibility.

It is most informative to look at the effects of avidin on a series of biotinylated cysteine mutants to see how a pattern readily emerges from the data. Figure 26 shows representative experiments for six sites staggered along the S5 helix of the pore. As we move from sites at the N-terminus to sites at the C-terminus of S5, traversing the membrane, how does avidin accessibility change? Addition of avidin to the external side of the membrane

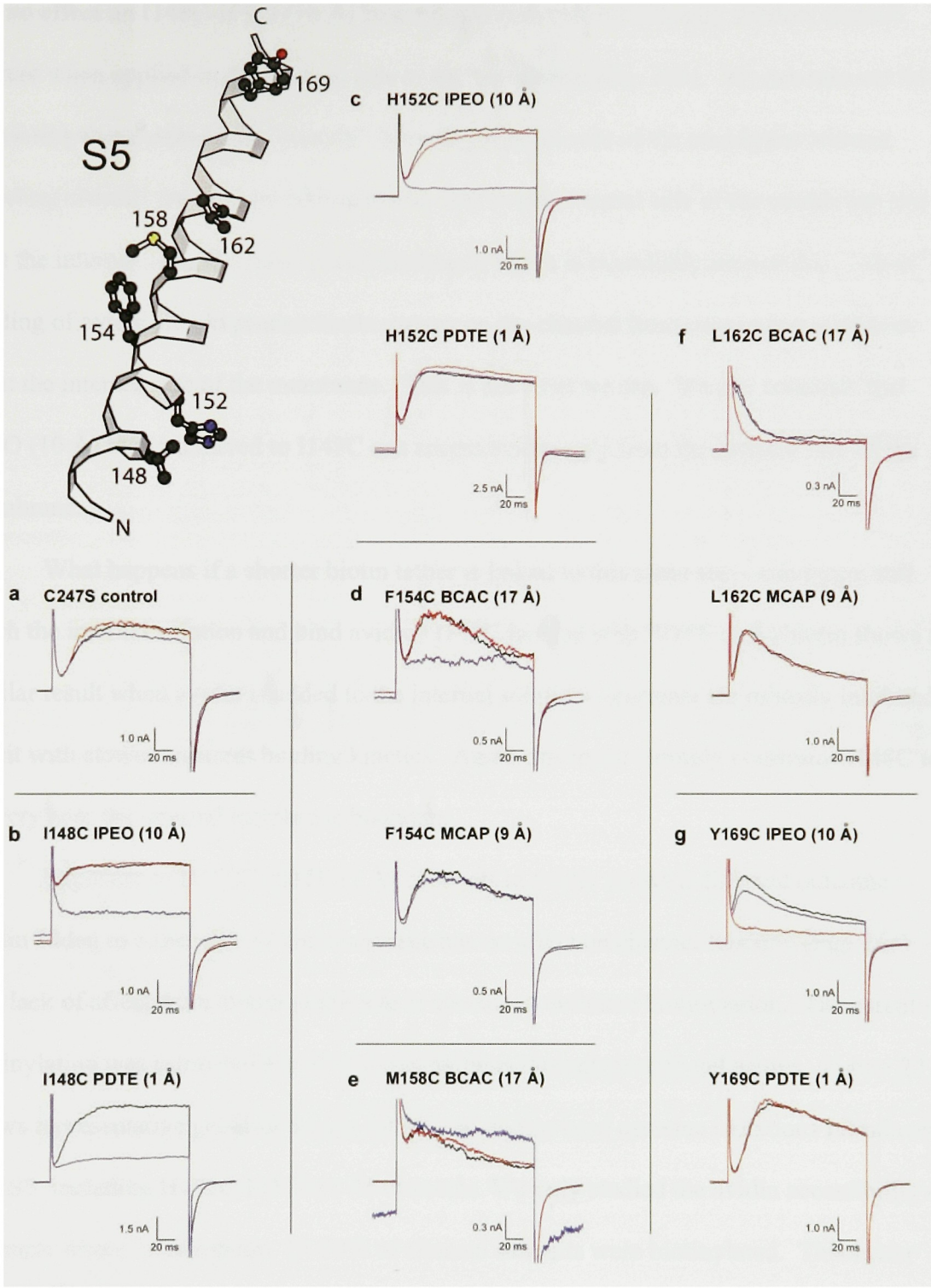

Figure 26

Representative traces showing the effects of avidin on biotinylated control **(a)** and S5 cysteine mutant channels **(b-g)**. An average of 2-3 traces is shown prior to avidin addition (black), after avidin addition to the extracellular side of the membrane (red) or after addition of avidin to the intracellular side of the membrane (blue).

has no effect on I148C-IPEO (10 Å) biotinylated channels but strongly inhibits channel current when applied to the internal side of the membrane (Fig. 26b). We can rule out the possibility that avidin binds "silently" from the external side of the membrane without affecting channel function by adding avidin first to the external side of the membrane and then the internal side. Because avidin binding to biotin is essentially irreversible, "silent" binding of avidin should protect biotin groups on the channel from subsequent inhibition from the internal side of the membrane. This is not what we see. We can conclude that IPEO (10 Å) biotin tethered to I148C can access avidin only from the internal side of the membrane.

What happens if a shorter biotin tether is linked to this same site—can biotin still reach the internal solution and bind avidin? I148C labeled with PDTE (1 Å) biotin shows a similar result when avidin is added to the internal solution—currents are robustly inhibited, albeit with slower apparent binding kinetics. Again this result strongly constrains I148C to be very near the internal membrane boundary.

Exposure of H152C-PDTE (1 Å) channels to avidin shows a different outcome—avidin added to either side of the membrane has no affect on channel function (Fig. 26c). The lack of affect from avidin at this site is not due to deficient biotinylation. The extent of biotinylation was estimated for all cysteine mutants through protein gel assays. Figure 27 shows representative gel-shift assays for several biotinylated cysteine mutations introduced into S5, including H152C-PDTE (1 Å) channels. We only studied the avidin accessibility of channels where, at minimum, 25-30% of channel subunits were biotinylated. This lower level of biotinylation translates to 70-75% of channel tetramers having at least one

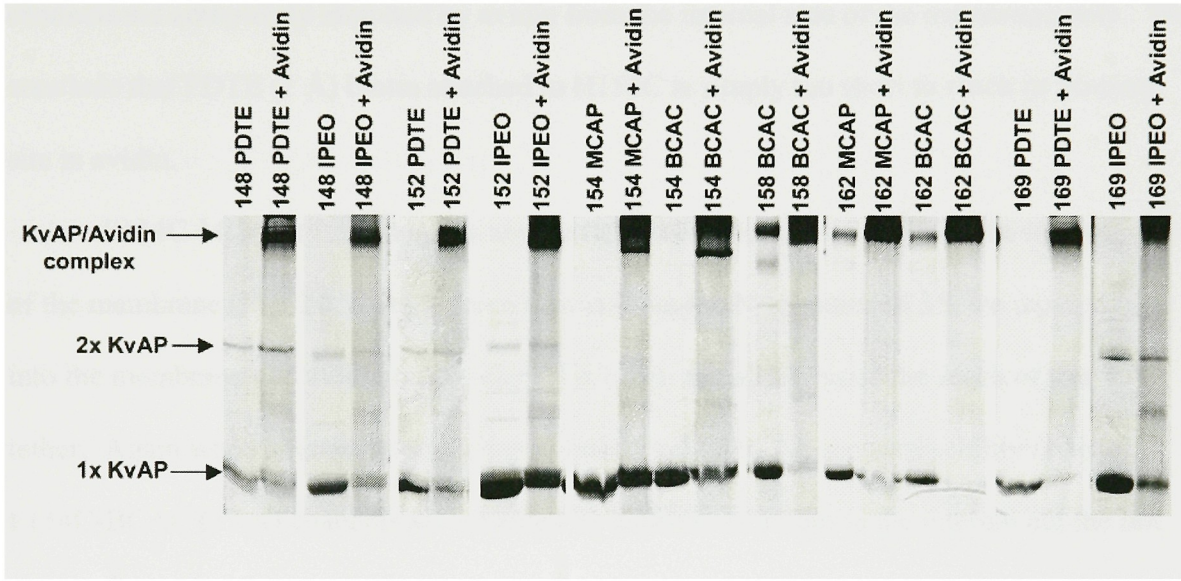

Figure 27

Estimating the extent of biotinylation through gel-shift assays. Biotinylated cysteine mutant channels were reconstituted and equal volumes of avidin or buffer were added to the channel containing vesicles. Vesicles were lysed by the addition of SDS sample buffer and were analyzed by SDS-PAGE. Most channels run as monomers (1x KvAP). For some mutations, disulfide-linked dimers are visible (2x KvAP). M158C and L162C channels show bands corresponding to non-disulfide linked channel tetramers at almost the same molecular weight as the KvAP/avidin complex. Extent of biotinylation can be estimated by the relative decrease in KvAP monomer band and increase in the KvAP/avidin complex band.

biotinylated subunit (i.e. $1-(0.75)^4$)—sufficient to see clear (although not necessarily complete) effects from avidin binding. Lack of effect from avidin at H152C-PDTE (1 Å) could reflect silent avidin binding or alternatively a longer biotin tether is required at this site in order to reach the intracellular solution and allow avidin binding to occur. When biotin is linked through a longer tether to H152C, it becomes accessible: H152C-IPEO (10 Å) channels are completely inhibited by avidin from the internal side of the membrane only. We conclude that PDTE (1 Å) biotin attached to H152C is simply too short to reach its binding site in avidin.

F154C-MCAP (9 Å) channels are unaffected by addition of avidin to the internal side of the membrane (Fig. 26d). As we move away from the N-terminus of S5, we move deeper into the membrane and avidin in the internal solution remains beyond the reach of this 9 Å tether. Again when a longer biotin tether is linked to F154C we see accessibility restored. F154C-BCAC (17 Å) channels are inhibited by addition of avidin to the internal but the not the external side of the membrane.

M158C-BCAC (17 Å) channels are unaffected by the addition of avidin to the external solution (Fig. 26e). Subsequent addition of internal avidin to the same membrane dramatically alters the gating of M158C-BCAC (17 Å) channels, leading to an increase in current at both positive and negative voltages. This effect, though different from what we see at other positions on the pore, is very reproducible and gives us confidence that the changes in channel function are due to internal avidin binding.

L162C is the most N-terminal position on S5 that we studied where avidin can bind from the external side of the membrane, although only when the site is labeled with the longest biotin tether. L162C-BCAC (17 Å) channels are not affected by internal avidin but

are inhibited by external avidin (Fig. 26f). A transition occurs on the S5 helix between residues M158 and L162, from sites that are able to bind avidin in the internal solution to sites that are able to bind avidin in the external solution. This transition presumably defines the mid-point of the membrane. Given that L162C lies near the middle of the membrane, it is not surprising that the shorter MCAP (9 Å) biotin attached to L162C is unable to reach avidin in the extracellular solution.

Residues near the C-terminus of S5, closer to the external boundary of the membrane, are accessible to external avidin when labeled with shorter biotin tethers. Y169C-IPEO (10 Å) channels are inhibited completely from external but not internal avidin; the small reduction by internal avidin (Fig. 26g) is similar to the control (Fig. 26a). Y169C-PDTE (1 Å) is unaffected by external avidin and must still lie several angstroms beneath the surface of the membrane.

From this scan of the S5 helix we see that avidin binding significantly disrupts channel function, allowing us to readily differentiate between accessible and inaccessible sites. We find that avidin accessibility to a site is dependent on the position of the site within the helix and the length of the biotin tether. This pattern of differential accessibility that we observe immediately suggests that our measurement detects positional changes in membrane depth.

Figure 28 maps the accessibility data for the four biotin tethers onto the structure of the KvAP pore. Data from channels biotinylated with MCAP biotin and IPEO biotin have been grouped together due to the similar length of their tether. These two tethers were used interchangeably in our study to obtain the greatest coverage of sites. MCAP biotin's greater reactivity towards free cysteines on the channel, owing to its methanethiosulfonate versus

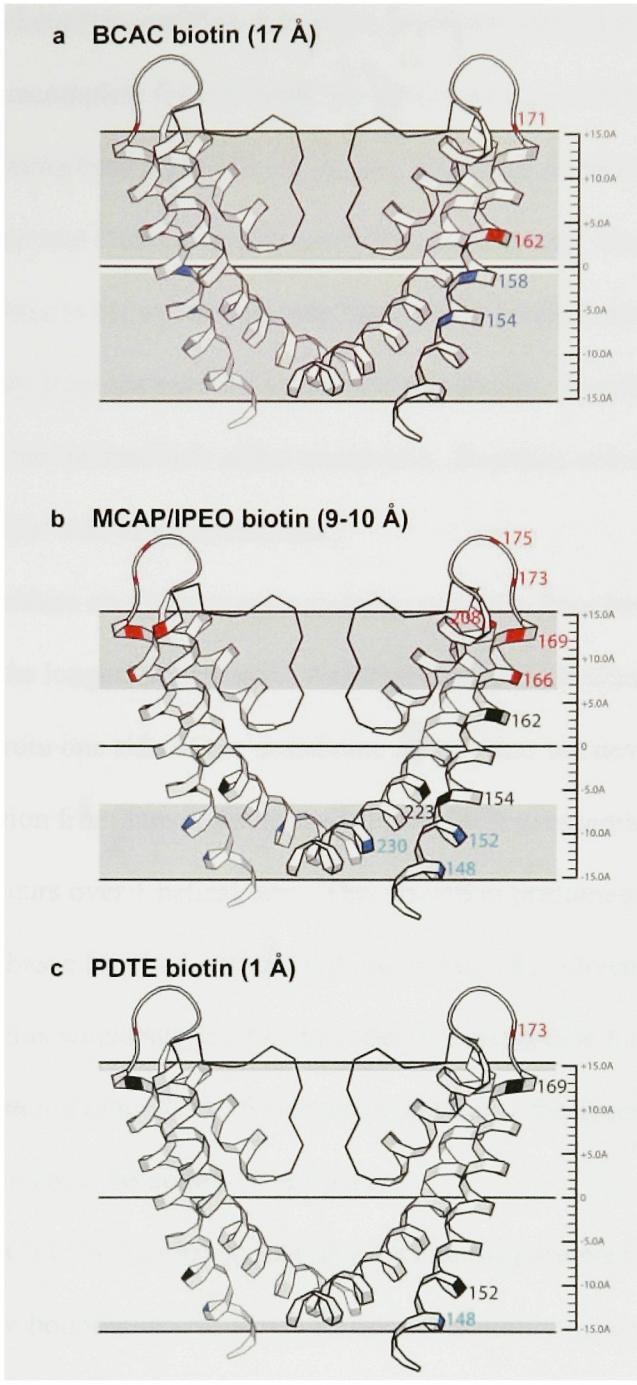

Figure 28

Avidin accessibility mapped onto the KvAP pore. Two subunits of the KvAP pore are shown. Residues are labeled by their number in the amino-acid sequence and are colored based on their avidin accessibility when labeled with **a**, BCAC, **b**, IPEO or MCAP and **c**, PDTE biotin. Red residues are accessible only from the external side of the membrane, blue residues are accessible only from the internal side of the membrane and black residues are inaccessible from either side of the membrane. Grey regions mark the estimated limits of avidin accessibility for each length biotin tether.

iodoacetamide group chemistry, enabled us to study positions where biotinylation with IPEO (10 Å) biotin was too incomplete for confident evaluation of accessibility. Three sites on the channel were studied using both the IPEO (10 Å) and MCAP (9 Å) biotin tethers and the accessibility in all cases was found to be the same (data not shown). Residues in Figure 28 are color coded according to the membrane side from which avidin bound. Residues colored red can bind avidin only from the external side of the membrane. Residues colored blue can bind avidin only from the internal side of the membrane. Residues colored black are unable to bind avidin from either side of the membrane.

Notably, no residues on the pore are accessible to avidin from both sides of the membrane even with the longest tether used. Avidin can bind at all sites biotinylated with BCAC (17 Å) biotin from one side of the membrane or the other but never from both sides (Fig. 28a). The transition from internally accessible (M158C) to externally accessible (L162C) sites in S5 occurs over 1 helical turn. This transition presumably defines the mid-point of the lipid membrane (marked with a solid line in Fig. 28). Given our estimate that the BCAC tether is 17 Å, this would suggest that the effective membrane thickness as a barrier to avidin accessibility is minimally ~29 Å. Since we do not know the accessibility of residues 159-161, the membrane could be up to ~10 Å thicker.

From the BCAC (17 Å) biotin accessibility data on the pore we can define approximate membrane boundaries. How well do our accessibility measurements with the shorter biotin tethers correspond to these membrane boundaries? Figure 28b shows the combined accessibility data for residues biotinylated with IPEO (10 Å) and MCAP (9 Å) biotin. For sites biotinylated with IPEO (10 Å) and MCAP (9 Å) biotin, avidin should be able to bind biotin attached to all residues whose α-carbon lies within 9-10 Å of the external

and internal solution (area shaded light grey in Fig. 28b), leaving a ~ 13 Å band of sites in the middle of the membrane that cannot bind avidin at all. The data are remarkably consistent with this image. Residues F154C and L162C are accessible when labeled with BCAC biotin (Fig. 26d,f) but are inaccessible when labeled with MCAP (9 Å) or IPEO (10 Å) biotin. F154 and L162 lie 11 Å apart which would suggest from our measurement with MCAP (9 Å) biotin, that the membrane is minimally 29 Å thick as a barrier to avidin accessibility—the same as our estimate derived from accessibility of residues labeled with BCAC (17 Å) biotin. Flanking these inaccessible sites in the central portion of the membrane are multiple residues that are accessible from one side of the membrane or the other when labeled with MCAP (9 Å) or IPEO (10 Å) biotin. These accessible residues lie within about 10 Å of the external or internal membrane boundary.

PDTE biotin has a very short tether (estimated to be ~1 Å) and only residues very near the membrane surface should be accessible to avidin when labeled with PDTE biotin. We can empirically define the limits of avidin accessibility to PDTE (1 Å) labeled sites by asking: how close can two PDTE (1 Å) biotinylated sites lie and still bind avidin from opposite sides of the membrane? The maximum distance between accessible sites for the PDTE (1 Å) biotin tether is defined by the accessibility of I148C-PDTE (1 Å) to internal avidin and Y173C-PDTE (1 Å) to external avidin. These two residues are separated by 31 Å. H152C-PDTE (1 Å) and Y169C-PDTE (1 Å), 23 Å apart, both lie too far beneath the membrane surface to bind avidin. Thus the accessibility data from the pore indicates that when the α-carbon of PDTE-biotinylated residues lies within a central band of membrane 23-31 Å thick, these residues will be completely inaccessible to avidin. This will be an important point later when considering the accessibility data for the voltage-sensor paddle.

The calibration of our assay using the KvAP pore suggests that using biotin-avidin accessibility data we can reliably deduce the approximate depth of a residue relative to the plane of the membrane. We now turn to the voltage sensor whose topology in the membrane we know less about.

The S1 and S2 helices

In the crystal structures of the KvAP channel with and without Fab fragments, the S1 and S2 segments form a helical cuff that surrounds the pore. The S1 and S2 helices both start and end in what would correspond to the interior of the membrane with the short loop connecting S1 and S2 dipping down towards the middle of the membrane. This is a surprising configuration given that the S1–S2 loops of *Shaker* and some other eukaryotic Kv channels are glycosylated[106], indicating an extracellular location. The S1-S2 loop in *Shaker* is 19 amino acids longer than in KvAP, providing the possibility that the loop could snake out of the membrane and back to join S1-S2 helices arranged as in the KvAP structure. However a recent study of KvAP channels in lipid vesicles using electron paramagnetic resonance spectroscopy suggests that residues in the S1-S2 loop are water-accessible[108]. Given these apparent discrepancies, how does the configuration of the S1-S2 helices in the crystal structures relate to their position in functioning channels in membranes?

We investigated the accessibility of the S1 and S2 segments of KvAP with our biotin-avidin assay to learn more about their orientation in the membrane. As seen in the pore, most sites on S1 and S2 were robustly affected by avidin binding and we could readily differentiate between internally accessible, externally accessible, and inaccessible sites (Fig. 29). For residues near both ends of the S2 helix we observed that avidin binding has an

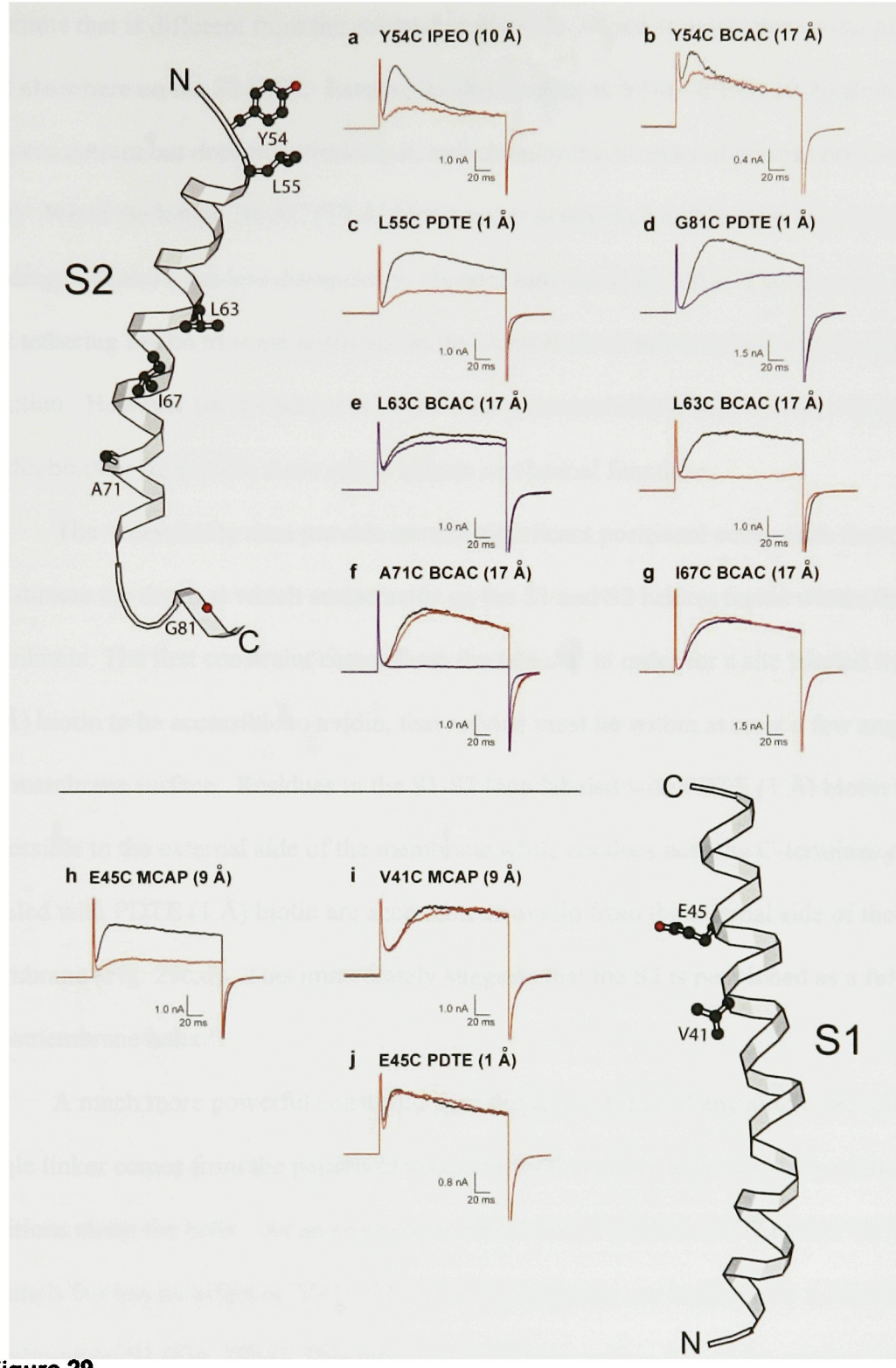

Figure 29

Representative traces showing the effect of avidin on biotinylated cysteines in S2 **(a-g)** and S1 **(h-i)**. An average of 2-3 current traces is shown in the absence (black), or presence of external (red) or internal (blue) avidin.

outcome that is different from the complete inhibition we see at most sites on the pore, S1 and elsewhere on the S2 helix. External avidin binding to Y54C-IPEO (10 Å) channels reduces current but does not eliminate it, and changes the kinetics of current activation (Fig. 29a). When the longer BCAC (17 Å) biotin tether is attached to this same site, avidin binding becomes even less disruptive to channel function (Fig. 29b). These results indicate that tethering avidin to some positions on the channel alters but does not abolish channel function. However for the purposes of our binary accessibility assay, we can still detect avidin binding from these more subtle affects on channel function.

The accessibility data provide several significant positional constraints that enable us to estimate the depth at which amino acids on the S1 and S2 helices reside within the membrane. The first constraint comes from the fact that in order for a site labeled with PDTE (1 Å) biotin to be accessible to avidin, that residue must lie within at most a few angstroms of the membrane surface. Residues in the S1-S2 loop labeled with PDTE (1 Å) biotin are accessible to the external side of the membrane while residues near the C-terminus of S2 labeled with PDTE (1 Å) biotin are accessible to avidin from the internal side of the membrane (Fig. 29c,d). This immediately suggests that the S2 is positioned as a fully transmembrane helix.

A much more powerful constraint than the accessibility of any single site with any single linker comes from the pattern of accessibility that arises from the study of different positions along the helix. As an example, external avidin inhibits E45C-MCAP (9 Å) channels but has no affect on V41C-MCAP (9 Å) channels one helical turn further into the membrane on S1 (Fig. 29h,i). This tells us that E45 lies within 9 Å of the external membrane but V41 lies further than 9Å beneath the membrane surface and so cannot be captured by

avidin. Complementary information is also derived from comparing the same site with tethers of different length. If we link the PDTE (1 Å) tether to E45C, external avidin has no affect (Fig. 29j). These experiments indicate that E45C is within 9 Å of the external solution (because when labeled with MCAP biotin it is accessible to external avidin) but is at least several angstroms from the membrane surface (because when labeled with PDTE biotin it is inaccessible to external avidin). The total pattern of accessibility that we see along the S1 and S2 helices provides information about the position of the helix with respect to the membrane.

It is important to note that as in the pore, no residues on S1 or S2 are accessible to both sides of the membrane even with the longest linker used. In fact, on S2 we find a site that cannot be accessed from either side of the membrane even when labeled with BCAC (17 Å) biotin. Figure 29e,f shows that L63C-BCAC (17 Å) binds external but not internal avidin while A71C-BCAC (17 Å) binds internal but not external avidin. I67C-BCAC (17 Å), which lies between these externally and internally accessible sites, is unaffected by avidin added to either side of the membrane (Fig. 29g). Silent avidin binding within the middle of the helix seems unlikely, particularly in the context of the complete inhibition we see at neighboring sites. Another possibility is that BCAC (17 Å) biotin tethered to I67C is somehow buried within the protein or distorted so that it cannot quite reach avidin on either side of the membrane. However we see no evidence that biotin is sequestered within the membrane for any site on the pore which we know to lie at the center of the channel and must make contacts with the surrounding voltage sensors. An alternative possibility is that the effective length of the BCAC (17 Å) tether is in fact less than half the width of the membrane and

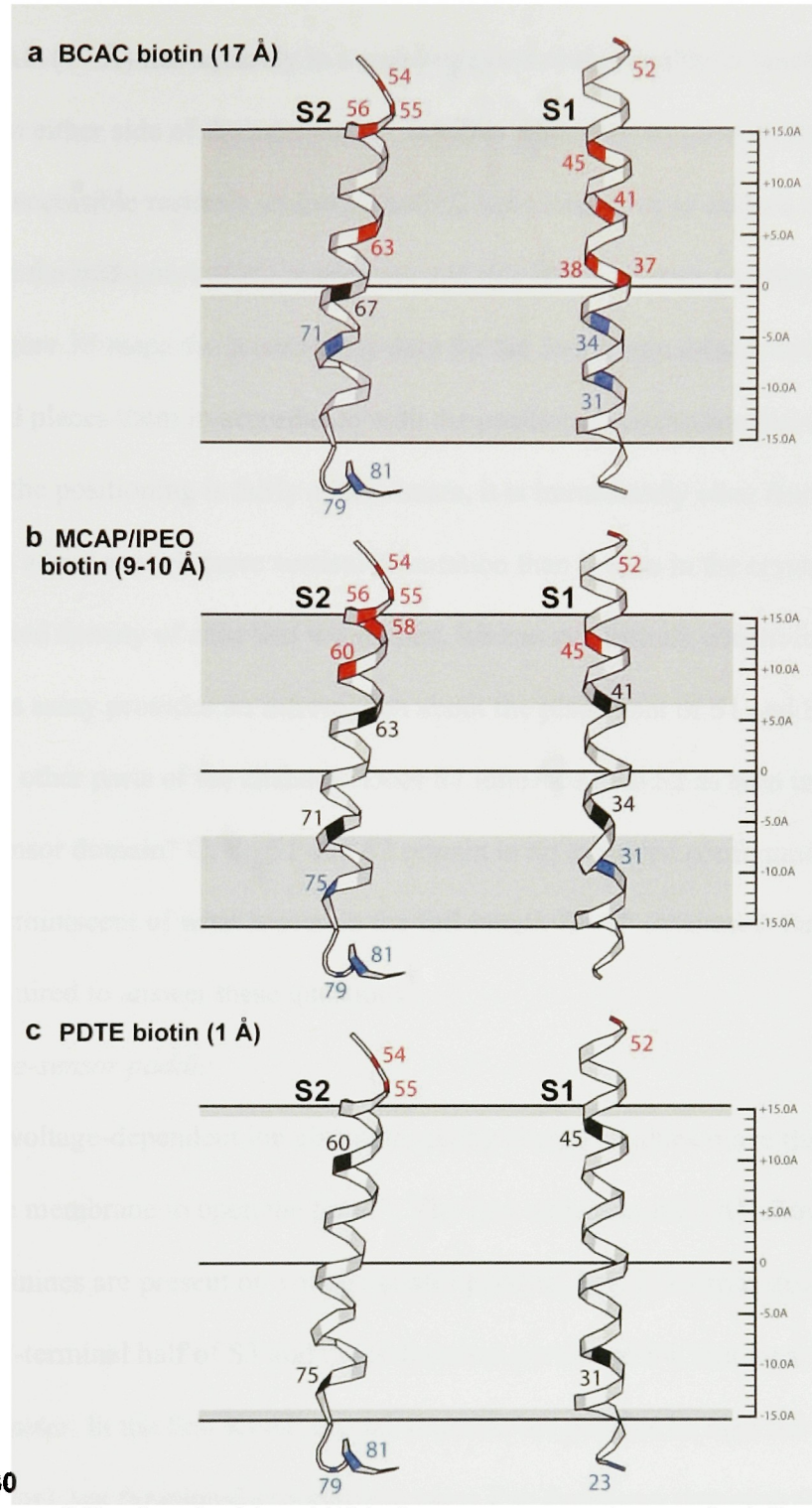

Figure 30

Avidin accessibility data for S1 and S2 indicate a transmembrane orientation. S1 and S2 are approximately positioned within the membrane to be in agreement with the biotin-avidin accessibility constraints. Residues are colored based on their avidin accessibility when labeled with **a,** BCAC biotin, **b,** IPEO or MCAP biotin and **c,** PDTE biotin. Red residues indicate accessiblity to external avidin only, blue residues indicate internal accessibility only and black residues are inaccessible.

I67C-BCAC (17 Å) lies squarely in a narrow region that is unable to reach avidin in the solution on either side of the membrane. In either case the transition from externally to internally accessible residues on the S1 and S2 helix allows us to deduce which residues reside near the mid-point of the membrane and this forms another positional constraint.

Figure 30 maps the accessibility data for the four biotin tethers onto the S1 and S2 helices and places them in accordance with the positional constraints derived from the data. Although the positioning is fairly approximate, it is immediately clear from these data that the helices adopt a much more vertical orientation than is seen in the crystal structure. Due to the limited density of sites that we studied, we can not entirely constrain the pitch of either helix. This assay provides no information about the placement of S1 and S2 relative to each other or to other parts of the channel. Does S1 interface with S2 as seen in the isolated voltage-sensor domain? Or do S1 and S2 remain in an extended configuration that encircles the pore reminiscent of what is seen in the full-length KvAP structure? Further experiments will be required to answer these questions.

The voltage-sensor paddle

In voltage-dependent ion channels, gating charge residues move through the electric field of the membrane to open the pore[94]. The first structure of KvAP shows that the gating charge arginines are present on voltage-sensor paddles, helical hairpin structures formed from the C-terminal half of S3 and the N-terminal portion of S4, that lie at the channel's outer perimeter. In the first KvAP crystal structure the paddles lie near the intracellular side of the channel, yet functional experiments using Fab fragments demonstrate that the paddles become exposed to the extracellular solution during membrane depolarization. These observations suggest that the voltage-sensor paddles might move a large distance through the

lipid membrane in response to changes in membrane voltage. How deep inside the membrane do the paddles reside when the membrane is hyperpolarized and far do they move when the channel opens?

In an initial study we tested the motions of the voltage-sensor paddles by site-specifically labeling multiple residues on the paddle with IPEO biotin and analyzing the accessibility of these sites to avidin. Here we present the results from that initial study against the backdrop of our accessibility measurements on the pore and S1- S2 helices, which provide an important comparison. In addition we investigate the accessibility of sites on the paddle labeled with longer and shorter biotin tethers to obtain additional constraints that help us to refine our model of the gating motions of the paddle.

Figure 31 shows data from our scan of sites on the voltage-sensor paddle labeled with BCAC (17 Å), IPEO (10 Å) and PDTE (1 Å) biotin tethers (MCAP biotin was not used). Avidin binding had detectable effects on channel function for all sites on the voltage-sensor paddle (with a single exception on S3b), enabling us to derive a clear pattern of accessibility for the three biotin tethers. In many cases, avidin binding led to complete inhibition. Partial inhibition for certain sites on S4 could be explained by incomplete biotinylation as determined by protein gel assays. For most sites on S3b, avidin binding led to partial inhibition with altered kinetics (Fig. 31a,b), reminiscent of the effects of avidin binding seen at sites near the N- and C-terminus of S2 (Fig. 29a,b). We could not detect changes to L108C-BCAC (17 Å) channel function after avidin addition, although avidin binding resulted in partial inhibition when L108C was labeled with a shorter biotin tether. Avidin binding to this site may be functionally silent if the tether is sufficiently long.

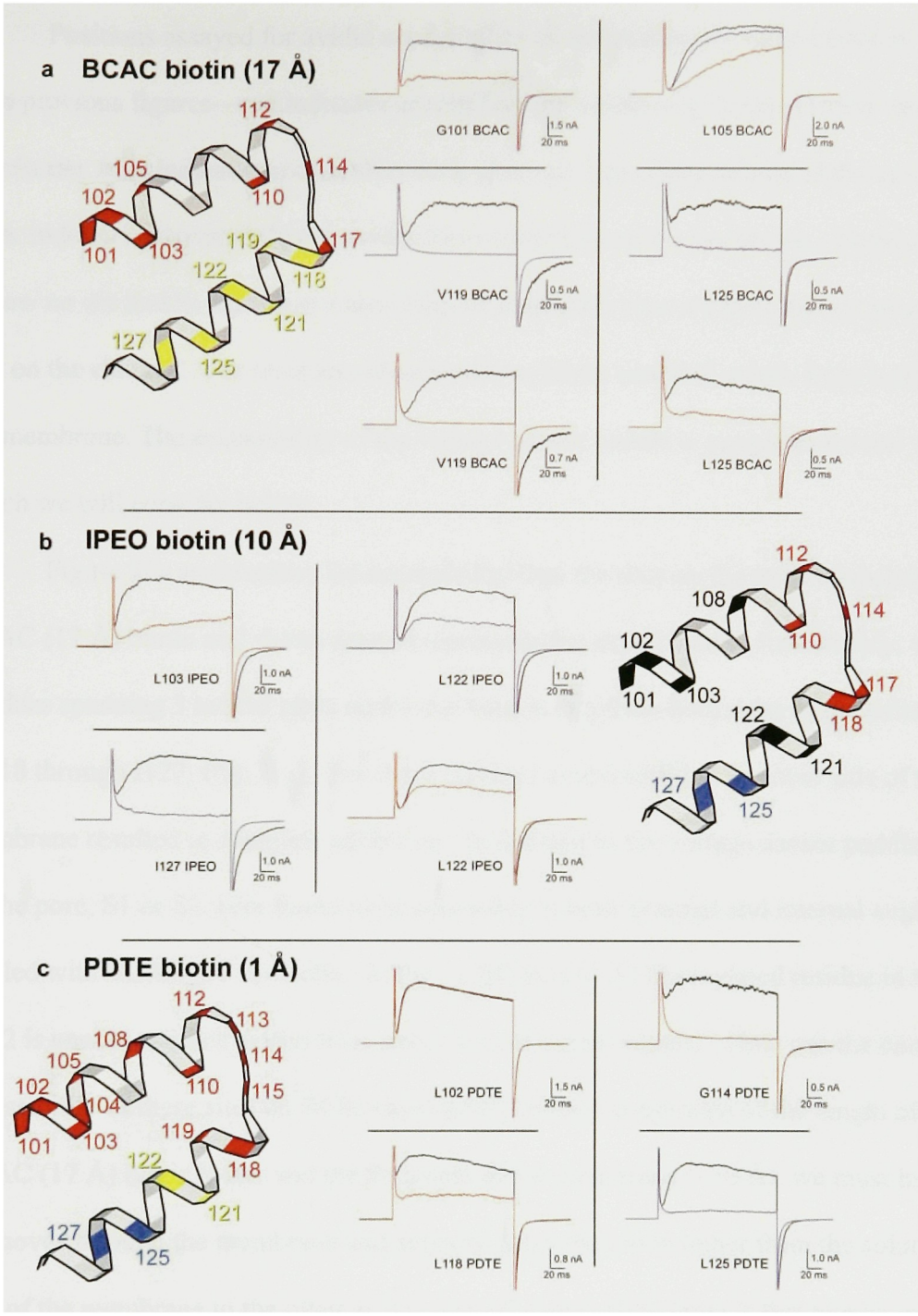

Figure 31

Avidin accessibility of the voltage-sensor paddle. Effects of avidin on paddle cysteine mutants biotinylated with **a,** BCAC, **b,** IPEO or MCAP and **c,** PDTE biotin. Traces show currents prior to (black) and after addition of external (red) or internal (blue) avidin. Paddle structure is shown and color coded for each length biotin tether. Red residues are accessible only from the external side of the membrane, blue residues are accessible only from the internal side of the membrane, black residues are inaccessible and yellow residues are accessible from both sides of the membrane.

Positions assayed for avidin accessibility on the paddle are color-coded in Figure 31 as in previous figures—red indicates accessibility to avidin only from external side of the membrane, blue indicates accessibility to avidin only from internal side of the membrane and black indicates inaccessibility to avidin from either side of the membrane. Residues colored yellow on the paddle represent a new class of accessible sites we have not yet seen anywhere else on the channel. For residues colored yellow, biotin can bind avidin from both sides of the membrane. The accessibility of the voltage-sensor paddle is unique in several respects which we will consider below.

Figure 31a summarizes the accessibility data for sites on the paddle labeled with BCAC (17 Å) biotin and shows several representative experiments. Remarkably, a stretch of residues spanning 3 helical turns on S4 can bind avidin from both sides of the membrane (L118 through I127, Fig. 31a). For these residues avidin addition to either side of the membrane resulted in complete inhibition. In contrast to the voltage-sensor paddle, no sites on the pore, S1 or S2 were found to be accessible to both external and internal avidin when labeled with BCAC (17 Å) biotin. In fact, a BCAC (17 Å) biotinylated residue in the middle of S2 is unable to reach avidin from either side of the membrane. How can the dual accessibility of these sites on S4 be explained? Given our estimate of the length of the BCAC (17 Å) biotin tether and the thickness of the membrane (~30 Å), we must invoke that S4 moves through the membrane and actually drags the biotin tether from the solution on one side of the membrane to the other as the channel gates. How large is this movement? The distance between L118 and I127 is nearly 15 Å. In order to account for ~15 Å of the S4 helix having dual accessibility when labeled with BCAC (17 Å) biotin, the voltage-sensor paddle must move at least 15 Å perpendicular to the membrane. This finding is important

not only because it indicates that the voltage-sensor paddles move a large distance through the membrane but it implies that the paddles must move through a lipid environment where a bulky chemical structure such as biotin and its linker would go unimpeded. In contrast to S4, BCAC biotinylated sites on S3B are able to bind avidin only from the external side of the membrane (Fig. 31a). These results indicate that the S4 segment is a distinctively mobile part of the channel, as we might expect is necessary in order to ferry the gating charges across the membrane.

Figure 31b summarizes the accessibility data for residues on the voltage-sensor paddle labeled with IPEO biotin (10 Å tether). Remarkably, even the shorter IPEO (10 Å) biotin linked to sites on S4 is able to access avidin in both the internal and external solution. L121C-IPEO (10 Å) and L122C-IPEO (10 Å) can bind to avidin from both sides of the membrane (Fig 31b). Although biotinylation at position L122C was incomplete, avidin added to either side of the membrane caused a reproducible reduction in current. Subsequent addition of avidin to the opposite side of the membrane caused no further inhibition, indicating that the biotin groups were completely bound after addition of avidin to the first side of the membrane. Again the accessibility of the S4 segment is markedly different than seen for any other part of the channel. Given that IPEO biotin has an effective tether length of 10 Å and the membrane thickness is at least ~31 Å, the voltage-sensor paddle must move at least ~11 Å perpendicular to the membrane plane in order to account for the dual accessibility we see at positions L121C-IPEO (10 Å) and L122C-IPEO (10 Å). This estimate of S4 motion is independent from the estimate derived above from the BCAC (17 Å) biotin accessibility data.

The pattern of accessibility for residues on the voltage-sensor paddle labeled with IPEO (10 Å) biotin is unique in another respect. All residues on S3b and S4 are accessible to avidin from one side of the membrane or the other when labeled with IPEO (10 Å) biotin. In comparison, on the pore, S1 and S2, we find multiple residues that are inaccessible to avidin on either side when labeled with this biotin tether or the similar length MCAP (9 Å) biotin tether. Again this suggests that the paddle must undergo a sizable motion in order to bring the α-carbon of all residues within 10 Å of either the internal or external membrane boundary.

Figure 31c maps the PDTE (1 Å) biotin accessibility data onto the paddle. Some sites on both S3b and S4 labeled with this short biotin tether reside too far beneath the membrane surface to bind avidin. However, avidin in the extracellular solution can grab biotinylated residues on the tip of the paddle and on the first helical turn of S4 including L118C-PDTE (1 Å). Just 2 helical turns away on S4, L125C-PDTE (1 Å) binds avidin from the internal side of the membrane. Remarkably, L118 and L125 are separated by just 10 Å on the S4 helix. Recall that the closest PDTE (1 Å) biotinylated residues on the pore that bind avidin from opposite sides of the membrane are 31 Å apart. Again the only way to understand the unique pattern of accessibility that we see on S4 is to invoke that the voltage-sensor paddles move a large distance during the gating process to bring L125C within a few angstroms of the internal membrane boundary and L118C within a few angstroms of the external membrane boundary. To account for the accessibility of PDTE (1 Å) biotinylated sites on S4, this region of the paddle must move 13 Å to 21 Å perpendicular to the plane of the membrane.

Thus, the accessibility data from the three biotin tethers all independently indicate that the voltage-sensor paddle moves a large distance so that the region containing arginine residues changes its vertical depth by at least 15 Å. The large motion of the paddle implies

that most biotinylated sites will be able to reach avidin only in some gating states of the channel and not in others and therefore avidin binding will depend on membrane voltage. For biotinylated sites that are externally accessible to avidin, we investigated whether membrane depolarization was required, by studying the effect of depolarization frequency on the rate of channel inhibition. Figure 32a shows that for G112C-IPEO (10 Å), near the tip of the voltage-sensor paddle, inhibition from the external solution required depolarization: higher frequencies gave higher rates of inhibition. Moreover G112C-IPEO (10 Å) can be protected from external avidin by keeping the membrane at negative voltages (green trace, Fig. 32b). However, protection from inhibition by external avidin by holding the membrane at negative voltages is incomplete. In particular, if the wait at negative voltages is long enough, inhibition occurs but at a low rate (Fig. 32a). This finding is explained on the basis of thermal fluctuations of the voltage sensors. Although probably four voltage-sensor paddles have to move to open the pore, individual paddle movements must occasionally occur even at negative voltages.

We find that membrane depolarization is required at all sites on the paddle to allow PDTE (1 Å) and IPEO (10 Å) biotin groups to bind avidin in the external solution. However, the state-dependence of avidin binding is lost for most sites on the paddle when labeled with the longer BCAC (17 Å) biotin tether. For these BCAC (17 Å) biotinylated residues we observe complete or near complete effects due to avidin binding with the first depolarization after addition of avidin to the recording chamber. In Figure 32c, binding of external avidin to L110C-IPEO (10 Å) channels incompletely inhibits channel current. As with G112C-IPEO (10 Å), inhibition occurs only following membrane depolarization—the first depolarization after addition avidin (shown in green) looks like control traces (Fig. 32d). Avidin binding to

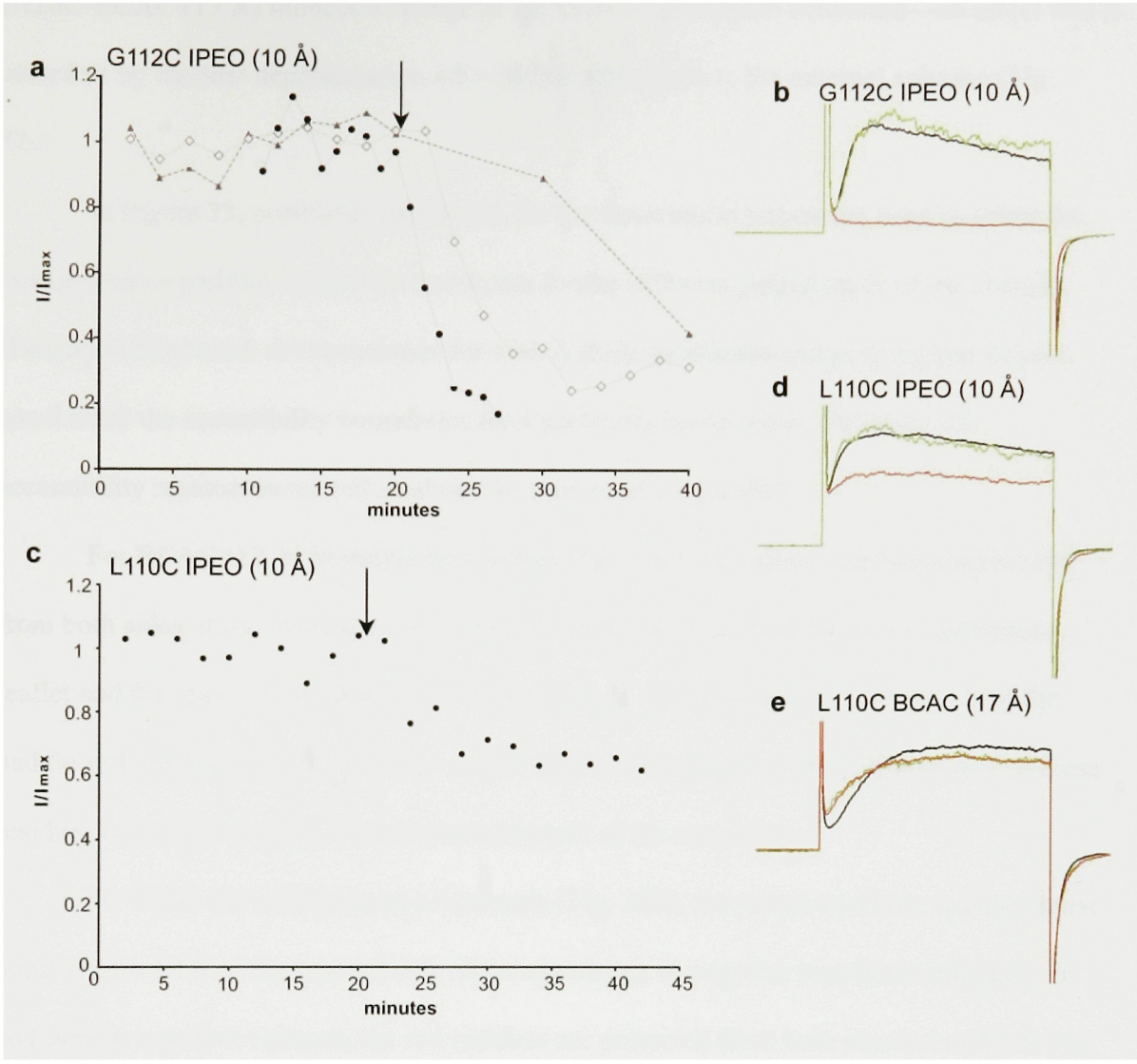

Figure 32

Exposure of the paddle to avidin in the extracellular solution requires membrane depolarization. **a,** G112C IPEO normalized (to the average control) currents elicted by depolarization to +100 mV every 60 s (circles), 120 s (diamonds) or 600 s (triangles) are shown before and after the addition of avidin to the external side (arrow). **b,** G112C IPEO current records from (a) elicited by depolarization every 120 s. **c,** L110C IPEO normalized currents in response to depolarization to 100 mV every 120 s. Avidin addition (arrow) does not inhibit channels until after depolarization has occured. **d,** L110C IPEO current records shown in (c). **e,** L110C BCAC channels exhibit the full effects of external avidin by the first depolarization. For **b,d,** and **e,** the average of 3 traces prior to (black) and 10-15 min after addition (red) of external avidin is shown. The first depolarization after avidin addition is shown in green.

L110C-BCAC (17 Å) induces a change in the kinetics of channel activation—an affect that is complete by the first depolarization after addition of avidin to the external solution (Fig. 32e).

In Figure 33, positional constraints for the three biotin tethers are used to orient the voltage-sensor paddles within the membrane for the different gating states of the channel. Horizontal lines mark the boundaries for a 31 Å thick membrane and grey regions in each panel mark the accessibility boundaries for a particular biotin tether. What do the accessibility measurements tell us about the motion of the paddle?

For BCAC (17 Å) biotinylated residues (Fig. 33a), all yellow residues bind avidin from both sides of the membrane and therefore must move between the lower membrane leaflet and the upper membrane leaflet during gating. Red residues on S3b, the tip of the paddle and the first helical turn of S4 cannot bind avidin in the internal solution and so these residues can never descend beneath the mid-point of the membrane.

For IPEO (10 Å) biotinylated channels (Fig. 33b), the yellow and blue residues must come within 10 Å of the internal side of the membrane at negative membrane voltages. In addition, at negative voltages, the red residues are protected from both external and internal avidin and so must reside further than 10 Å from the surface of both sides of the membrane. At positive voltages, red and yellow residues, including all of S3b, the tip of the paddle and the first two and a half helical turns of S4 become accessible to external avidin and must therefore be within 10 Å of the external solution.

The PDTE (1 Å) biotin accessibility data (Fig. 33c) inform us that at negative voltages, when the channel is closed, parts of the voltage-sensor paddle must reside very close to the intracellular solution to enable the blue residues to bind avidin with this very

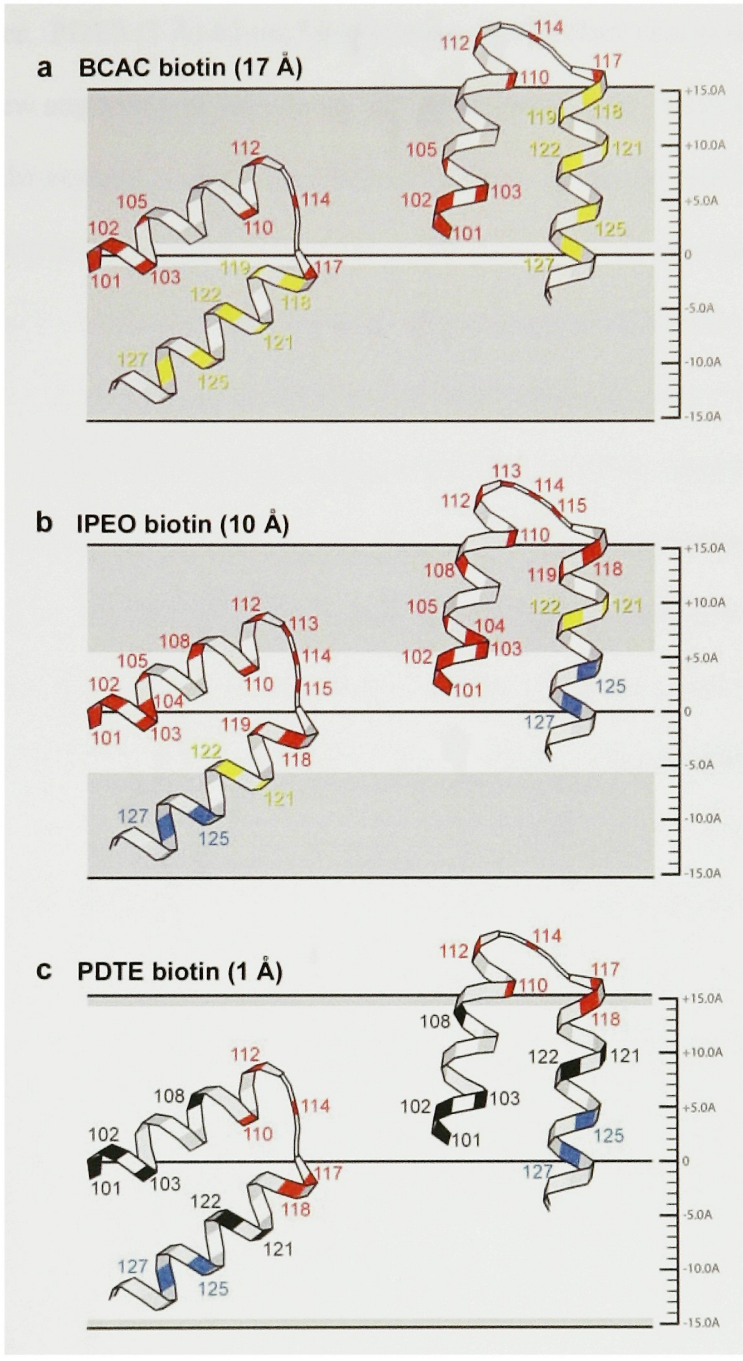

Figure 33

Position of the voltage-sensor paddle within the membrane in the closed (left) and opened (right) state of the channel. Paddle approximately positioned in accordance with the avidin accessibility data for residues labeled with **a,** BCAC, **b,** IPEO, and **c,** PDTE biotin. Grey regions mark the boundaries for avidin accessibility for each length biotin tether.

short biotin tether. PDTE (1 Å) biotinylated residues on the third helical turn of S4 must come within a few angstroms of the internal side of the membrane. At positive membrane voltages, when the channel is opened, all the red PDTE (1 Å) biotinylated residues on the tip of the paddle move to within a few angstroms of the external membrane boundary and the paddle must assume a more vertical orientation. Black residues remain several angstroms below the membrane surface and are inaccessible from either side of the membrane.

The three accessibility data sets independently describe very similar features of the paddle motion and orientation within the membrane. The most important consensus of the accessibility data is that the paddle translates S4 a large distance through the lipid as the channel gates. Data from all three biotin tethers also indicate that at negative voltages, S3b must remain above S4, in a similar orientation to the voltage-sensor paddles in the KvAP-6E1 Fab crystal structure. This constraint arises from the differences in accessibility to internal avidin for sites on S3b and S4. No sites on S3b can bind avidin from the internal side of the membrane even with labeled with the longest biotin tether. Yet multiple sites on S4 are accessible to internal avidin even labeled with the shortest biotin tether.

However, Figure 33 shows that the positional constraints derived from accessibility measurements made with the three tethers can not be satisfied with a single solution for the position of the paddle in a closed and opened configuration. The minor inconsistencies we find in the constraints derived from accessibility measurements with different length biotin tethers could reflect the limited resolution of our assay. Alternatively, and more interestingly, these discrepancies might arise because our model is inadequately describing some feature of paddle motion.

The PDTE (1 Å) accessibility data suggest that when the membrane is depolarized, the tip of the paddle, two helical turns on S3b and one helical turn on S4, all move to within a few angstroms of the external surface of the membrane and the paddle assumes a vertical orientation. A slightly more tilted, exposed orientation for the paddle of the opened channel is described by the IPEO (10 Å) biotin data, constrained by the fact that all of S3b must be within 10 Å of the external side of the membrane at positive membrane voltages. This disparity hinges on the accessibility measurement of a single site. L108C-PDTE (1 Å) channels are inaccessible to external avidin and this constrains the paddle to reside deeper within the membrane and in a more vertical position in the opened configuration than is indicated by the IPEO (10 Å) biotin accessibility data.

More significant than any inconsistency resulting from the outcome of a single site are discrepancies that arise when comparing the overall pattern of accessibility for the three biotin tethers. BCAC (17 Å) biotinylated residues on S3b, the tip of the paddle and the first turn of S4 can never bind avidin from the internal side of the membrane and so must remain in the upper half of the membrane in the closed configuration. Positioning the paddle to satisfy this constraint places the S4 segment too far from the internal solution to account for the accessibility of IPEO (10 Å) and PDTE (1 Å) labeled sites to internal avidin. This inconsistency can be reconciled if the voltage-sensor paddle interface is allowed to crack open slightly (~ 20 ° angle between S3b and S4) in the closed state of the channel, allowing S4 to move closer to the internal side of the membrane while S3b resides in the upper leaflet near the middle of the membrane. Only a small motion of S4 relative to S3b would be required to satisfy the data. However, S3b and S4 come together to form a tightly packed

interface that does not deviate in three different crystal structures, indicating that the paddle unit is clearly a very stable structure and a large movement of S4 relative to S3b is not likely.

Although the biotin-avidin assay as a method of molecular measurement may be inadequate to resolve these details of the paddle structure during gating, the accessibility data unequivocally indicates that the motion of the voltage-sensor paddle is large. In moving from their opened to their closed position, the centre of mass of the paddle translates a minimum of ~11 Å through the membrane from inside to out, and the paddles tilt from a somewhat horizontal to a more vertical orientation. The flexible S3 loop attaches the voltage-sensor paddle to the body of the channel and serves as the hinge-point for the paddle motion. Figure 33 illustrates that sites on S3b, close to the hinge point, will be translated substantially less through the thickness of the membrane than sites on S4—for example, L105 on S3b will be displaced by ~ 6Å while the R117 on S4 will be displaced by ~16 Å during gating. This aspect of the paddle motion is reflected in the unique pattern of avidin accessibility that we see for the S4 segment. This may also explain why avidin binding to some sites on S3b biotinylated with the longer tethers does not significantly disrupt channel gating.

In summary, we have used biotin-avidin accessibility as a method to probe the structure of KvAP channels in membranes. From our calibration with the KvAP pore and our study of the voltage-sensor we find that the voltage-sensor paddles are a uniquely mobile part of the channel. In the next chapter we will synthesize the findings from these accessibility measurements with other structural and functional studies of KvAP, as well as eukaryotic channels to consider how the design of the voltage-sensors enables the membrane electric field to perform mechanical work to open and close the pore.

CHAPTER 7: CONCLUSIONS AND DISCUSSION

In the preceding chapters, I have presented the first strokes of a structural portrait of the voltage-dependent gating process in a Kv channel. This work has been a collaborative effort at many levels. However, I would like to begin this concluding chapter by presenting my perspective on how our understanding of the mechanistic design of these channels has evolved over the past four years and in what ways my thesis work has contributed to this evolution.

Prior to the structural and functional studies of KvAP, the prevailing models for Kv channel architecture all placed the S4 segment with its constellation of gating charges, adjacent to the pore in an aqueous, protein-lined canal, shielded from the lipid by the other segments of the voltage sensor[37-39]. It was thought that the voltage sensor was designed by the same fundamental energetic principle as the pore forming domain—charges are not favored to be in contact with the hydrophobic core of the membrane and to alleviate this cost a mostly aqueous pathway evolved to move the gating charge residues across the membrane's electric field. While there was disagreement as to the exact nature of the gating motion of the S4 segment—whether a rotation, a translation, or both—a general consensus

existed that the movement was not very large. The structure of the gating canal surrounding the S4 segment was thought to form a highly focused electric field, so that the gating charges could be effectively transferred across the field with a fairly subtle motion.

When I joined the lab in 2000, an intense effort was already underway to obtain a structure of a Kv channel. Youxing Jiang, Alice Lee and Jiayun Chen had cloned KvAP and were using it in crystallization trials. I began to investigate the electrophysiological properties of purified KvAP channels reconstituted into membranes. At the time, essentially nothing was known about how the functional properties of prokaryotic Kv channels would compare to well-studied eukaryotic Kv channels. If we were to ever see a structure of one of these proteins, this is something we would want to understand in great detail. My functional analysis of KvAP demonstrated that remarkably this prokaryotic channel with an unknown physiological role possessed all the functional properties of neuronal Kv channels responsible for nerve impulses. I demonstrated that there was fundamental conservation of the voltage-sensor structure throughout the evolutionary tree by showing that KvAP is inhibited by tarantula voltage-sensor toxins that evolved specifically to inhibit voltage-dependent channels in the eukaryotic prey of these spiders.

I developed a biochemical assay using purified KvAP channels to rapidly isolate interacting toxins. This assay allowed me to compare the toxin binding characteristics of the KvAP isolated voltage-sensor domain (S1-S4) and the full-length channel. This comparison showed that in the absence of the pore-forming domain, the isolated voltage-sensor domain retained the structural features that form the tarantula toxin receptor. The voltage-sensor domain was in fact completely sufficient to extract toxins from venom. This further strengthened the idea that tarantula toxins interact with a conserved receptor on the KvAP

voltage sensor to bring about channel inhibition, in a completely analogous manner to how these toxins target eukaryotic channels.

The first structure of KvAP was a considerable departure from the expected architecture for the voltage sensor. The voltage sensors held by Fab fragments adopted a non-native conformation, hinting at their inherent flexibility and dynamic nature. While the KvAP-6E1 structure lacked the simple, explicit eloquence of other crystal structures like KcsA, for example, it did suggest a possible mechanism for gating charge movement—the gating charge residues were located on voltage-sensor paddle units at the channel perimeter and could move at the protein-lipid interface through the membrane's electric field. However because this mechanism was inferred from a crystal structure in a clearly non-physiological conformation and was so radically different from what was previously envisioned, further experiments were required to test and explore this structure-based hypothesis. I became involved at this point in interpreting the first structure of the KvAP channel, carrying out experiments on functioning channels to investigate the movement of the paddles within the membrane during channel gating. I used Fab fragments and (with Youxing) tethered biotin and avidin to probe the position of the paddles relative to the membrane plane. These functional studies strongly substantiated the idea that the voltage-sensor paddles moved at the protein lipid interface, where they could drag bulky chemical tags and that they moved a large distance, some 15-20 Å perpendicular to the membrane plane.

After this first structure-function study, it was immediately clear that we would want to see more crystal structures of the KvAP channel to better understand its physiological conformations. I worked with Alice Lee to identify new crystal forms of the channel and I

eventually solved a structure of KvAP in the absence of Fab fragments. While this structure is low-resolution, the basic architecture of the channel is clearly resolved. This second channel structure lent strong support for the idea that the voltage-sensor paddles are stable units but attached to the channel through flexible hinges that allow the paddles to move relative to the pore, completely consistent with the dynamic properties of the voltage-sensor paddle evident from the first biotin-avidin accessibility studies.

The biotin-avidin accessibility assay proved to be an invaluable tool to allow me to probe the structure of the KvAP channel within the membrane. It was actually imperative to have such an assay given the critical importance of the lipid membrane to maintain the flexible voltage sensor in a physiological conformation. I returned to the biotin-avidin assay in the last months of my thesis work, to conduct more rigorous controls and compare the accessibility of the voltage-sensor paddle with other parts of the channel, using biotin tethers of different lengths. The inescapable conclusion from my biotin-avidin experiments is that the voltage-sensor paddle is a uniquely dynamic part of the channel, as we might expect is required in order to carry out its role transporting gating charge residues through the membrane.

There are two significant conclusions regarding the mechanism of voltage-dependent gating that can be drawn from the combined structural and functional studies of KvAP I have just described. The first conclusion is that the S4 segment translates a substantial distance (minimum of ~15 Å) through the membrane as the channel moves from its closed to its opened conformation. The second conclusion is that the S4 segment carries out this motion at the perimeter of the channel, moving at the protein-lipid interface. These two features are embodied in a conceptual model of the electromechanical coupling process shown in Figure

34. The voltage-sensor paddles are positioned at depths within the membrane according to the constraints derived from the biotin-avidin accessibility data. In the closed channel, the voltage-sensor paddles are held beneath the surface of the membrane by the large electric field (Fig. 34a). In the pore of the closed channel, the S5 and S6 helices are arranged as they are in KcsA, with the S6 helices forming a bundle at the intracellular face of the channel that prevents the passage of ions. Upon membrane depolarization the voltage-sensor paddles move a large distance through the lipid to expose the tip of the helix-turn-helix to the extracellular solution (Fig. 34b). This motion pulls on the S4-S5 linker, to which the paddle is directly attached, which in turn pulls on the S5 helix. The S6 helices follow the motion of the S5 helices, bending at the gating hinge glycine to expand the diameter of the intracellular mouth of the pore and adopt the conformation that we observe in the two crystal structures of the channel.

This conceptual model envisions how the motion of the voltage-sensor paddle, driven by the membrane electric field, could induce pore opening. However, there are several aspects of this model that are not constrained by my data. The biotin-avidin accessibility measurements report on the position of residues within the paddle relative to the plane of the membrane, but the assay provides no information about where residues within the paddle are located relative to other regions of the channel. The voltage-sensor paddles could lie tangential to the channel's outer surface or could be pointed in a radial direction away from it. The flexibility of the paddle's connections to the body of the channel would allow either orientation. As I will discuss below, studies of eukaryotic Kv channels suggest that the paddle is more likely to be positioned in a tangential orientation, in a manner similar to what I have depicted in Figure 34, to allow for interactions between residues on the paddle and

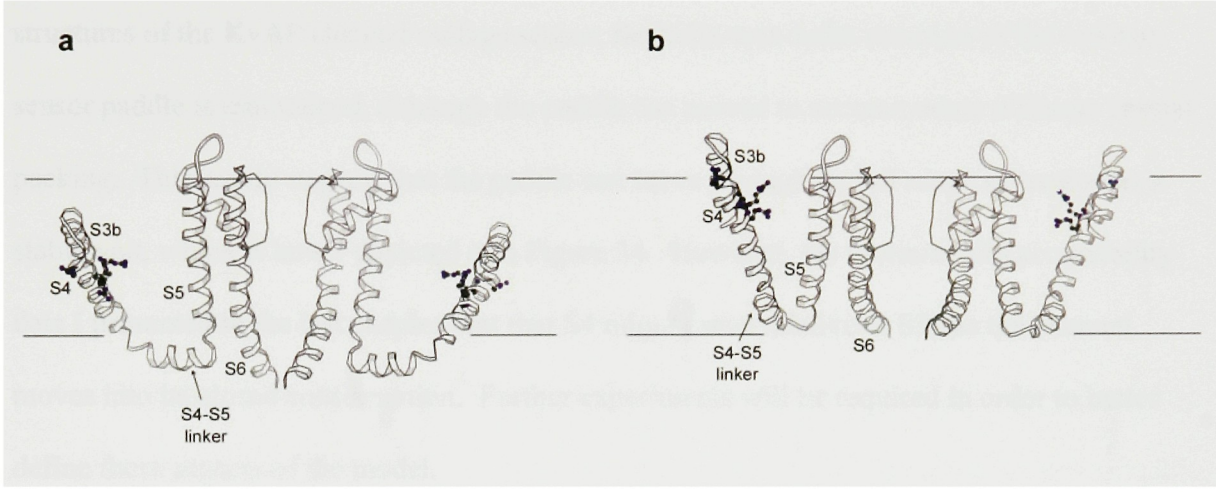

Figure 34

Conceptual model of the voltage-dependent gating process. Model for the closed **(a)** and opened **(b)** KvAP channel. Voltage-sensor paddles are positioned at depths within the membrane based on biotin-avidin accessibility measurements. The four gating charge arginines on the S4 are shown as ball and stick. Pore of the closed channel is modeled on the KcsA pore.

other parts of the channel. The S1,S2 and S3a helices have been omitted from my model. While the biotin-avidin accessibility data indicate that S1 and S2 are positioned in the functioning KvAP channel as transmembrane helices, I have no information about their relative placement with respect to each other, to the paddle or to the pore. A third aspect of this model that I can not fully constrain with my data is whether the well-packed paddle interface is preserved throughout the gating motions of the channel. In three crystal structures of the KvAP channel voltage sensor, the helix-turn-helix structure of the voltage-sensor paddle is maintained, although the paddle has moved to accommodate different crystal packing. This would suggest that the paddle can move through its full range of motion as a stable unit, which is how I depicted it in Figure 34. However, the biotin-avidin accessibility data I presented in the last chapter hint that S4 might move relative to S3b as the channel moves into its closed conformation. Further experiments will be required in order to better define these aspects of the model.

The fundamental conclusion of my thesis work, that the gating charge residues on S4 are carried a large distance through the membrane at the protein lipid interface, is different from previously envisioned models of gating charge movement derived from studies of eukaryotic channels that I described. What is the source of this discrepancy? The amino-acid sequence, functional and pharmacological properties of KvAP all indicate that it is closely related to eukaryotic Kv channels and undergoes essentially the same voltage-dependent conformational changes. Therefore, any structural model of voltage-dependent gating derived from structural and functional studies of KvAP should be consistent with the data from studies of voltage-dependent gating in eukaryotic Kv channels. I will now consider

several significant constraints derived from studies in other laboratories, primarily of eukaryotic Kv channels, in the context of the conceptual model that I have proposed.

Gating charge

The voltage sensitivity of voltage-dependent channels arises from the motion of multiple gating charge amino-acids through the electric field of the membrane[34,94]. Can the motion of the voltage-sensor paddle, deduced from the biotin-avidin accessibility studies of KvAP, account for the gating charge measured in eukaryotic Kv channels? Figure 35 positions the voltage-sensor paddle in a closed and opened conformation based on the constraints derived from the biotin-avidin accessibility data. The first four arginines on the S4 segment (R117, R120, R123, R126) are shown. In *Shaker*, movement of the homologous S4 arginine residues through the membrane's electric field constitutes most of the channel's measured gating charge[18,19]. In KvAP, we find that in the closed conformation arginines 126, 123 and possibly 120 will be able to extend their positively charged guanidinium group to the internal lipid head group layer. Arginine 117 will remain near the mid-point of the membrane. In the opened conformation, arginines 117, 120, and probably 123 can extend to the external solution or lipid head group layer, whereas arginine 126 will be close to the external side but remain within the membrane. The transfer of these four arginine residues across much of the thickness of the membrane is compatible with the total gating charge in the *Shaker* channel of 3-3.5 elementary charge units per voltage-sensor[17-19].

If the S3b segment follows the motion of the S4 segment during gating, should charged amino-acids on S3b also contribute to the measured gating charge? In Figure 35a, I have shown the paddle descending beneath the surface of the membrane boundary. However this boundary is based on the limits of avidin accessibility for biotinylated sites on the paddle

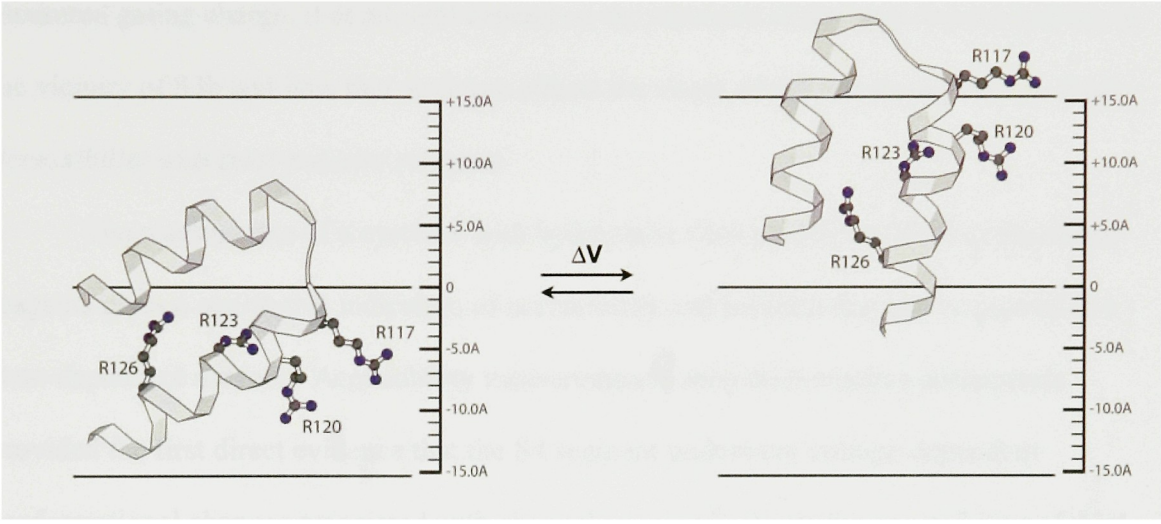

Figure 35

Gating charge movement in KvAP. Deduced positions of the voltage-sensor paddles in the closed (a) and opened (b) conformation. Gating charge arginine side chains on S4 are shown as ball and stick representations.

and is not representative of the lipid-water interface. The lipid membrane in reality is fluid and compressible. In the closed configuration of the channel, the membrane may not be continuous over S3b, particularly taking into consideration that some eukaryotic Kv channels, including *Shaker*, possess an elaborated S3-S4 loop containing multiple acidic and polar residues. Therefore the extent to which charged residues on S3b contribute to the measured gating charge, if at all, will depend on the structure of the lipid-water interface in the vicinity of S3b and how that structure affects the shape of the membrane electric field.

Accessibility with thiol-reactive reagents

The reaction rate of a cysteine with hydrophilic thiol modifying MTS or mercurial reagents gives a qualitative indication of accessibility and location that can be probed in a state-dependent manner. Accessibility measurements using thiol reactive compounds provided the first direct evidence that the S4 segment underwent voltage-dependent conformational changes associated with channel opening[26]. While the accessibility of thiol reactive compounds would seem to convey the same information as the biotin-avidin accessibility assay, there are important differences between these techniques. First, studies in eukaryotic channels using thiol reactive reagents are actually measuring cysteine reactivity with a small thiol reactive reagent, of which the accessibility of the cysteine to the reagent is just one component[110]. In contrast, the biotin-avidin assay is a true measure of accessibility of a tethered biotin to avidin. Moreover, the size of the probe in the two assays is very different. MTS reagents are sufficiently small to diffuse into crevices within the channel to react. Avidin, in comparison, is far too large to penetrate into crevices. Thus, these two assays report very different information. The calibration of the biotin-avidin assay using the

KvAP pore confirmed that avidin accessibility reports on the position of the α-carbon of biotinylated cysteine with respect to the membrane surface.

Despite these differences, the results from MTS "accessibility" studies in eukaryotic voltage-dependent ion channels are entirely consistent with the large translational movement of S4 indicated by the biotin-avidin data. Studies by Isacoff and colleagues showed that in *Shaker*, as the channel moves from a closed to an opened conformation, residues A359-R368 (equivalent to residues G114-R123 in KvAP) move from inaccessible to externally accessible positions, able to react with extracellular MTS reagents[23,25]. At the same time, channel activation moves residues R365-S376 (equivalent to residues R120-I131 in KvAP) from internally accessible to inaccessible positions. The state-dependent change in accessibility of a minimum of 9 residues (~13 Å on a α-helix) is most simply explained with a large translation of S4.

A very similar pattern of state-dependent accessibility was obtained by Yusaf et al. who investigated the reactivity of introduced cysteines on the *Shaker* S4 with mercurial agents only from the extracellular solution[24]. One difference between these studies is that Yusaf et al. found that L367C was not accessible to external parachloromercuribenzenesulphonate (PCMBS) suggesting that one or two fewer residues becomes exposed to the extracellular solution with membrane depolarization. This difference may arise from the different charge and size of the thiol modifying compounds used in the two studies. Horn and colleagues probed the state-dependent accessibility of residues in the S4 segment in the human skeletal muscle voltage-dependent Na^+ channel with MTSET. They found that a minimum of 6 residues became exposed to the external solution with membrane depolarization[26,27].

Thus, in eukaryotic voltage-dependent ion channels, the accessibility of a large number of sites on the S4 segment depends on the gating state of the channel (Fig. 36). Whether or not a residue is accessible to extracellular or intracellular thiol reactive compounds appears to be determined simply by its position along the length of the S4 segment, compatible with a translational motion. The data with thiol reactive compounds from eukaryotic voltage-dependent channels is therefore completely consistent with the biotin-avidin data from KvAP in terms of the size of the voltage-dependent motion of S4. Moreover, Figure 36 shows that in KvAP, *Shaker*, and the Na_v channel, the transition from external to internal accessibility is centered over essentially the same residues—between the second and third arginine on the S4 segment.

One argument cited as evidence against a large translational motion of the *Shaker* S4 segment has been that the state-dependent accessibility of sites at the N-terminus of the S4 is weak. This would be inconsistent with a model in which S4 descends beneath the surface of the membrane, as seen in Figure 34. However, this argument is not quite justified. Isacoff and colleagues initially found only a two-fold increase in reactivity for A359C at the N-terminus of S4 upon channel activation relative to the holding voltage of -80 mV[23]. Yusaf et al. went on to demonstrate that external accessibility to thiol reactive agents was very steeply dependent on the membrane holding voltage. Even at very negative voltages where channel openings were rare, cysteines on S4 were not fully protected from reaction with thiol reactive compounds[24]. For example, L361C is 50% inhibited by external PCMBS after 2 minutes holding at -100 mV but only 10% inhibited when holding at -140 mV for the same time period. This observation prompted Isacoff and colleagues to reinvestigate the weak state-dependence of the reactivity that they had observed for position A359C. They subsequently

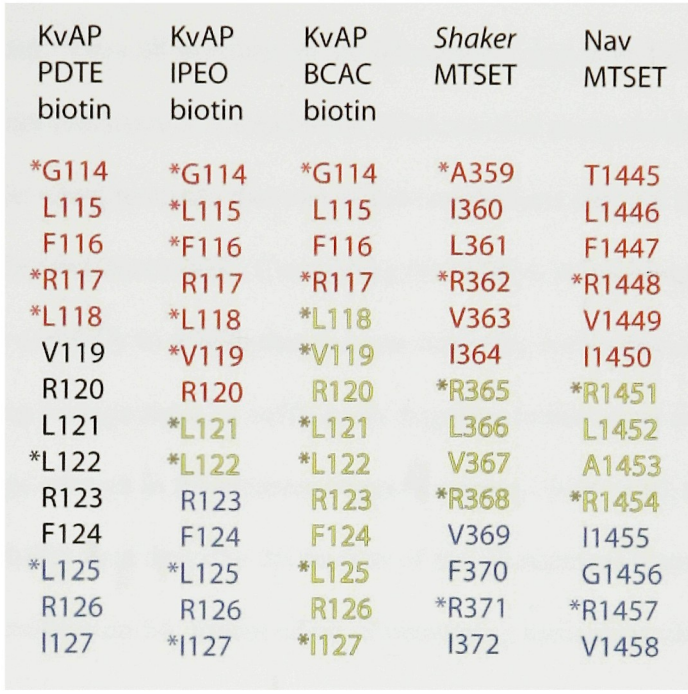

KvAP PDTE biotin	KvAP IPEO biotin	KvAP BCAC biotin	*Shaker* MTSET	Nav MTSET
*G114	*G114	*G114	*A359	T1445
L115	*L115	L115	I360	L1446
F116	*F116	F116	L361	F1447
*R117	R117	*R117	*R362	*R1448
*L118	*L118	*L118	V363	V1449
V119	*V119	*V119	I364	I1450
R120	R120	R120	*R365	*R1451
L121	*L121	*L121	L366	L1452
*L122	*L122	*L122	V367	A1453
R123	R123	R123	*R368	*R1454
F124	F124	F124	V369	I1455
*L125	*L125	*L125	F370	G1456
R126	R126	R126	*R371	*R1457
I127	*I127	*I127	I372	V1458

Figure 36

Comparsion of accessibility for residues on S4 of KvAP, *Shaker* [11,12] and the human skeletal voltage-dependent Na+ channel (Nav)[9,14]. Residues colored red are accessible only from the external side of the membrane, residues colored blue are only accessible from the internal side of the membrane and residues colored yellow are accessible to both sides of the membrane. Asterix mark the residues whose accessibility has been tested, accessibility of intervening residues is inferred.

found that the rate of inhibition did indeed depend on holding voltage and that MTS modification was in fact 80-fold slower at -120 mV than at fully activated membrane voltages[25]. They went on to show that reactivity of A359C with extracellular MTSET reagents correlated well with the voltage-dependence of gating charge movement measured for the cysteine mutant. Thus all residues on the S4 segment that have been carefully tested exhibit state-dependent reactivity to extracellular thiol reactive compounds. This example highlights some of the considerations that can affect conclusions derived from state-dependent accessibility measurements. Comparing the relative reaction rates between two states has to be done carefully to ensure that the two states are well separated—in this case the membrane holding voltage must be sufficiently negative to minimize independent motions of the voltage sensors in the absence of pore opening. It is worth noting that the biotin-avidin accessibility data describe the motion of the S4 segment from the simple pattern of accessibility for residues on S4, independent of measuring state-dependent accessibility for individual residues.

The state-dependent accessibility of sites on S3b in eukaryotic voltage-dependent channels has been less thoroughly investigated. Gandhi et al. and Gonzalez et al. found no or very modest state-dependent reactivity (~2-fold slower with the channel held at -110 mV) respectively at a total of four different residues on the N-terminal portion of the S3b segment of *Shaker* that they probed with MTSET (equivalent to residues A100, G101,L103, and L105 on KvAP)[111,112]. Nguyen et al. investigated the accessibility of two residues (equivalent to G101, E107 on KvAP) on the S3b segment of a voltage-dependent Na^+ channel with both cationic MTSET and anionic MTSES reagents and found 2-10-fold differences in the reaction rates between channels held at -150 mV or 0 mV[113]. However, the reaction rates of

the cysteines introduced into S3b in all three studies, are 10-1,000-fold slower than either the reaction rate of MTSET with β-mercaptoethanol in solution[110] or (a more telling comparison) cysteines introduced into the S6 helix of the *Shaker* channel that are thought to line the ion conduction pathway[114]. Comparably slow MTSET reaction rates are found for cysteines introduced into S4 but only at sites that lie at the limits of internal or external accessibility (e.g. R368C from the internal side of the membrane in the closed state or the external side of the membrane in the opened state.)

What do these slow reaction rates imply? Despite being widely used as a tool to define membrane boundaries, MTS accessibility has not been systematically studied in ion channels of known structure to delineate how reaction rates of thiol modifying reagents are affected by the local chemical environment. However, a systematic study of cysteine reactivity on the N-terminal amphipathic helix of KcsA channels reconstituted into membranes found 10^2-10^3 –fold differences in reaction rates for residues along the helix probed with positively charged thiol reactive compounds[115]. The differences in reactivity for sites along the helix correlated well with the accessibility of the EPR spin-labeled sites to water or lipid soluble quenchers[116]. This result raises the possibility that slow but appreciable reactivity can occur even for residues in a predominantly lipid environment. Alternatively the slow reactivity of these reagents could be ascribed to steric hindrance from protein packing. Further investigation will be required to understand the water-lipid-protein environment surrounding S3b in both the opened and closed channel and how this affects the MTS reactivity.

Fluorescence

Two main experimental approaches have been carried out on *Shaker* channels labeled with fluorescent dyes. The first experimental strategy has monitored the voltage-dependent changes in fluorescence intensity of labeled residues and attempted to correlate these changes with different gating conformations of the protein. Voltage-dependent changes in fluorescence intensity are seen at many sites throughout the channel including multiple residues on S1, S2, S3b, S4, S5 and S6 segments[31-33,111]. Within a helix, the magnitude and direction of the fluorescence changes that occur upon membrane depolarization varies greatly between consecutive residues[33]. While voltage-dependent changes in fluorescence intensity are certainly reflecting some change in channel conformation, because they are so widespread and without a cohesive pattern, it has been difficult to extract the exact physical nature of the conformational change.

One prediction of the large motion of the S4 segment through the lipid would be that some residues would move from an aqueous to a lipid exposed environment depending on the gating state of the channel. Therefore the spectral emission of a fluorophore linked to these sites would likely change in a systematic manner with membrane voltage as the fluorophore moves between a high and a low dielectric medium. Bezanilla and colleagues investigated this possibility. They covalently linked tetramethylrhodamine (TMR) maleimide to either M356C on the S3-S4 linker or A359C on the very N-terminus of S4 of *Shaker* and then monitored changes in the emission spectrum of TMR with depolarization[32]. TMR is a symmetric fluorophore and lacks a significant dipole making it a fairly poor environmental sensitive probe, exhibiting only a modest shift in emission depending on the polarity of the solvent. Nevertheless, in a cuvette, Bezanilla and colleagues demonstrated

that the emission maximum of TMR shifts to shorter wavelengths by 9 nm when the fluorophore is moved from water to ethanol. In comparison, the emission spectrum of TMR on the labeled channels was the same as for the fluorophore in water and did not change with membrane voltage. They interpreted this result to mean that the very N-terminus of S4 does not enter a lipid environment. However there are several uncertainties in the measurement that are not addressed. First, how much of the fluorescence spectrum is due to non-specific background from fluorophores not bound to cysteines on the S4 segment? Bezanilla and colleagues controlled for background labeling by subtracting the fluorescence spectrum of uninjected oocytes from their signal but it is unclear how much error that procedure introduced and whether it affected their ability to detect the small shift in wavelength that would occur if TMR entered the membrane. The fluorophore in these experiments was linked to the α-carbon of the cysteine through ~ 8 Å tether and therefore is placed at a distance from the S4 segment, which might affect its local environment. In addition, TMR maleimide is a zwitterionic compound that has been shown to be membrane impermeant and therefore might not be a good indicator of lipid accessibility. TMR maleimide has in fact been used as a marker of solution accessibility for residues in the *Shaker* voltage sensor and has been shown to bind to A359C only upon membrane depolarization[31,111]. No other positions on the channel were tested as a control to ensure that they could measure spectral changes from the partitioning of this fluorophore into lipid membranes. This type of fluorescence experiment could be very informative if more sites were investigated, including some known to lie within the core of the membrane, and were labeled with a more appropriate hydrophobic, environmentally sensitive probe.

The second type of fluorescence measurement has attempted to derive distance constraints between two labeled sites on the channel using fluorescence resonance energy transfer (FRET). Two studies by Cha et al. and Glauner et al. both investigated the energy transfer between identical residues on different subunits of the *Shaker* channel[35,36]. Cha et al. monitored luminescence energy transfer between a chelated terbium compound donor and a fluroscein acceptor through changes in the lifetime of the terbium luminescent state. Glauner et al. labeled sites with two organic dyes and monitored FRET efficiency by the rate of donor photobleaching. From their data, both groups extracted the absolute distance between identical sites on the S3-S4 linker or S4 segment of neighboring subunits in the closed and opened state of the channel to assess S4 motion during gating. Cha et al. contended that at intermediate voltages, the independent motion of the voltage sensors would allow for some S4 segments to be in their opened position while others remained in their closed position and so they could obtain a measure of translational motion, perpendicular to the membrane plane. However, this method is inherently insensitive to translational motion perpendicular to the membrane due to the fact that the sites are far apart. As an example, if two sites are separated by 40 Å in the closed state and one subunit undergoes a 10 Å displacement perpendicular to the membrane plane, the distance between the sites will only increase by 1.2 Å. In theory FRET can accurately measure these small changes in the distance between fluorphores, but in practice it is not entirely clear that either study has.

One problem is that the two studies show marked inconsistencies in both the absolute distances measured between the same residues and the relative distance changes that occur with depolarization. Glauner et al. find uniformly larger absolute distances between sites (e.g. 53 Å distance between S352 in adjacent subunits in the closed state in comparison to the

29 Å distance that Cha et al. measured). Glauner et al. offer no controls to show that their experimental system is capable of accurately measuring the distance between two sites. Cha et al. show that the distance measurement they obtain for two sites on the pore is within 1 Å of the distance between homologous residues on the KcsA structure. However, more important than the absolute distances between sites on S4 are the voltage-dependent changes in distance that reflect movement of the gating charge and neither study offers controls to show that they can track movement. This is a particular concern considering that the terbium chelate, for example, is linked to the α-carbon of the S4 cysteine through a ~17 Å tether, which would place the fluorophore a large distance from the S4 segment. The two studies show complete inconsistency in the direction of distance changes that occur with depolarization. Cha et al. find that S351, S352, and N353 move +1.1 Å, 0 Å, -1.3 Å respectively (between residues on diagonally related subunits) with channel activation while Glauner et al. find those same three residues move -9.2 Å, +2.0 Å, and +6.4 Å. So the conclusion from the two studies is that residues move different distances in the opposite direction.

The only consensus between the studies is that the pattern of alternating distance changes seen at consecutive residues suggests a rotation of the S4 helix so that some residues move closer to each other and some further away with channel activation. Is this rotation accompanied by translation of the S4 segment? Cha et al. could measure distance changes as a function of membrane voltage which Glauner et al. could not because they were detecting energy transfer through the rate of irreversible photobleaching of the donor fluorophore. Cha et al. argue that because of the independent motion of the voltage sensors, the distance between fluorophores on neighboring subunits should be a maximum at intermediate

voltages if a large translational movement is occurring, but this is not what they observe. They find very small (1-2 Å) changes in the distances between identical sites on two subunits that increase or decrease monotonically with membrane voltage. They interpret this result as an indication that there is very little translational motion of S4 and gating charge transfer occurs simply through a rotation of S4 by ~180 ° through a focused electric field.

However this interpretation is not very satisfying for several reasons. First, if a helix is ~10 Å in width, some residues on the helix that rotate by 180 ° should move ~20 Å further apart, at least measured diagonally across the channel. This change in distance would be somewhat less if the helix were tilted or the rotation was less than 180 °. However, Cha et al. only measure at maximum a ~1-2 Å change in distance between identical sites on diagonally related subunits with channel activation. This distance change is too small to account for even the rotation that they propose. Another unsubstantiated aspect of their interpretation is that if the S4 segment only rotates to transfer its gating charge arginines through a focused electric field, residues between the gating charge arginines should move in the opposite direction. So while the arginines move from the intracellular to the extracellular side of the membrane with depolarization, the hydrophobic residues in between should move from the extracellular to the intracellular solution. This is not what has been observed in the MTS accessibility experiments I described above where there accessibility appears to depend only on position of the residue along the axial length of the S4 segment and not its radial position on the face of the helix[23-25]. Despite the uncertainties in the FRET measurements and their interpretations, these two studies have strongly influenced the prevailing models for S4 motion. For example, Isacoff and colleagues, whose MTS accessibility data is very

consistent with a large translational movement of S4 have invoked smaller motions of the helix within aqueous crevices to account for their FRET data[38,111].

Cross-links between S4 and S5

Several recent reports have shown that in *Shaker*, disulfide and metal cross-bridges form between residues on the N-terminus of S4 and the C-terminus of S5 when pairs of residues are mutated to cysteine or histidine[111,117-120]. The formation of these cross-links is an important constraint, indicating that in some states of the channel, the top of S4 can reach very near subunits of the pore. However while the specificity of the cross-links have been vouched for in each study, taken together as a set of data, the cross-links are not very specific. For example, F416C on the C-terminal portion of S5 is reported to form cross-links with 7 positions on the S3-S4 linker and N-terminus of S4 (N353C, Q354C, A355C, M356C, S357C, A359C, and R362C)[111,119]. Even within a single study, Gandhi et al. reported that F416C forms a disulfide with 4 consecutive residues on the S3-S4 linker, encompassing all faces of a helical wheel[111]. Similarly A359C on the N-terminus of S4 has been shown to cross-link with both F416C and E418C despite that the homologous residues in the KvAP pore structure are on opposite sides of the helix (with E418C apparently pointing into the core of the pore)[111,119,120]. The methodologies used to form cross-bridges in the different studies varied from air-oxidation, to treatment with 50-100 μM Copper phenanthroline (an oxidizing agent), to 0.2% H_2O_2 to various concentrations of Cd^{2+}. Some harsher oxidizing methods or higher concentrations of Cd^{2+} could trap transient interactions.

Another possible explanation for the lack of specificity evident in the combined data from these studies is that the S4 segment is inherently very flexible. Sivaprasadarao and colleagues reported that L361C at the N-terminus of S4 forms a disulfide between

neighboring subunits with air-oxidation or treatment with copper phenanthroline[121]. R362C and R365C channels also show a reduction in current with exposure to copper phenanthroline that is reversed with TCEP, suggestive that a disulfide cross-link has formed[120]. It is difficult to understand this degree of mobility in a model where the S4 is restrained within a protein canal and is entirely consistent with the dynamic nature of the S4 segment evident from the biotin-avidin accessibility studies.

Membrane depolarization was apparently required for cross-links to form between A359C-F416C[111] and R362C-F416C[119], consistent with the paddle motion that would place the N-terminus of S4 close to the membrane surface to make contacts with the residues on the C-terminus of S5 only in the opened state of the channel (Fig 34b). However, Sivaprasadarao and colleagues report that cross-links between S4 and the pore can form in the closed state of the channel and these would be entirely inconsistent with a large translational motion of S4[120]. They show that R362C-A419C forms a Cd^{2+} cross-bridge while the channels are held at -100 mV (although the Cd^{2+} concentration that they use is 1000 times the Kd for the Cd^{2+} binding site formed from those two residues as reported by Papazian and colleagues)[117]. Sivaprasadarao and colleagues use tandem dimers in which each subunit contains a single cysteine mutation of the pair to show that L361C-E418C crosslinks between subunits form with treatment of copper phenanthroline while holding at -120 mV[120]. This ability to form these cross-links in the closed channel is difficult to understand in the context of a translational motion of S4. The formation of cross-links between the N-terminus of S4 and the C-terminus of S5 is inconsistent not only with the biotin avidin accessibility data but also with measurements of the reactivity of S4 cysteine mutants in *Shaker* which clearly indicate that residues L361C and R362C are inaccessible to

thiol reactive agents in the closed state of the channel[23,24]. It is also rather surprising, given the apparent lack of specificity of the cross-links that some residues very near each other appear to cross-link only in the open state while others are able to cross-link in the closed state. For example, R362C forms a cross-link with F416C only in the open state while that same S4 cysteine mutation can cross-link with A419C, one helical turn away on S5, in the closed state[119,120]. This degree of specificity seems particularly unlikely given that R362C on its own can apparently form a disulfide between S4 segments on neighboring subunits.

Salt-bridges

Papazian and colleagues employed second-site suppressor analysis to investigate the role of highly conserved acidic and basic residues within the *Shaker* voltage sensor[88-90]. In these experiments, single charge reversing mutations that disrupted channel protein maturation and function were identified. These deleterious mutations could be specifically rescued by the introduction of a second charge reversing mutation, pointing to the existence of structurally and functionally important ionic interactions within the *Shaker* voltage sensor. With this strategy, Papazian and colleagues proposed that electrostatic interactions exist between E293 in S2 with D316 in S3a and K374 in S4 as well as between E283 in S2 with the third and the fourth gating charge arginine residues on S4, R368 and R371. All of these charged residues are conserved in KvAP, except K374.

Papazian and colleagues proposed that the salt-bridges in *Shaker* likely break and reform as the channel gates. Part of the basis for this conclusion was derived from differences in MTS accessibility that are found for members of a salt-bridge pair. For example, E283C is accessible to MTS reagents only from the external side of the membrane while R371C is accessible to MTS reagents only from the internal side of the membrane, and

R368C is accessible to both sides depending on the gating state of the channel[89]. Thus E283C was proposed to interact with R368 in a closed state of the channel and R371 in fully activated state—a proposal that was consistent with the functional effects of double charge reversal mutations[89]. These results suggest that ionic interactions between the voltage-sensor paddle and the S2 segment may assist in gating charge movement.

In KvAP, the biotin-avidin accessibility measurements indicate that the analogous acidic residue on S2, E62, resides closer to the external side of the membrane in both the opened and closed state of the channel while the dynamic S4 segment moves its third and fourth arginine residue from the lower membrane leaflet to the upper membrane leaflet with channel activation, analogous to the accessibility that is observed for those residues in *Shaker*. In the structure of the KvAP isolated voltage sensor, a different set of salt-bridges are visible, although this may represent a snapshot of transient interactions which occur during gating. The ionic interactions proposed by Papazian and colleagues, along with the disulfide and metal cross-bridge interactions described above suggest that the paddle remains in close proximity with residues in other parts of the voltage sensor and the pore throughout the gating process. These results help to constrain the possible orientation of the paddle within the membrane, a feature that is not well described by the structural and functional studies of KvAP. If the paddle is positioned tangentially as depicted in Figure 34, these charged residues on the paddle would largely be directed towards the body of the channel, favoring the formation of salt-bridge interactions.

Proton currents

Bezanilla and colleagues used histidine scanning mutagenesis to investigate the gating motions of the S4 segment in *Shaker*. Their rationale in this set of elegant experiments

was that if displacement of the voltage-sensor resulted in exposure of an introduced histidine to the bulk solution, then its charge could be titrated by the pH of the surrounding solution. They found that indeed, the gating charge in the R365H and R368H mutant channels could be titrated by the pH of both the intracellular and extracellular solution[28,29]. At acidic pH, the histidine could carry a positive charge across the membrane field and act as a surrogate gating charge, while at basic pH, the unprotonated histidine would not contribute to the measured gating currents. Both K374 and R377, the fifth and sixth basic residue on S4 do not contribute to the measured gating charge in Shaker and when mutated to histidine did not contribute to the gating charge at any pH, substantiating that these residues do not cross through the membrane's electric field[29].

These results indicate that R365H and R368H, the second and third arginine residues in S4, fully change their accessibility from internal to external exposure with membrane depolarization. In the presence of a transmembrane pH gradient, R365H and R368H become proton transporters. The maximum rate of transport occurs near the voltage of half-maximal charge displacement where voltage sensor transitions would be most frequent, consistent with the idea that the histidine residues are shuttling protons, one at a time, across the membrane with each stroke of the voltage-sensor. At strongly hyperpolarized and depolarized voltages, where the voltage dependence of gating charge movement is saturated, the proton transport rate is near zero, consistent with the idea that the histidine spends most of its time in one conformation.

In contrast, the first and fourth arginine on S4 (R362 and R371), when mutated to histidine generate voltage-dependent proton channels[29,30]. In a transmembrane pH gradient, R362H conducts protons only at hyperpolarized voltages while R371H conducts only at

depolarized voltages. Non-stationary noise analysis of R362H currents indicated that conductance of the channel in a 10^4-fold proton gradient was 40 fs indicating that at -100 mV, 56,000 protons pass through the voltage sensor per second. This rapid rate of proton passage suggested that the histidine at position 362 is driven by membrane voltage to a position accessible to both external and internal solutions, creating a true proton pore and not a transporter.

These results substantiate the idea that membrane depolarization triggers conformational changes in the voltage sensor that affect the accessibility of residues throughout the S4 segment. What further constraints do these experiments place on the possible environment or motion of the S4 segment? The formation of the R362H proton channel was presented as strong evidence for the presence of aqueous crevices that deeply penetrate into the membrane surrounding S4, allowing a single histidine residue to form a bridge between them in the closed state of the channel. This proton pore is sufficiently narrow to exclude thiol reactive agents which can not access ~9 residues in the closed state of the channel[23,25]. Could a proton pathway be generated by the packing of S4 against the remainder of the channel? Do we know to what extent water molecules penetrate the membrane in order to hydrate charged amino-acid side chains? Without a better understanding of the packing of the voltage sensor and the nature of the protein-lipid-water interface surrounding the S4 segment, the formation of artificial proton pores does not entirely discriminate between models of S4 motion or voltage sensor organization.

Lipid exposure of the voltage-sensor paddle

One of the most audible arguments against the position of the voltage-sensor paddle at the protein-lipid interface was that it was energetically unreasonable to place the gating

charge arginines within the hydrophobic core of the membrane. Is this a valid argument—what is the energetic cost of placing the charged S4 segment within the membrane? Recent studies by von Heijne and colleagues help to address this question. They measured the efficiency of translocon-mediated transmembrane insertion for single helical segments with different amino-acid sequences. von Heijne and colleagues found that single helices containing a charged amino acid, arginine for example, within the middle of the segment can be inserted into the membrane if the energetic cost of the arginine residue is compensated for with an increased number of hydrophobic residues[122]. The S4 sequence of voltage-dependent channels is very hydrophobic aside from the gating charge residues. von Heijne and colleagues showed that a segment corresponding to the KvAP S4 sequence can partition into the membrane with ~50% probability in the absence of any other part of the channel[123]. Their work suggests that the probability of membrane insertion for the S4 is balanced by a combination of hydrophobic and electrostatic forces: the hydrophobic residues of the S4 segment prefer to remain within the oily core of the lipid while the arginine residues prefer to reside in aqueous solution or near the membrane interface. In the context of the channel, the energetic cost of the S4 segment is likely to be further alleviated by the formation of salt-bridge interactions between the gating charge residues and conserved acid residues within other segments of the voltage sensor. This result clearly indicates that based on energetic considerations alone, placing the S4 arginines at the protein-lipid interface is not unreasonable.

von Heijne and colleagues also found that the energetic contribution of arginine is steeply dependent on its position within the segment and the cost of the arginine rises sharply when placed near the middle of the segment[123]. This suggests that arginines positioned near

the edges of the hydrophobic core of the membrane can participate in electrostatic interactions with lipid head-groups or benefit from hydration with water molecules. Crystallographic studies of soluble proteins have shown that water molecules can hydrate charged amino-acids buried within the protein core. For example, a glutamate inserted into the core of staphylococcal nuclease was observed to be hydrated by a chain of waters linking it with the bulk solution[124]. A better appreciation of the complexities of the lipid-water interface surrounding the S4 segment could affect the interpretation of certain functional results proposed to be inconsistent with the paddle model—for example the transmembrane proton pathways formed with histidine mutations mentioned above.

It is interesting to note that in the crystal structure of another voltage-sensitive membrane protein, MscS, a prokaryotic mechanosensitive channel, arginine residues are also found at the protein-lipid interface[125]. The MscS channel opens in response to membrane tension and its opening is modulated by membrane voltage. The MscS channel is entirely unrelated in amino acid sequence or structure to members of the voltage-dependent cation channel family, yet it appears to have very similar structural elements. The MscS channel contains helical hairpins at the periphery of the membrane spanning region with three arginine residues facing into the lipid. A detailed molecular mechanism has not been defined in these channels, although the arginine residues are thought to underlie its voltage-modulation by moving through the lipid in response to membrane depolarization.

A recent EPR study of KvAP channels reconstituted into lipid vesicles provided direct evidence that many of the residues of the S4 segment are exposed to lipid[108]. In this study, Perozo and colleagues measured the accessibility of spin-labeled side-chains to lipid-soluble and water-soluble paramagnetic agents to distinguish between lipid-accessible and

water-accessible sites. The vesicles lack a transmembrane voltage so presumably the KvAP channels during the experiment are in an inactivated conformation with the voltage-sensor paddles maintained in their opened configuration. The EPR data points to one face of the voltage-sensor paddle being almost fully-lipid exposed—the same face that would sit within the lipid if the paddle were to position its gating charge arginines towards the body of the channel as depicted in Figure 34. The opposite face of the paddle is accessible to water only near the tip of the helix-turn-helix and to a mixture of lipid and protein at all other sites.

Are the arginine positions on S4 specifically shielded from the lipid? The EPR data show that arginine 117 is in fact mostly lipid exposed, arginine 120 has mixed aqueous/lipid exposure and arginines 123 and 126 are inaccessible to either and presumably are interacting with other parts of the channel protein. Of course to evaluate the accessibility of different residues, the gating charge arginines have been mutated individually to cysteine and modified with the spin label, which precludes the formation of native ionic interactions between the arginine side chain and acidic residues elsewhere on the channel. In addition the EPR probe, is linked to the α-carbon of the cysteine through a ~5-6 Å tether and so may incorrectly estimate the extent of water or lipid accessibility for a given residue. Nevertheless, the overall pattern of accessibility is consistent with the idea that the voltage-sensor paddle lies at the protein-lipid interface.

Voltage-sensor toxins

Tarantula voltage-sensor toxins are small protein toxins that bind to the voltage sensor from the extracellular side of the membrane and alter channel function. The best studied member of this family of toxins is hanatoxin, which inhibits the eukaryotic Kv2.1 channel with 10-100 nM affinity[55]. Mutational studies in eukaryotic channels suggest that

voltage-sensor toxins recognize a very localized receptor on the voltage sensor. Only a few residues on the S3b segment have been implicated in forming the toxin interaction surface[52,73]. Initial studies of hanatoxin inhibition suggested that the toxin binds to the voltage-sensor of the closed channel and alters the energetics of channel activation[51]. Based on the very slow apparent binding kinetics, hanatoxin was thought to remain bound to the voltage-sensor throughout the gating process. The action of hanatoxin was therefore suggested to be inconsistent with a voltage-dependent gating mechanism in which the S3b segment resides beneath the surface of the membrane in the closed state of the channel, inaccessible to the extracellular solution[126].

I identified VSTX1, another member of this toxin family from the same spider, as an inhibitor of KvAP channel function with an apparent Kd of approximately ~25 nM for the channel reconstituted into membranes. Studies by Seok-Yong Lee in our lab, have shown that VSTX1 has intrinsically low affinity for purified KvAP channels in detergent and that much of the binding energy of the toxin-channel interaction comes from the toxin's interaction with lipid membranes[127]. This observation indicates that the tarantula voltage-sensor toxins target their receptor on the voltage-sensor paddle through the lipid membrane, entirely consistent with the idea that the voltage-sensor paddle lies at the protein-lipid interface. The low-affinity of the channel-toxin interaction raises the possibility that these toxins can bind and dissociate rapidly in the timescale of the gating process which would invalidate the assumption underlying the conclusion that these toxins bind to the closed conformation of the paddle. It is also possible that the toxins protrude into the membrane far enough to interact with S3b in the closed state of the channel. Members of other families of voltage-sensor toxins from other venomous animals, like *Centruroides* toxin II, a β-scorpion

toxin, have also been shown to partition into the lipid membrane, suggesting this is a more general strategy used by venomous animals for targeting the voltage-sensor[128].

In summary, from my thesis work I conclude that the S4 segment forms part of a helix-turn-helix structure—the voltage-sensor paddle—that lies at the perimeter of the channel, at the protein-lipid interface. The voltage-sensor paddles are attached to the body of the channel through flexible connections that allow them to move within the membrane. In response to membrane depolarization, the movement of the voltage-sensor paddle translates the S4 segment and its gating charge residues a minimum of 15 Å through the lipid, a conformational change that induces pore opening. This new conceptual understanding of gating charge movement is based on the crystallographic, biochemical and functional studies of KvAP that I have presented in the preceding chapters. This model is actually consistent with much of the data derived from functional studies of eukaryotic Kv channels. However, it represents a fundamentally different perspective on the mechanistic design of the voltage sensor and the dynamics of voltage-dependent channels in the membrane.

MATERIALS AND METHODS

KvAP channel protein preparation and analysis

KvAP channel protein (methionine14-lysine295) inserted into the pQE60 vector (Qiagen) with a C-terminal hexahistidine tag, was expressed in XL1-Blue cell cultures grown in LB medium supplemented with 10 mM $BaCl_2$ on induction with 0.4 mM isopropyl-β-D-thiogalactopyranoside (IPTG). Cells were harvested and lysed in 50 mM Tris, pH 8.0, and 100 mM KCl, containing Leupeptin, Pepstatin, Aprotinin and phenylmethylsulphonyl fluoride (Sigma) to inhibit proteases. Protein was then extracted from the cell lysate for 3 hours at room temperature in the above solution by adding 40 mM decylmaltoside (DM) and purified on a Talon Co^{2+} affinity column (Clontech). The protein was maintained in 5 mM DM, 20 mM Tris, pH 8.0, and 100 mM KCl. Nonspecifically bound protein was washed using 15 mM imidazole added to the above buffer, and the channel then eluted with 400 mM imidazole. Immediately after elution, 1.0 unit of thrombin (Roche) per 3.0 mg channel was added to cleave the hexahistidine sequence overnight at room temperature. Protein was concentrated to ~15 mg/ml and run on a Superdex-200 (10/30) column (Pharmacia) in the above buffer. Maldi time of flight mass spectrometry (PerSeptive

Biosystems Voyager-STR) and N-terminal sequencing analysis (Rockefeller University Protein/DNA Technology Center) indicated that the KvAP protein undergoes a modification during expression in which the first five residues of the encoded construct are replaced with a single leucine residue in the expressed channel protein.

The isolated voltage sensor (methionine1-lysine147) inserted into the pQE60 vector with a C-terminal hexa-histidine sequence was prepared by the same protocol as above except that no $BaCl_2$ was added to the bacterial cultures during growth and lower concentrations of imidazole were used for the affinity purification on Co^{2+} resin: the column was washed with 10mM imidazole and the isolated voltage-sensor was eluted off the column with 300 mM imidazole.

Fab purification

IgGs from mouse hybridoma cell culture supernatant were initially purified by Q-Sepharose chromatography. Fab fragment of the antibody was obtained by papain proteolysis (Worthington) followed by Q-Sepharose chromatography.

Electrophysiology

KvAP channels were reconstituted from DM into lipid vesicles as described[129], to give a final protein concentration of between 20 to 1200 μg/ml. Planar lipid bilayers of POPE (15 mg/ml) and POPG (5 mg/ml) in decane were painted over a 300 μm hole in a polysterene partition separating the internal and external solutions. To induce fusion of channel-containing vesicles, solution on the side to which vesicles were added (*cis*) contained 150 mM KCl, 10 mM Hepes, pH 7.0 and the opposite side (*trans*) contained 15 mM KCl, 10 mM Hepes, pH 7.0. After the appearance of channels in the membrane, ion concentration on the *trans* side was increased to 150 mM KCl or 15mM KCl plus 135 mM NaCl for measurement

of K^+ selectivity. For voltage activation curves shown in Figure 5a, the membrane was stepped to various test voltages and then returned to –100 mV. Currents were recorded 10 ms following the return to –100 mV, normalized to the current measured following the +10 mV test voltage, and graphed as a function of test voltage. Membrane voltage was controlled and current recorded using an Axopatch 200B amplifier with a Digidata 1322A analogue to digital converter and Axoclamp software (Axon Instruments).

For investigation of toxin function, the membrane holding potential was –100 mV and the membrane stepped to +100 mV for 200 ms every 2 minutes to monitor the extent of channel inhibition. Bovine serum albumin (0.5 mg /ml) was added to the recording chamber prior to toxin addition to prevent non-specific interaction of the toxin with surfaces of the recording chamber. Toxin concentrations were determined using the calculated extinction coefficient for 280 nm absorbance.

To measure functional effects from Fab fragments, the membrane holding potential was –100 mV and the membrane stepped to +100 mV for 200 ms every 2-10 minutes to monitor the extent of channel inhibition.

To measure avidin accessibility to biotinylated channels, the cysteine-mutant, biotinylated channels were reconstituted into membranes and studied using various voltage protocols prior to and after addition of 40-100 μg/ml avidin (Pierce) to the solution on one side of the membrane.

Reverse-phase HPLC

Analytical gradient HPLC was performed on an Agilent 1100 series instrument with UV detection using a Vydac C18 column (5 μm,4.6×250 mm) at a flow rate of 1 ml /min using a two component mobile phase system in which mobile phase A is 0.1% TFA in water and

mobile phase B is 90% acteonitrile and 0.1% TFA in water. Absorbance was monitored at 214 nm and 280 nm.

Mass spectrometry

MALDI-TOF mass spectrometry was used for characterization of toxin fractions to determine mass and estimate purity. Toxin samples were diluted into a saturated solution of α-cyano-4-hydroxycinnamic acid matrix in 30% acetonitrile, 0.1% TFA in water to a final concentration of approximately 10-100 nM. Spectra were acquired using a MALDI-TOF mass spectrometer Voyager-DE STR (PE Biosystem) operating in reflectron, delayed extraction mode. Spectra from 200 individual laser shots were averaged (using 0.5 ns-data channel width) with software provided by the manufacturer. The spectra were calibrated and analyzed using Data Explorer (PE Biosystem). For tandem mass spectrometry, proteolytic fragments of reduced and alkylated toxins were crystallized with 2,5-dihydroxybenzoic acid matrix in 60% methanol, 2% acetic acid in water and analyzed on a MALDI-Ion Trap MS Thermo Finnigan LCQ-DECAXP mass spectrometer with a home-made MALDI source[130].

Toxin biochemistry

CTX was produced recombinantly as previously described[131]. Venom from *G. spatulata* spiders was purchased from Spider Pharm (Yarnell, AZ). Venom was diluted 10-fold in 0.1% trifluoroacetic acid (TFA) in water, clarified by centrifugation and filtered through a 0.22 μm cellulose acetate filter. The resulting supernatant was fractionated using a linear gradient from 22% to 56% mobile phase B over 150min. The peak eluting at ~59 min contained mostly VSTX1. Homogenous VSTX1 could be obtained through a second purification step using a 2 min isocratic flow of 30% mobile phase B followed by a linear gradient from 30% to 42% mobile phase B over 40min. Purified VSTX1 was analyzed by

Maldi time of flight mass spectrometry. The first 32 residues of the VSTX1 sequence were determined using Edman chemistry (Rockefeller University Protein/DNA Technology Center). The identity and order of the final two residues was determined using tandem mass spectrometry on the C terminal toxin fragment obtained from a Lys-C proteolysis of the reduced and alkylated VSTX1.

Toxin extraction from venom using immobilized KvAP voltage-sensor domain and full-length KvAP channel

Isolated KvAP voltage-sensor domain and full-length channel was expressed and purified as described but without thrombin cleavage so that the channel proteins contained a C-terminal hexahistidine tag. Purified protein (10-15 mg/ml) was applied to a 0.1 ml Talon Co^{2+} affinity column to saturate the resin. Venom from *Grammostola spatulata* spiders (SpiderPharm, Yarnell, AZ) was diluted ten fold into 20 mM Tris, pH 8.0, 100 mM KCl, and 10 mM DM and applied (0.1 ml) either to a column saturated with isolated voltage-sensor domain, to a column saturated with full-length channel or to a control column with Co^{2+} resin alone. All three columns were washed extensively to minimize non-specifically bound toxins, first in the above buffer, then in the above buffer with 15 mM imidazole. Remaining protein was eluted from the columns with 0.1ml of 400mM imidazole in the above buffer and reduced with 50 mM DTT at 37°C for 2 hours to improve separation by HPLC. Equal volumes of eluted, reduced protein from the three pull-down columns were run using a 2 minute isocratic flow of 25% mobile phase B, followed by a 25% -55% B linear gradient over 40 minutes.

Toxin identification from channel protein pull-down assay

Individual peaks from the toxin pull-down assay were collected and analyzed by MALDI-TOF mass spectrometry and in some cases Edman sequencing. The peak corresponding to

VSTX1 has, within error of measurement, the same mass and retention time as the reduced native toxin run on the HPLC gradient used for the pull-down assay.

The peak corresponding to VSTX2 from the pull-down assay was subject to Edman sequencing (Rockefeller University Protein/DNA Technology Center) which yielded the N-terminal 30 residues. The toxin was reduced with 10 mM DTT for 2 hours at 37° C, alkylated with 100 mM iodoacetamide in the dark for an additional 2 hours and then repurified using a 22-56% B linear gradient over 40 minutes. Reduced, alkylated VSTX2 was dried under vacuum and resuspended in 100 mM potassium phosphate buffer, pH 7.0 and cleaved with Asp-N endoproteinase for 45 minutes. The identity and order of the final two residues was then determined by tandem mass spectrometry analysis of the 2981.4 Da fragment of reduced and alkylated VSTX2.

The peak corresponding to GSMTX4 from the pull-down assay was also subject to Edman sequencing which provided the N-terminal 23 residues. The initial sequence and mass corresponded to that of GSMTX4. The peak corresponding to GSMTX4 from the pull-down assay has the same retention time as reduced native GSMTX4, purified from whole venom as described.

The mass of VSTX3 determined from the pull-down assay guided us in isolating impure fractions of native VSTX3 from whole venom. These venom fractions were reduced and purified on the same gradient used for the toxin pull-down assay. A single peak had, within error of measurement, the same retention time and mass as the peak corresponding to VSTX3 from the pull-down assay. Edman sequencing of this peak provided the first 32 residues of the VSTX3 sequence. VSTX3 was reduced, alkylated with iodoacetamide and repurified as described above, resuspended in 50 mM MES, pH 6.0 and treated with Glu-C endoproteinase

for 1 hour. The identity and order of the final two residues of VSTX3 were determined by tandem mass spectrometry analysis of the 2260.1 Da fragment of the reduced alkylated toxin.

Toxin purification from venom

GSMTX4 were purified as described. VSTX1 was purified as described above. To purify VSTX2 and VSTX3, whole venom was fractionated on a linear 22-56% B gradient over 150 minutes. The fraction containing VSTX2 eluted between 46-52 minutes. VSTX2 was purified to homogeneity on a second gradient consisting of a two minute isocratic period at 25% B, followed by a linear 25-45% B gradient over 40 minutes. The fraction of whole venom containing VSTX3 eluted between 38-45 minutes. Extensive attempts to purify VSTX3 on a second gradient using a variety of different mobile phase systems were unsuccessful. A fraction of whole venom in which the VSTX3 was the dominant mass signal was used for functional experiments.

Production of recombinant toxins

The genes for both VSTX1 and VSTX3 were synthesized using two oligonucleotide duplexes ligated into pGEX-4T-2 (Amersham Biosciences) with SalI and BamHI restriction sites and confirmed by sequencing. The sense strand for VSTX1 was as follows: 5'GAATGCGGTAAATTTATGTGGAAAT GCAAAAACAGCAACGATTGCTGCAAAGATTTAGTGTGCAGCAGCCGCTGG AAATGGTGCGTGTTAGCCAGCCCGTTT 3'. The sense strand for VSTX3 was as follows: 5'GATTGCTTAGGCTGGTTTAAAGGCTGCGATCCGGATAACGAT AAATGCTGCGAAGGCTATAAATGCAACCGCCGCGATAAATGGTGCAAATATAAA TTATGG 3'. Recombinant toxin fusion protein was expressed in BL21-DE3 cells grown in LB medium on induction with 1.0 mM isopropyl-β-D-thiogalactopyranoside for three hours

at 37°C. Expressed fusion protein was maintained in 50 mM Tris-HCl, pH 7.5, 200 mM NaCl and purified on glutathione sepharose resin (Amersham Biosciences) by batch method. Following elution from the resin with 5 mM glutathione, the toxin was cleaved from the fusion protein with thrombin (1 unit per 2 mg fusion protein) overnight at room temperature. Recombinant VSTX1 was purified from the cleavage reaction using a 2 minute isocratic step at 30% B, followed by a 30-42% B linear gradient over 40 minutes. Recombinant VSTX3 was initially fractionated using a 2 minute isocratic step at 25% B, followed by a 25-45% B linear gradient over 40 minutes. The fractions eluting between approximately 12.5 –30.5 minutes all corresponded to toxins of the correct recombinant VSTX3 mass. These fractions were pooled together, dried under vacuum and resuspended in 20 mM Tris, pH 8.0, 100 mM KCl, and 10 mM DM for affinity purification on a KvAP voltage-sensor column domain generated as detailed above. Pooled recombinant VSTX3 fractions retained by the voltage-sensor domain were isolated using the same protocol to affinity purify toxins from whole venom described above except that following elution from the resin, bound toxins were not reduced but run on reverse-phase HPLC using a two minute isocratic flow of 0% B followed by a linear 0-73% B gradient over 30 minutes.

Biotinylation

EZ-Link PEO-Iodoacetyl Biotin ((+)-Biotinyl-iodoacetamidyl-3, 6-dioxaoctanediamine) (IPEO biotin) was obtained from Pierce. Biotin-[2-(2-pyridyldithio)ethylamide] (PDTE biotin), N-Biotinylcaproylaminoethyl Methanethiosulfonate (MCAP biotin), and N-Biotinylcaproylaminocaproylaminoethyl Methanethiosulfonate (BCAC biotin) were obtained from Toronto Research Chemicals, Inc.

All biotinylation studies were carried out using a KvAP channel in which the single endogenous cysteine was mutated to serine (C247S). This mutant showed no detectable electrophysiological differences when compared to wild-type KvAP. Single cysteine mutations were then added to the channel using the QuickChange method (Stratagene) and confirmed by sequencing the entire gene. Mutant channels were expressed and purified by the same protocol as wild-type KvAP channels, except that prior to gel filtration, mutant KvAP channels were incubated with 1 mM TCEP for 1 hour. Immediately after gel filtration, mutant channels (at 0.5–1.0 mg ml^{-1}) were incubated with 2-4 mM biotin reagent for 4-5 hours at room temperature in the dark, and then reconstituted into lipid vesicles for electrophysiological analysis. Samples of reconstituted channels in vesicles were complexed with avidin (Pierce) and run on an SDS gel to assess the extent of biotinylation.

REFERENCE LIST

1. Hille,B. Ion Channels of Excitable Membranes. Sinauer Associates, Inc., Sunderland, MA (2001).

2. Hodgkin,A.L. & Huxley,A.F. A quantitative description of membrane current and its application to conduction and excitation in nerve. *J. Physiol.* **117**, 500-544 (1952).

3. Hodgkin,A.L. & Huxley,A.F. Currents carried by sodium and potassium ions through the membrane of the giant axon of Loligo. *J. Physiol.* **116**, 449-472 (1952).

4. Hodgkin,A.L. & Huxley,A.F. The components of membrane conductance in the giant axon of Loligo. *J. Physiol.* **116**, 473-496 (1952).

5. Hodgkin,A.L. & Huxley,A.F. The dual effect of membrane potential on sodium conductance in the giant axon of Loligo. *J. Physiol.* **116**, 497-506 (1952).

6. Doyle,D.A. *et al.* The structure of the potassium channel: molecular basis of K^+ conduction and selectivity. *Science* **280**, 69-77 (1998).

7. Zhou,Y., Morais-Cabral,J.H., Kaufman,A. & MacKinnon,R. Chemistry of ion coordination and hydration revealed by a K^+ channel- Fab complex at 2.0 A resolution. *Nature* **414**, 43-48 (2001).

8. Heginbotham,L., Lu,Z., Abramson,T. & MacKinnon,R. Mutations in the K^+ channel signature sequence. *Biophys. J.* **66**, 1061-1067 (1994).

9. MacKinnon,R. Determination of the subunit stoichiometry of a voltage-activated potassium channel. *Nature* **350**, 232-235 (1991).

10. Perozo,E., Cortes,D.M. & Cuello,L.G. Structural rearrangements underlying K^+-channel activation gating. *Science* **285**, 73-78 (1999).

11. Armstrong,C.M. Interaction of tetraethylammonium ion derivatives with the potassium channels of giant axons. *J. Gen. Physiol.* **58**, 413-437 (1971).

12. del Camino,D. & Yellen,G. Tight steric closure at the intracellular activation gate of a voltage-gated K^+ channel. *Neuron* **32**, 649-656 (2001).

13. del Camino,D., Holmgren,M., Liu,Y. & Yellen,G. Blocker protection in the pore of a voltage-gated K^+ channel and its structural implications. *Nature* **403**, 321-325 (2000).

14. Jiang,Y. *et al.* The open pore conformation of potassium channels. *Nature* **417**, 523-526 (2002).

15. Magidovich E. & Yifrach, O. Conserved gating hinge in ligand- and voltage-dependent K+ channels. *Biochemistry* **43**, 13242-13247 (2005).

16. Armstrong,C.M. & Bezanilla,F. Charge movement associated with the opening and closing of the activation gates of the Na^+ channels. *J. Gen. Physiol.* **63**, 533-552 (1974).

17. Schoppa,N.E., McCormack,K., Tanouye,M.A. & Sigworth,F.J. The size of gating charge in wild-type and mutant Shaker potassium channels. *Science* **255**, 1712-1715 (1992).

18. Aggarwal,S.K. & MacKinnon,R. Contribution of the S4 segment to gating charge in the Shaker K^+ channel. *Neuron* **16**, 1169-1177 (1996).

19. Seoh,S.A., Sigg,D., Papazian,D.M. & Bezanilla,F. Voltage-sensing residues in the S2 and S4 segments of the Shaker K^+ channel. *Neuron* **16**, 1159-1167 (1996).

20. Noda,M. *et al.* Primary structure of Electrophorus electricus sodium channel deduced from cDNA sequence. *Nature* **312**, 121-127 (1984).

21. Tanabe,T. *et al.* Primary structure of the receptor for calcium channel blockers from skeletal muscle. *Nature* **328**, 313-318 (1987).

22. Tempel,B.L., Papazian,D.M., Schwarz,T.L., Jan,L.Y. & Jan,Y.N. Sequence of a probable potassium channel component encoded at Shaker locus of Drosophila. *Science* **237**, 770-775 (1987).

23. Larsson,H.P., Baker,O.S., Dhillon,D.S. & Isacoff,E.Y. Transmembrane movement of the Shaker K^+ channel S4. *Neuron* **16**, 387-397 (1996).

24. Yusaf,S.P., Wray,D. & Sivaprasadarao,A. Measurement of the movement of the S4 segment during the activation of a voltage-gated potassium channel. *Pflugers Arch.* **433**, 91-97 (1996).

25. Baker,O.S., Larsson,H.P., Mannuzzu,L.M. & Isacoff,E.Y. Three transmembrane conformations and sequence-dependent displacement of the S4 domain in Shaker K^+ channel gating. *Neuron* **20**, 1283-1294 (1998).

26. Yang,N. & Horn,R. Evidence for voltage-dependent S4 movement in sodium channels. *Neuron* **15**, 213-218 (1995).

27. Yang,N., George,A.L. & Horn,R. Molecular basis of charge movement in voltage-gated sodium channels. *Neuron* **16**, 113-122 (1996).

28. Starace,D.M., Stefani,E. & Bezanilla,F. Voltage-dependent proton transport by the voltage sensor of the Shaker K^+ channel. *Neuron* **19**, 1319-1327 (1997).

29. Starace D.M. & Bezanilla, F. Histidine scanning mutagenesis of basic residues of the S4 segment of the shaker K^+ channel. *J.Gen.Physiol.* **117**, 469-490 (2001).

30. Starace D.M. & Bezanilla, F. A proton pore in a potassium channel voltage sensor reveals a focused electric field. *Nature* **427**, 548-553 (2004).

31. Mannuzzu,L.M., Moronne,M.M. & Isacoff,E.Y. Direct physical measure of conformational rearrangement underlying potassium channel gating. *Science* **271**, 213-216 (1996).

32. Cha,A. & Bezanilla,F. Characterizing voltage-dependent conformational changes in the Shaker K^+ channel with fluorescence. *Neuron* **19**, 1127-1140 (1997).

33. Gandhi C.S., Loots, E., & Isacoff, E.Y. Reconstructing voltage sensor-pore interaction from a fluorescence scan of a voltage-gated K^+ channel. *Neuron* **27**, 585-595 (2000).

34. Bezanilla,F. The voltage sensor in voltage-dependent ion channels. *Physiol Rev.* **80**, 555-592 (2000).

35. Cha,A., Snyder,G.E., Selvin,P.R. & Bezanilla,F. Atomic scale movement of the voltage-sensing region in a potassium channel measured via spectroscopy. *Nature* **402**, 809-813 (1999).

36. Glauner,K.S., Mannuzzu,L.M., Gandhi,C.S. & Isacoff,E.Y. Spectroscopic mapping of voltage sensor movement in the Shaker potassium channel. *Nature* **402**, 813-817 (1999).

37. Horn,R. Coupled Movements in Voltage-gated Ion Channels. *J. Gen. Physiol* **120**, 449-453 (2002).

38. Gandhi,C.S. & Isacoff,E.Y. Molecular models of voltage sensing. *J. Gen. Physiol* **120**, 455-463 (2002).

39. Bezanilla,F. Voltage sensor movements. *J. Gen. Physiol* **120**, 465-473 (2002).

40. Ren,D. *et al.* A prokaryotic voltage-gated sodium channel. *Science* **294**, 2372-2375 (2001).

41. MacKinnon,R., Cohen,S.L., Kuo,A., Lee,A. & Chait,B.T. Structural conservation in prokaryotic and eukaryotic potassium channels. *Science* **280**, 106-109 (1998).

42. Miller,C., Moczydlowski,E., Latorre,R. & Phillips,M. Charybdotoxin, a protein inhibitor of single Ca2+-activated K+ channels from mammalian skeletal muscle. *Nature* **313**, 316-318 (1985).

43. MacKinnon,R. & Miller,C. Mechanism of charybdotoxin block of the high-conductance, Ca^{2+}-activated K^+ channel. *J. Gen. Physiol.* **91**, 335-349 (1988).

44. Garcia,M.L., Garcia-Calvo,M., Hidalgo,P., Lee,A. & MacKinnon,R. Purification and characterization of three inhibitors of voltage-dependent K^+ channels from *Leiurus quinquestriatus var. hebraeus* venom. *Biochemistry* **33**, 6834-6839 (1994).

45. Goldstein,S.A., Pheasant,D.J. & Miller,C. The charybdotoxin receptor of a Shaker K^+ channel: peptide and channel residues mediating molecular recognition. *Neuron* **12**, 1377-1388 (1994).

46. Yifrach,O. & MacKinnon,R. Energetics of pore opening in a voltage-gated K^+ channel. *cell* **111**, 231-239 (2002).

47. Zagotta,W.N., Hoshi,T. & Aldrich,R.W. Shaker potassium channel gating. III: Evaluation of kinetic models for activation. *J. Gen. Physiol.* **103**, 321-362 (1994).

48. Schoppa,N.E. & Sigworth,F.J. Activation of Shaker potassium channels. III. An activation gating model for wild-type and V2 mutant channels. *J. Gen. Physiol* **111**, 313-342 (1998).

49. Hoshi,T., Zagotta,W.N. & Aldrich,R.W. Biophysical and molecular mechanisms of Shaker potassium channel inactivation. *Science* **250**, 533-538 (1990).

50. Hoshi,T., Zagotta,W.N. & Aldrich,R.W. Two types of inactivation in Shaker K+ channels: effects of alterations in the carboxy-terminal region. *Neuron* **7**, 547-556 (1991).

51. Swartz,K.J. & MacKinnon,R. Hanatoxin modifies the gating of a voltage-dependent K^+ channel through multiple binding sites. *Neuron* **18**, 665-673 (1997).

52. Swartz,K.J. & MacKinnon,R. Mapping the receptor site for hanatoxin, a gating modifier of voltage-dependent K^+ channels. *Neuron* **18**, 675-682 (1997).

53. McDonough,S.I., Lampe,R.A., Keith,R.A. & Bean,B.P. Voltage-dependent inhibition of N- and P-type calcium channels by the peptide toxin omega-grammotoxin-SIA. *Mol. Pharmacol.* **52**, 1095-1104 (1997).

54. Suchyna,T.M. *et al.* Identification of a peptide toxin from Grammostola spatulata spider venom that blocks cation-selective stretch-activated channels. *J. Gen. Physiol* **115**, 583-598 (2000).

55. Swartz,K.J. & MacKinnon,R. An inhibitor of the Kv2.1 potassium channel isolated from the venom of a Chilean tarantula. *Neuron* **15**, 941-949 (1995).

56. Marvin,L. *et al.* Isolation, amino acid sequence and functional assays of SGTx1. The first toxin purified from the venom of the spider scodra griseipes. *Eur. J. Biochem.* **265**, 572-579 (1999).

57. Middleton,R.E. *et al.* Two Tarantula Peptides Inhibit Activation of Multiple Sodium Channels. *Biochemistry* **41**, 14734-14747 (2002).

58. Diochot,S., Drici,M.D., Moinier,D., Fink,M. & Lazdunski,M. Effects of phrixotoxins on the Kv4 family of potassium channels and implications for the role of Ito1 in cardiac electrogenesis. *Br. J. Pharmacol.* **126**, 251-263 (1999).

59. Sanguinetti,M.C. *et al.* Heteropodatoxins: peptides isolated from spider venom that block Kv4.2 potassium channels. *Mol. Pharmacol.* **51**, 491-498 (1997).

60. Li-Smerin,Y. & Swartz,K.J. Gating modifier toxins reveal a conserved structural motif in voltage- gated Ca^{2+} and K^+ channels. *Proc Natl Acad Sci U S A.* **95**, 8585-8589 (1998).

61. Ellinor,P.T., Zhang,J.F., Horne,W.A. & Tsien,R.W. Structural determinants of the blockade of N-type calcium channels by a peptide neurotoxin. *Nature* **372**, 272-275 (1994).

62. Hidalgo,P. & MacKinnon,R. Revealing the architecture of a K^+ channel pore through mutant cycles with a peptide inhibitor. *Science* **268**, 307-310 (1995).

63. Tytgat,J., Debont,T., Carmeliet,E. & Daenens,P. The alpha-dendrotoxin footprint on a mammalian potassium channel. *J. Biol. Chem.* **270**, 24776-24781 (1995).

64. Chang,N.S., French,R.J., Lipkind,G.M., Fozzard,H.A. & Dudley S Jr. Predominant interactions between mu-conotoxin Arg-13 and the skeletal muscle Na^+ channel localized by mutant cycle analysis. *Biochemistry* **37**, 4407-4419 (1998).

65. Jin,W., Klem,A.M., Lewis,J.H. & Lu,Z. Mechanisms of inward-rectifier K^+ channel inhibition by tertiapin-Q. *Biochemistry* **38**, 14294-14301 (1999).

66. Imredy,J.P. & MacKinnon,R. Energetic and structural interactions between delta-dendrotoxin and a voltage-gated potassium channel. *J. Mol. Biol.* **296**, 1283-1294 (2000).

67. Cahalan,M.D. Modification of sodium channel gating in frog myelinated nerve fibres by Centruroides sculpturatus scorpion venom. *J. Physiol.* **244**, 511-534 (1975).

68. Catterall,W.A. Binding of scorpion toxin to receptor sites associated with sodium channels in frog muscle. Correlation of voltage-dependent binding with activation. *J. Gen. Physiol* **74**, 375-391 (1979).

69. Wang,G.K. & Strichartz,G. Kinetic analysis of the action of Leiurus scorpion alpha-toxin on ionic currents in myelinated nerve. *J. Gen. Physiol* **86**, 739-762 (1985).

70. Shon,K.J. *et al.* Delta-conotoxin GmVIA, a novel peptide from the venom of Conus gloriamaris. *Biochemistry* **33**, 11420-11425 (1994).

71. Sheets,M.F. & Hanck,D.A. Voltage-dependent open-state inactivation of cardiac sodium channels: gating current studies with Anthopleurin-A toxin. *J. Gen. Physiol* **106**, 617-640 (1995).

72. McDonough,S.I., Mintz,I.M. & Bean,B.P. Alteration of P-type calcium channel gating by the spider toxin omega-Aga-IVA. *Biophys. J.* **72**, 2117-2128 (1997).

73. Li-Smerin,Y. & Swartz,K.J. Localization and molecular determinants of the Hanatoxin receptors on the voltage-sensing domains of a K^+ channel. *J. Gen. Physiol* **115**, 673-684 (2000).

74. Takahashi,H. *et al.* Solution structure of hanatoxin1, a gating modifier of voltage-dependent K^+ channels: common surface features of gating modifier toxins. *J. Mol. Biol.* **297**, 771-780 (2000).

75. Rogers,J.C., Qu,Y., Tanada,T.N., Scheuer,T. & Catterall,W.A. Molecular determinants of high affinity binding of alpha-scorpion toxin and sea anemone toxin in the S3-S4 extracellular loop in domain IV of the Na^+ channel alpha subunit. *J. Biol. Chem.* **271**, 15950-15962 (1996).

76. Cestele,S. *et al.* Voltage sensor-trapping: enhanced activation of sodium channels by beta-scorpion toxin bound to the S3-S4 loop in domain II. *Neuron* **21**, 919-931 (1998).

77. Kinoshita,E. *et al.* Novel wasp toxin discriminates between neuronal and cardiac sodium channels. *Mol. Pharmacol.* **59**, 1457-1463 (2001).

78. Lu,Z., Klem,A.M. & Ramu,Y. Ion conduction pore is conserved among potassium channels. *Nature* **413**, 809-813 (2001).

79. Takeuchi,K. *et al.* Solution structure of omega-grammotoxin SIA, a gating modifier of P/Q and N-type Ca^{2+} channel. *J. Mol. Biol.* **321**, 517-526 (2002).

80. Oswald,R.E., Suchyna,T.M., McFeeters,R., Gottlieb,P. & Sachs,F. Solution structure of peptide toxins that block mechanosensitive ion channels. *J. Biol. Chem.* **277**, 34443-34450 (2002).

81. Lee,C.W. *et al.* Solution Structure and Functional Characterization of SGTx1, a Modifier of Kv2.1 Channel Gating. *Biochemistry* **43**, 890-897 (2004).

82. Wang,J.M. *et al.* Molecular surface of tarantula toxins interacting with voltage sensors in Kv channels. *J. Gen. Physiol* **123**, 455-467 (2004).

83. Lee,S.Y. & MacKinnon,R. A membrane-access mechansim of ion channel inhibition by voltage sensor toxins from spider venom. *Nature* **430**, 232-235 (2004).

84. Diochot,S., Drici,M.D., Moinier,D., Fink,M. & Lazdunski,M. Effects of phrixotoxins on the Kv4 family of potassium channels and implications for the role of Ito1 in cardiac electrogenesis. *Br. J. Pharmacol.* **126**, 251-263 (1999).

85. Jiang,Y. *et al.* Crystal structure and mechanism of a calcium-gated potassium channel. *Nature* **417**, 515-522 (2002).

86. Carson,M. Ribbons. *Methods in Enzymology* **277**, 493-505 (1997).

87. Papazian,D.M. *et al.* Electrostatic interactions of S4 voltage sensor in Shaker K^+ channel. *Neuron* **14**, 1293-1301 (1995).

88. Tiwari-Woodruff,S.K., Schulteis,C.T., Mock,A.F. & Papazian,D.M. Electrostatic interactions between transmembrane segments mediate folding of Shaker K^+ channel subunits. *Biophys. J.* **72**, 1489-1500 (1997).

89. Tiwari-Woodruff,S.K., Lin,M.A., Schulteis,C.T. & Papazian,D.M. Voltage-dependent structural interactions in the Shaker K^+ channel. *J. Gen. Physiol* **115**, 123-138 (2000).

90. Papazian,D.M., Silverman,W.R., Lin,M.C., Tiwari-Woodruff,S.K. & Tang,C.Y. Structural organization of the voltage sensor in voltage-dependent potassium channels. *Novartis. Found. Symp.* **245**, 178-190 (2002).

91. Slatin,S.L., Qiu,X.Q., Jakes,K.S. & Finkelstein,A. Identification of a translocated protein segment in a voltage-dependent channel. *Nature* **371**, 158-161 (1994).

92. Qiu,X.Q., Jakes,K.S., Finkelstein,A. & Slatin,S.L. Site-specific biotinylation of colicin Ia. A probe for protein conformation in the membrane. *J. Biol. Chem.* **269**, 7483-7488 (1994).

93. Qiu,X.Q., Jakes,K.S., Kienker,P.K., Finkelstein,A. & Slatin,S.L. Major transmembrane movement associated with colicin Ia channel gating. *J. Gen. Physiol* **107**, 313-328 (1996).

94. Sigworth,F.J. Voltage gating of ion channels. *Q. Rev. Biophys.* **27**, 1-40 (1994).

95. Collaborative Computational Project,N.4. The CCP4 Suite: Programs for X-ray crystallography. *Acta Cryst.* **D50**, 760-763 (1994).

96. Knablein J,*et al.* $Ta_6Br_{12}^{2+}$ a tool for phase determination of large biological assemblies by X-ray crystallography. *J Mol Biol* **270**, 1-7 (1997).

97. Sheldrick, G.M. Patterson superposition and ab initio phasing. *Methods Enzymol.* **276**, 628-641 (1997).

98. Terwilliger, T.C. SOLVE and RESOLVE: automated structure solution and density modification. *Methods Enzymol.* **374**, 22-37 (2003).

99. Zhou,Y. & MacKinnon,R. The occupancy of ions in the K+ selectivity filter: Charge balance and coupling of ion binding to a protein conformational change underlie high conduction rates. *J. Mol. Biol.* **333**, 965-975 (2003).

100. Vagin,A.&. Teplyakov, A. MOLREP: an automated program for molecular replacement. *J.Appl.Cryst.* **30**,1022-1025 (1997).

101. de La Fortelle,E. & Bricogne,G. Maximum-Likelihood heavy-atom parameter refinement for multiple isomorphous replacement and multiwavelength anomalous diffraction methods. *Methods in Enzymology* **276**, 472-494 (1997).

102. Cowtan,K. DM: an automated procedure for phase improvement by density modification. *Joint CCP4 and ESF-EACBM newsletter on protein crystallography* **31**, 34-38 (1994).

103. Jones,T.A., Zou,J.Y., Cowan,S.W. & Kjeldgaard,M. Improved methods for building protein models in electron density maps and the location of errors in these models. *Acta Cryst.* **A47**, 110-119 (1991).

104. Brunger,A.T. *et al.* Crystallography & NMR system: A new software suite for macromolecular structure determination. *Acta Cryst.* **D54**, 905-921 (1998).

105. DeLano,W.L. The PyMOL Molecular Graphics System on World Wide Web http://www.pymol.org. 2002.

106. Santacruz-Toloza,L., Huang,Y., John,S.A. & Papazian,D.M. Glycosylation of Shaker potassium channel protein in insect cell culture and in Xenopus oocytes. *Biochemistry* **33**, 5607-5613 (1994).

107. Blaustein,R.O., Cole,P.A., Williams,C. & Miller,C. Tethered blockers as molecular 'tape measures' for a voltage-gated K^+ channel. *Nat. Struct. Biol.* **7**, 309-311 (2000).

108. Cuello,L.G., Cortes,D.M. & Perozo,E. Molecular architecture of the KvaP voltage-dependent K^+ channel in lipid bilayer. *Science* . **306**, 491-495 (2004).

109. Pugliese,L., Coda,A., Malcovati,M. & Bolognesi,M. Three-dimensional structure of the tetragonal crystal form of egg-white avidin in its functional complex with biotin at 2.7 A resolution. *J. Mol. Biol.* **231**, 698-710 (1993).

110. Karlin,A. & Akabas,M.H. Substituted-cysteine accessibility method. *Methods Enzymol.* **293**, 123-145 (1998).

111. Gandhi,C.S., Clark,E., Loots,E., Pralle,A. & Isacoff,E.Y. The orientation and molecular movement of a K^+ channel voltage-sensing domain. *Neuron* **40**, 515-525 (2003).

112. Gonzalez,C., Morera,F.J., Rosenmann,E., Alvarez,O. & Latorre,R. S3b amino acid residues do not shuttle across the bilayer in voltage-dependent Shaker K^+ channels. *Proc. Natl. Acad. Sci. U. S. A* **102**, 5020-5025 (2005).

113. Nguyen,T.P. & Horn,R. Movement and crevices around a sodium channel S3 segment. *J Gen. Physiol* **120**, 419-436 (2002).

114. Liu,Y., Holmgren,M., Jurman,M.E. & Yellen,G. Gated access to the pore of a voltage-dependent K^+ channel. *Neuron* **19**, 175-184 (1997).

115. Li,J. *et al.* Reactions of cysteines substituted in the amphipathic N-terminal tail of a bacterial potassium channel with hydrophilic and hydrophobic maleimides. *Proc. Natl. Acad. Sci. U. S. A* **99**, 11605-11610 (2002).

116. Cortes,D.M., Cuello,L.G. & Perozo,E. Molecular architecture of full-length KcsA: role of cytoplasmic domains in ion permeation and activation gating. *J Gen. Physiol* **117**, 165-180 (2001).

117. Laine,M. *et al.* Atomic proximity between S4 segment and pore domain in Shaker potassium channels. *Neuron* **39**, 467-481 (2003).

118. Neale,E.J., Elliott,D.J., Hunter,M. & Sivaprasadarao,A. Evidence for intersubunit interactions between S4 and S5 transmembrane segments of the Shaker potassium channel. *J Biol Chem.* **278**, 29079-29085 (2003).

119. Broomand,A., Mannikko,R., Larsson,H.P. & Elinder,F. Molecular movement of the voltage sensor in a K channel. *J Gen. Physiol* **122**, 741-748 (2003).

120. Elliott,D.J. *et al.* Molecular mechanism of voltage sensor movements in a potassium channel. *EMBO J* **23**, 4717-4726 (2004).

121. Aziz,Q.H., Partridge,C.J., Munsey,T.S. & Sivaprasadarao,A. Depolarization induces intersubunit cross-linking in a S4 cysteine mutant of the Shaker potassium channel. *J. Biol. Chem.* **277**, 42719-42725 (2002).

122. Hessa,T. *et al.* Recognition of transmembrane helices by the endoplasmic reticulum translocon. *Nature* **433**, 377-381 (2005).

123. Hessa,T., White,S.H. & von Heijne,G. Membrane insertion of a potassium-channel voltage sensor. *Science* **307**, 1427 (2005).

124. Dwyer,J.J. *et al.* High apparent dielectric constants in the interior of a protein reflect water penetration. *Biophys. J* **79**, 1610-1620 (2000).

125. Bass,R.B., Strop,P., Barclay,M. & Rees,D.C. Crystal structure of escherichia coli MscS, a voltage-modulated and mechanosensitive channel. *Science* **298**, 1582-1587 (2002).

126. Lee,H.C., Wang,J.M. & Swartz,K.J. Interaction between extracellular Hanatoxin and the resting conformation of the voltage-sensor paddle in Kv channels. *Neuron* **40**, 527-536 (2003).

127. Lee,S.Y. & MacKinnon,R. A membrane-access mechanism of ion channel inhibition by voltage sensor toxins from spider venom. *Nature* **430**, 232-235 (2004).

128. Smith,J.J., Alphy,S., Seibert,A.L. & Blumenthal,K.M. Differential phospholipid binding by site 3 and site 4 toxins. Implications for structural variability between voltage-sensitive sodium channel domains. *J Biol Chem.* **280**, 11127-11133 (2005).

129. Heginbotham,L., LeMasurier,M., Kolmakova-Partensky,L. & Miller,C. Single *Streptomyces lividans* K^+ channels. Functional asymmetries and sidedness of proton activation. *J. Gen. Physiol.* **114**, 551-560 (1999).

130. Krutchinsky,A.N., Kalkum,M. & Chait,B.T. Automatic identification of proteins with a MALDI-quadrupole ion trap mass spectrometer. *Anal. Chem.* **73**, 5066-5077 (2001).

131. Park,C.S., Hausdorff,S.F. & Miller,C. Design, synthesis, and functional expression of a gene for charybdotoxin, a peptide blocker of K^+ channels. *Proc. Natl. Acad. Sci. USA* **88**, 2046-2050 (1991).